Electric stress on motorwindings due to switching in an industrial surrounding

Croes, A.

Award date:
1995

EG/95/789

FACULTY OF ELECTRICAL ENGINEERING

Section Electrical Energy Systems

Electric stress on motorwindings due to switching in an industrial surrounding.

Alan Croes

EG/95/789.A

M. Sc. graduation report coached by:
Supervisor: Prof.ir. G.C. Damstra
Coach : Dr.ir. R.P.P. Smeets
Eindhoven, August 1995.

EINDHOVEN UNIVERSITY OF TECHNOLOGY

THE NETHERLANDS

Summary

This thesis involves the electric faults in 3kV motors. The research was conducted at the Eindhoven University of Technology in cooperation with ISLA refinery in Curacao. At ISLA they experienced a high motor failure rate for their 3kV motors. The main source of failure was found to be electric breakdown in the motor insulation, probably due to switching surges. The objective of this study was to analyze the probability of the height of the occurring switching surges and their influence on the motor insulation. This includes the propagation of the surge in the industrial network and the distribution of the resulting wavefront over the motor windings. The work was divided into five topics and combined in a dedicated software program written for ISLA for calculating the electric stress on motor windings due to switching in an industrial surrounding.

The stress on the insulation is due to the inhomogeneous distribution of steep-fronted surges over the coils. The coil insulation will experience practically the whole surge amplitude and not partially as in normal operation. This effect is known to be the main cause of insulation degradation due to switching surges and will be the main issue of our investigation. Literature study showed a much lower probability of occurrence of steep-fronted surges when switching off then when switching in. This resulted in concentrating the research on surges made when switching in.

Several parameters of the time dependent transient phenomena which influence the height of the making surge (pre-ignition) were investigated. With the Monte Carlo method for the statistical variation, the calculation was implemented into the program. With the static energy relation the theoretical maximum of the closing surge (breakdown) was calculated, no statistical variation was used since the probability of breakdown was low. The influence of the network was divided into the propagation in the busbar and through the cable. The investigation of the influence of the cable showed, both in calculations and measurements, that within the range of 30 till 200 m the effect of damping could be neglected in further calculations. On the other hand the busbar setup has a great influence on the construction of the final wavefront at the motor terminal. Several setups were investigated and resulted in little difference between the steepness of the wavefront of vacuum breakers and oil breakers. The difference found, dependents on the other connected items near the motor under consideration. A compensation capacitor connected next to the motor is a severe case, while a motor is significantly less stressed if it is connected to the end of the busbar. For the distribution of the steep fronted waveform over the motor winding, a high frequent motor model was used. Several possibilities were found in the literature, and a lumped components model with a coil as smallest element was chosen. An estimation of the high frequent motor parameters was made. These parameters do not vary much, and show at most 10% difference in the result when calculated with extreme values.

For the degradation of the motor insulation, a literature study was conducted. Several deterioration mechanisms and methods of calculating the life time of the insulation were found. Since no specific knowledge about the motor winding insulation was present, an empirical formula related to age and to the number of switching operations was used in the program to only give an indication of the insulation degradation.

Samenvatting

Dit afstudeerwerk betreft het optreden van storingen in middenspanningsmotoren. Het onderzoek is verricht aan de Technische Universiteit Eindhoven in samenwerking met de raffinaderij ISLA in Curaçao. Op ISLA had men een vrij hoge uitval van hun 3kV motoren. De voornaamste reden voor deze uitval bleek elektrische doorslag te zijn, waarschijnlijk door steile golffronten vanwege schakelhandelingen. De doelstelling van dit onderzoek is om de kans op de golffronten en hun invloed op de isolatie in de motor windingen te onderzoeken. Hier is bij inbegrepen de propagatie van het golffront in het industrieel net en de distributie van het front over de motorspoelen. De resultaten van het werk zijn verwerkt in een computerprogramma waarmee de grootte van de overspanningen over de motorspoelen, afhankelijk van het industrieel net, berekend kunnen worden.

De verdeling van het golffront over de spoelen gebeurt inhomogeen bij voldoende steilheid. Het blijkt dat over de isolatie van de eerste spoel praktisch de volledige overspanning staat en niet een gedeelte zoals in normaal bedrijf. Het blijkt uit de literatuur dat de kans op steile golffronten veel kleiner is bij het uitschakelen dan bij het inschakelen. Hierdoor zal het onderzoek zal zich primair toeleggen op overspanningen over motorspoelen bij het inschakelen, vanwege de isolatie degradatie die hierdoor optreedt.

Verschillende parameters, van het tijdafhankelijk transiënt fenomeen, die invloed hebben op de hoogte van het front bij het inschakelen zijn onderzocht. Via de Monte Carlo methode voor statistische berekeningen is de berekening voor de hoogte van het front in het programma geïmplementeerd. Met de statische energie vergelijking is het theoretisch maximum van het front bij het uitschakelen berekend. Hierbij zijn geen statistische berekeningen gemaakt, vanwege de kleine waarschijnlijkheid van optreden, hoewel de grootte van het front vaak hoger is dan bij inschakelen. Bij het onderzoek naar de invloed van de kabel op het golffront bleek, uit berekeningen en metingen, dat de demping verwaarloosd kon worden bij een kabellengte van 30 tot 200 m. Echter het railsysteem bleek een grote invloed te hebben, veel meer dan de steilheid van de golffront bij het schakelen zelf. Verschillende configuraties zijn berekend en het bleek dat een compensatie condensator naast de motor een slechte keus was, terwijl een motor aangesloten aan het einde van de rail de laagste overspanning over de eerste spoel bleek te hebben. Voor de verdeling van het front over de motorspoelen is een hoogfrequent motor model gekozen, waarbij de spoel als kleinste eenheid is opgebouwd uit geconcentreerde componenten. Uit een schatting van de waarde voor de componenten bleek dat deze weinig varieerde, de variatie resulteerde in ±10% variatie in de hoogte van de overspanning over de eerste motorspoel.

Voor de degradatie van de motor isolatie is een literatuurstudie uitgevoerd. Verschillende verouderingsmechanismen en berekeningsmethoden voor de levensduur van de isolatie zijn gevonden. Hierbij is uitgegaan van een empirische vergelijking die afhankelijk is van de leeftijd van de motor en van het aantal schakelhandelingen. Deze vergelijking is in het programma alleen gebruikt ter indicatie van het isolerend vermogen van de motor isolatie.

Symbols

For the voltages the following styles were used:

normal	time dependant signals per unit	u_n = n^{th} phase of the supply voltage
CAPITAL	constant value per unit	U_{jump} = voltage jump
italic	signals in Volts	U_{jump} = 5.0 kV
		u_n = $\sqrt{2} \cdot 3 \sin \omega t$ (kV)

Other symbols:

# ...	number of ...
α	factor to determine presence of a compensation capacitor (0 = none / 1 = yes)
β_t	transient damping factor
C_C	total cable capacitance
C_{ground}	phase to phase cable capacitance
cos φ	power factor of a motor
C_{phase}	phase to phase cable capacitance
d	contact distance
E_{br}	breakdown field strength
Φ	closing angle
F_k	factor defined by dividing the slope of the breakdownvoltage by the maximum slope of the system power frequency voltage for switching in
I_{chop}	value of chopping current
κ	overshoot factor
L	motor inductance
μ	average of a normal distribution
P	motor power (W)
R	motor resistance
r	reflection coefficient of a wavefront
S	motor power (VA)
$\underline{\sigma}$	standard deviation
σ	standard deviation divided by μ given in percentages
τ	delay time of a wavefront on a cable
t	time
t_{d1}	pole delay time between pole 1 and pole 2
t_{d2}	pole delay time between pole 1 and pole 3
t_{rise}	rise time of the wavefront
TRV	transient recovery voltage
$\hat{u}$	1 unit = 1 pu $\approx$ 2.45 kV
U_F	height of the wavefront
v	closing velocity of the circuit-breaker
ω	frequency of the supply voltage
ω_{in}	frequency of the transient when switching in
Z_0	characteristic impedance

Table of Contents

1 Introduction

It is commonly known that motors in operation in an industrial surrounding are constantly under stress. This stress can be of electric, mechanical or thermal nature. ISLA refinery in Curacao is experiencing an increased level of electric stress on the motor windings of induction squirrel cage motors between 110 kW and 1 MW with a 3 kV 50 Hz supply system. The aim of this master thesis is to investigate the theory behind the electric stress on motor windings and if possible draw conclusions on better protection for the motors at the ISLA refinery.

To research the electric stress on motor windings, the investigation will focus on switching surges who are the main cause of this type of stress resulting in insulation failures. Since the first wavefront on the motor terminal on the first coils will be the worst, the research will focus on the initial wavefront over the first coil. The literature study on steep-fronted switching surges, their propagation in the system and distribution in the motor combined with the turn insulation capability resulted in dividing the research into five sections [1.1 - 1.7]:

- circuit-breaker — origin of switching surges
- cable — a "transmission line" between the breaker and the motor
- busbar setup — influence on the wavefront at the motor terminal, due to reflections
- motor — distribution of the wavefront in the motor windings
- degradation — withstand capability of the insulation

Circuit breaker

The objective is to determine if a probability function of the height of the switching surges is possible. By simplifying the three phase into a single phase circuit the transient phenomenon when switching can be calculated. Switching in and switching off will be separately researched. By using a normal distributed breakdown field strength to calculate the prestrikes when switching in, a probability of height can be introduced. Also the several factors influencing this phenomenon will be studied. The phenomenon when switching off will be researched for the various states a motor can be in; starting-, no load- or full load state. With the probability function one can see the influence of the circuit behind the breaker (towards the motor) and the influence of the circuit breaker itself. This will be expressed in a probability of height of the switching surge.

Cable

The length of cables used at ISLA lie in the range of 30 - 200 m. Their influence on the rise time of the wavefront and the height of the wavefront will be examined. For this purpose we will make use of the Elektromagnetic Transient Program (EMTP).

Busbar setup

The influence of the industrial surrounding of a motor is of importance in the construction of the final waveform on the motor terminal. The reflections and losses in a single phase model of the busbar will be calculated, with an option for different setup possibilities. These calculations will be done with the motor replaced by an impedance at the end of the motor cable. This simplification will be replaced afterward with a motor model, but when studying the different setups this will simplify the calculation.

Motor

For the calculation of the distribution of the surge over the motor windings a single phase circuit will be chosen. This model must be valid for the range of motors at ISLA. This model will replace the impedance used in the busbar calculations. By dividing the calculation in two, than using the results of the cable influence for the motor calculation and some simplifications in the motor model this can be done within reasonable computation time.

Degradation

For the degradation of the insulation system a study will be conducted into the causes of degradation, electrical, mechanical and thermal. The mechanism of each will be described in relation to the motor winding insulation. The aim is to translate the theory of the mechanisms of degradation into a degradation factor that can be calculated for the motor windings.

The results of these five sections will be implemented into a dedicated software program, with which ISLA can calculate the overvoltage over the motor windings. The input of this program will be divided into standard parameters, unique for each motor, and parameters for advanced use. By using the calculated parameters further advanced diagnostic can be used in relation to the industrial surrounding of the motor under consideration. An user guide with a test case will be supplemented.

To investigate the wavefronts and the overvoltages induced by the circuit breakers we will divide the problems into two actions: switching in and switching off the motor. In figure 2.1 the schematic circuit used in the modeling of the signals is drawn.

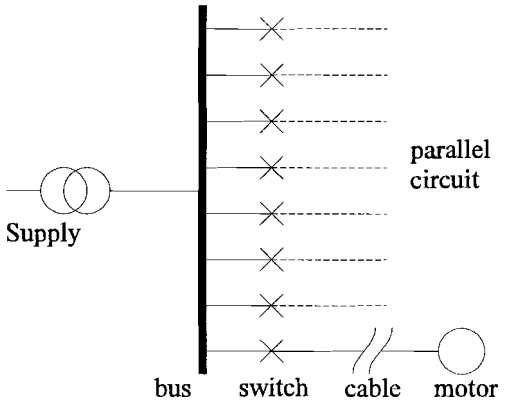

Fig 2.1: Schematic drawing

The supply for the motors is a three-phase non-grounded 50 Hz, 3 kV system. In our calculations the voltages are given in Volts/unit (peak rated line-to-ground voltage = 1 pu) unless otherwise mentioned.

$$1 \text{ unit} = \hat{u} = \frac{\sqrt{2}}{\sqrt{3}} 3 \text{ kV} \tag{2.1}$$

When closing the switch, there will be a pre-ignition. As a result a steep fronted surge will enter the cable and a transient phenomenon can be witnessed. By defining an overshoot factor (κ) and a frequency for the transient (ω_{in}) we can simplify the expression for this phenomenon.
When opening a switch the remaining energy in the circuit will cause a resonance with the cable capacitance, this transient phenomenon will also be simplified by defining an overshoot factor and a transient frequency.
The closing phenomenon can be witnessed as a damping high frequent sine superimposed on the system voltage (u_n). With a surge of 1pu this can be expressed by [2.1]:

$$\begin{aligned} u_{trans} &= u_n - U_{jump} \cdot e^{-\beta_t t} \cdot \cos(\omega_{in} t) \approx 1 \text{ pu} \cdot \left[1 - e^{-\beta_t t} \cdot \cos(\omega_{in} t)\right] \\ \beta_t &= \frac{-2\omega_{in}}{2\pi} \ln(\kappa - 1) \end{aligned} \tag{2.2}$$

The approximation made is only valid if $\omega_{in} \gg \omega$. Then u_n can be considered a constant compared to the transient phenomenon. Considering equation 2.2 without the approximation and κ=1.7 and ω_{in}=2π 1000 the transient is given by figure 2.2.

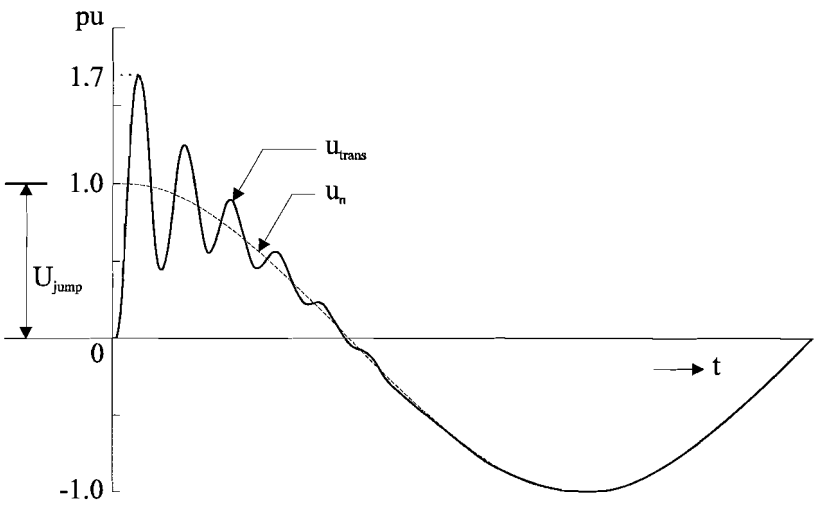

Fig 2.2: Transient voltage

When closing the switch in this example on $t = t_0$, the voltage jump was 1 pu resulting in a $\hat{u}_{trans} = 1.7$ pu (κ=1.7). After damping the voltage over the motor (u_B) will be the same as the supply voltage (u_n).

2.1 Switching in

2.1.1 Theory

When a circuit-breaker is switched in, there will be pre-ignition causing a steep wavefront traveling into the cable towards the motor. To determine the frequency of the transient we will transform the three phase circuit behind the switch into a single phase resonance electric circuit. This transformation allows us to calculate the transient phenomenon caused by a rapid change of voltage. When transforming we assumed equal transient phenomenon U_{b2} and U_{b3} (symmetrical) and ideal connection of the ground (second drawing figure 2.3).

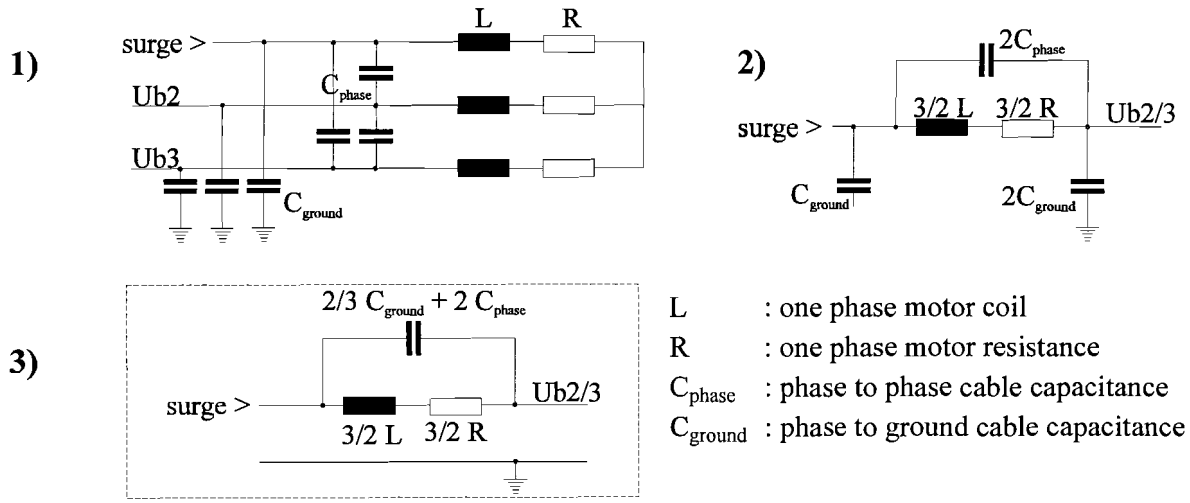

L : one phase motor coil
R : one phase motor resistance
C_{phase} : phase to phase cable capacitance
C_{ground} : phase to ground cable capacitance

Fig 2.3: Single phase electric circuit of the motor

The frequency of the transient (ω_{in}) will be the series resonance frequency of the single phase circuit in figure 2.3. With equation 2.24 we will calculate the low frequent value for the single phase coil value when switching in. When a filter is added parallel to the motor the value of the filter capacitor should be added to the phase to ground capacitance.

$$\omega_{in} = \frac{1}{\sqrt{\frac{3}{2}L \cdot \left(\frac{2}{3}C_{ground} + 2C_{phase}\right)}} \tag{2.3}$$

The three remaining parameters for each phase to define the height of this wavefront are:

- the voltage over the gap (u_{AB})
- the breakdown field strength (E_{br})
- the contact distance (d)

The latter two parameters define the breakdown voltage (u_{br}). When this is lower than the actual voltage a pre-ignition will occur. Assuming a constant closing velocity of the contacts (v), the breakdown voltage is a linear function of the contact distance. A factor F_k is used for our calculations:

$$F_k = \frac{E_{br} \cdot v}{\hat{u} \cdot \omega} \tag{2.4}$$

If the peak value of the supply voltage is given as 1 pu, the linear function of u_{br} depending on F_k can be given as (u_{br} per unit and u_{br} in kV):

$$\begin{aligned} u_{br} &= E_{br} v(t_c - t) \quad ; \quad t < t_c \\ u_{br} &= \frac{u_{br}}{\hat{u}} = \frac{E_{br} v}{\hat{u}\omega}\omega(t_c - t) = F_k \omega(t_c - t) \end{aligned} \tag{2.5}$$

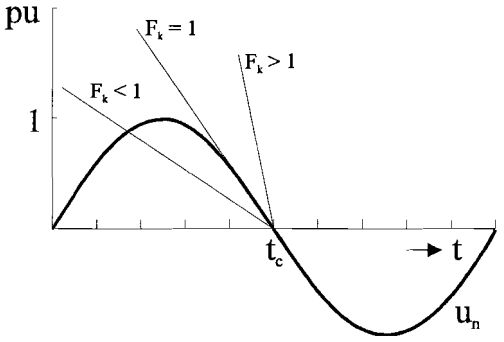

Fig 2.4: Function of u_{br} depending on F_k

For the three phase problem there are some variations of parameters that influence the breakdown voltage function of all three phases. The following actions were taken to cover all possible situations:

- random closing time, achieved by introducing a random closing angle (Φ) in the supply voltage.
- calculating for each cable and motor setup the transient frequency ω_{in}.
- normal distribution of the initial U_{br} achieved by using a normal distribution for the factor F_k and a constant v, $\hat{u}_n$.

Since there is a difference in the time of physical contact touch between the three switches for the three phases, a pole delay time is introduced. A delay time between closing of pole 1 and pole 2 (t_{d1}) and a delay time between closing of pole 1 and 3 (t_{d2}).

Switching in on t = 0 with a random Φ and known pole delay times a pre-ignition will occur on t = t_1 as shown in figure 2.5.

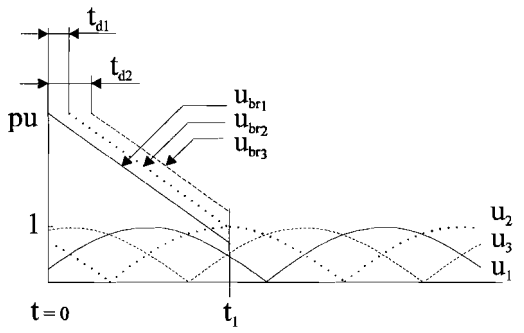

Fig 2.5: Switching in three phases

We made the following pre-assumptions for the calculations:

- The order of pre-ignition (pole 1 - 2 - 3) is the same as the phase order. In the program this is achieved by swapping all necessary parameters.
- The circuit breaker is physically closed in 10 ms ($u_{br} = F_k \pi (1 - 100 t)$; see equation 2.5). The 10 ms are chosen only to implement the time dependent breakdown voltage into the program. This has no influence whatsoever on the calculations.
- The overshoot $\kappa = 1.7$.
- The motor is connected close to the circuit breaker thus eliminating delay time of the wavefronts.
- The voltage of the non-grounded motor is zero before switching on.
- The supply voltage is not influenced by the circuit.

This results in the following initial situation:

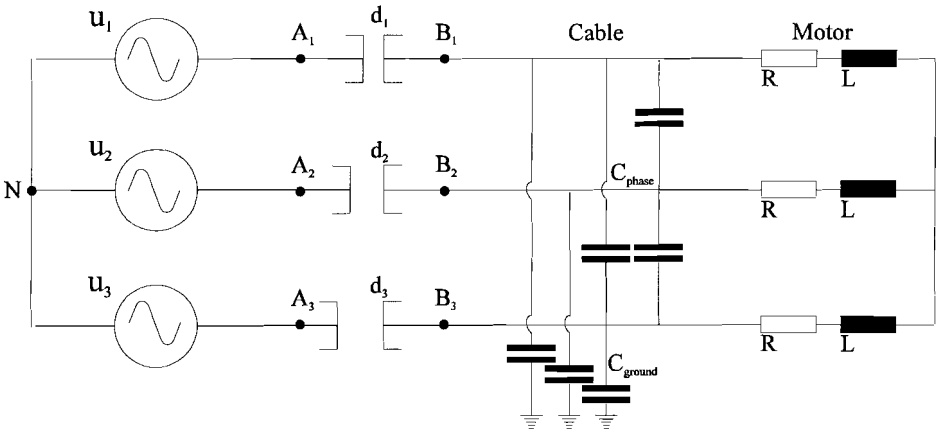

Fig 2.6: Electric circuit used for the calculations

The equations concerning the electric circuit of figure 2.6 will be:

$$\begin{aligned} u_1 &= \sin(\omega t - \Phi) \qquad \Phi = \text{random} \qquad & u_{br_1} &= F_{k_1}\pi\left[1-100\cdot t\right] \\ u_2 &= \sin(\omega t - \tfrac{2}{3}\pi - \Phi) & u_{br_2} &= F_{k_2}\pi\left[1-100\cdot(t-t_{d_1})\right] \\ u_3 &= \sin(\omega t - \tfrac{4}{3}\pi - \Phi) & u_{br_3} &= F_{k_3}\pi\left[1-100\cdot(t-t_{d_2})\right] \end{aligned} \tag{2.6}$$

The maximum voltage over the first pole $\hat{u}_{A1B1} = 1$ pu. The first pre-ignition will occur when $u_{A1B1} = u_1 > u_{br1}$. The height of this breakdown is $U_{t1} = u_1(t_1)$. After a transient phenomenon the voltage on B_2 and B_3 will become $u_1(t)$. The resulting voltages over the second and third pole with the transient phenomenon (see eq. 2.2) will be:

$$\begin{aligned} u_{A_2B_2} &= u_2 - u_{B_2N} = u_2 - u_{trans} \\ u_{A_3B_3} &= u_3 - u_{B_3N} = u_3 - u_{trans} \end{aligned} \tag{2.7}$$

$$\text{with:} \quad u_{trans} = u_1 - U_{t1}\cdot e^{-\beta_t(t-t_1)}\cdot\cos\left(\omega_{in}(t-t_1)\right) \approx u_1\left[1 - e^{-\beta_t(t-t_1)}\cdot\cos\left(\omega_{in}(t-t_1)\right)\right]$$

The maximum voltage across pole 2 ($\hat{u}_{A2B2}$) is at the maximum difference between u_1 and u_2 and the $\hat{u}_{trans}$ for this voltage jump:

$$\hat{u}_{A_2B_2} = u_2 - \hat{u}_{trans} = \tfrac{1}{2}\sqrt{3} + 1.7\,\tfrac{1}{2}\sqrt{3} \approx 2.3 \text{ pu} \tag{2.8}$$

After damping the maximum voltage will become the line voltage:

$$\hat{u}_{A_2B_2} = \sqrt{3}\,u_1 \approx 1.7 \text{ pu} \tag{2.9}$$

The second pre-breakdown occurs when $u_{A2B2} > u_{br2}$. The height of this breakdown is $U_{t2} = u_{A2B2}(t_2)$. The voltage on B_3 will jump from u_1' to 0.5 ($u_1' + u_2$), where u_1' is the momentary voltage over the motor.

The voltage across pole 3 will be:

$$u_{A_3B_3} = u_3 - \left[\tfrac{1}{2}(u_1' + u_2) - U_{jump}\cdot e^{-\beta_t(t-t_2)}\cdot\cos\left(\omega_{in}(t-t_2)\right)\right] \tag{2.10}$$

$$\text{with:} \quad u_1' = u_1 - U_{t_1}\cdot e^{-\beta_t(t-t_1)}\cdot\cos\left(\omega_{in}(t-t_1)\right)$$

$$U_{jump} = \tfrac{1}{2}\left[u_1'(t_2) + u_2(t_2)\right] - u_1'(t_2) = \tfrac{1}{2}\left[u_2(t_2) - u_1'(t_2)\right]$$

The maximum voltage across pole 3 for $t \to \infty$ is:

$$\hat{u}_{A_3B_3} = \left[u_3 - \tfrac{1}{2}(u_2 - u_1)\right]_{max} = 1.5\,\hat{u}_3 = 1.5 \text{ pu} \tag{2.11}$$

Results of calculations made with pole delay times of t_{d1} = 20 ms and t_{d2} = 40 ms, F_k = 10 (v = 1 m/s) and a transient frequency (f_{in}) of 1 kHz is presented in figure 2.7. The unrealistic values of t_{d1} and t_{d2} are only taken to emphasize the transient phenomenon in the plot.

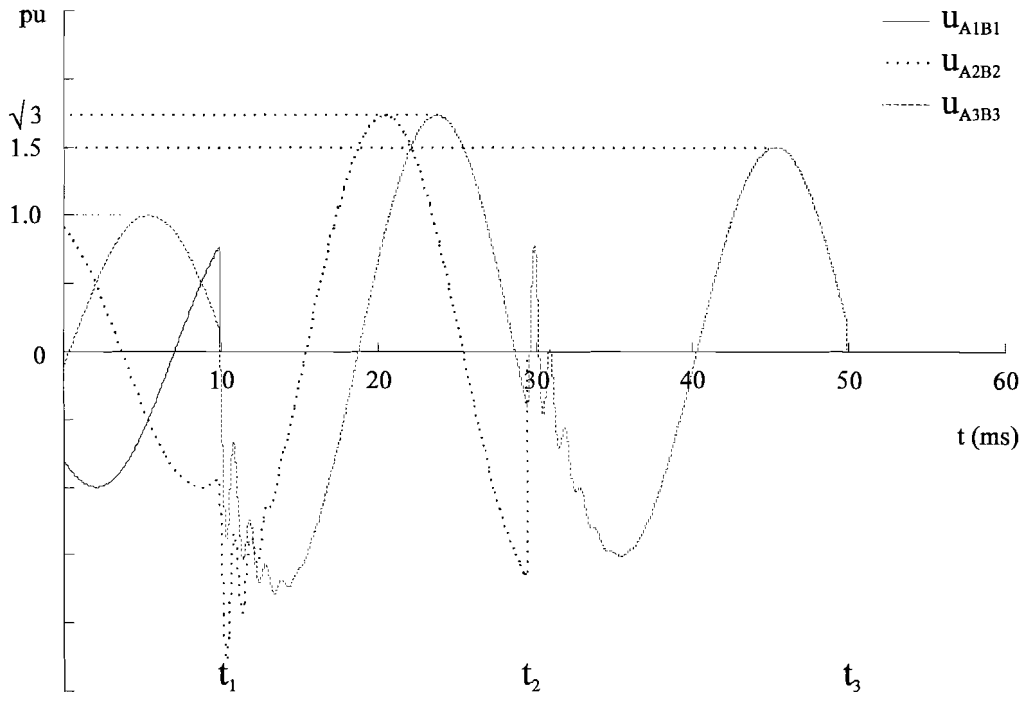

Fig 2.7: Transient phenomenon when switching on a three phase circuit breaker with long pole delay times

2.1.2 Statistical examination

A Monte-Carlo simulation examines the probability of occurrence of high wavefronts. This method uses for each single simulation random input parameters and by repeating this simulation with different random parameters a probability of occurrence can be obtained. By giving a parameter a normal distribution single can get a probability of occurrence with a normal distributed parameter. The number of simulations determines the accuracy of the result. A normal distribution is given by :

$$f(x) = \frac{1}{\underline{\sigma}\sqrt{2\pi}} e^{-\frac{(x-\mu)^2}{2\underline{\sigma}^2}} \quad \Rightarrow x \text{ is } N(\mu,\underline{\sigma}^2) \text{ distributed} \tag{2.12}$$

μ = average value of x

$\underline{\sigma}$ = standard deviation of x

According to [2.2] one can generate random numbers with a normal distribution in a computer program with equation 2.13.

$$x = \mu + \underline{\sigma}\sqrt{-\ln(X_1)}\cdot\cos(2\pi X_2) \tag{2.13}$$

X1, X2 = independent random numbers between zero and one

By defining σ as a percentage of the value of μ ($\sigma = \underline{\sigma}/\mu \cdot 100\%$), we can transform equation 2.13 into equation 2.14.

$$x = \mu\left[1 + \sigma\sqrt{-\ln(X_1)}\cdot\cos(2\pi X_2)\right] \tag{2.14}$$

The input parameters to determine the height of the wavefronts of pole 1, 2 and 3 were:

- n = 1000 simulations
- F_k = N(10,4) ; $\mu = 10$ and $\sigma = 20\%$ thus $\underline{\sigma}^2 = (0.20 \cdot 10)^2$ (see eq. 2.12)
- t_{d1} = 200 µs, t_{d2} = 400 µs
- f_{in} = 1 kHz

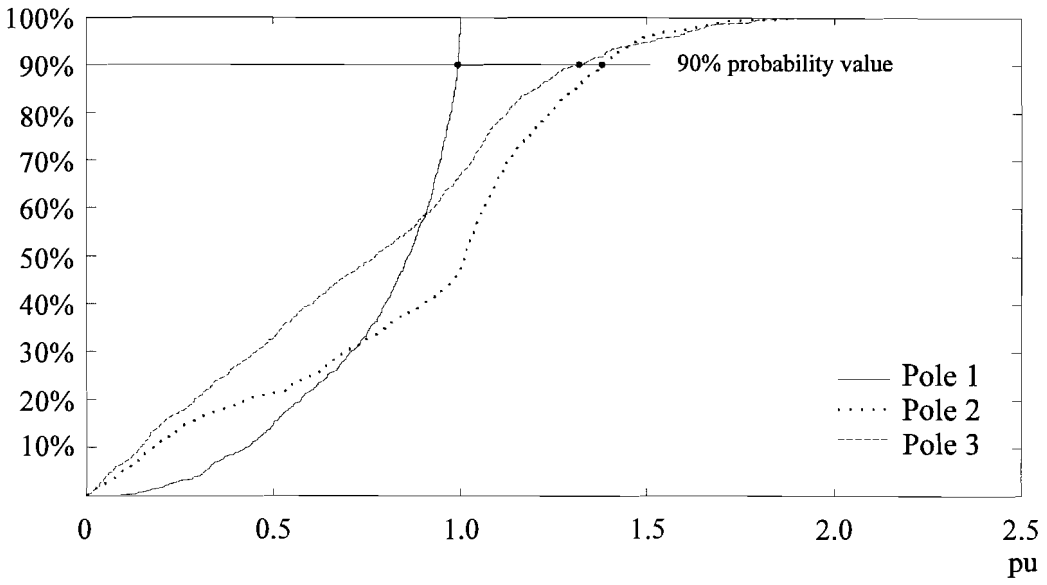

Fig 2.8: Probability of the height of the wavefronts

Pole 1 The maximum value of the height of the voltage jump is 1 pu as predicted. The height of the first pole to break down is near 1 pu because of the variance in F_k and the random closing angle allowing other phases to break down before phase 1. An example is shown in figure 2.5 where phase 2 is the first pole to break down.

Pole 2 The theoretical maximum of pole 2 (2.3 pu) is hardly reached since the gap will breakdown before the transient has reached its maximum and/or the difference between the two phases of $\sqrt{3}$ is not present. The order of phases to breakdown is still random.

Pole 3 There is only one possible phase left to break down. This results in a wider spread of possible heights of the third breakdown voltage.

When the transient frequency increases, with shorter cables (C<) and/or greater power (L<), we witnessed a right shift of the probability graph. This phenomenon is shown in figure 2.9, keeping the other input parameters equal to the ones used in figure 2.8.

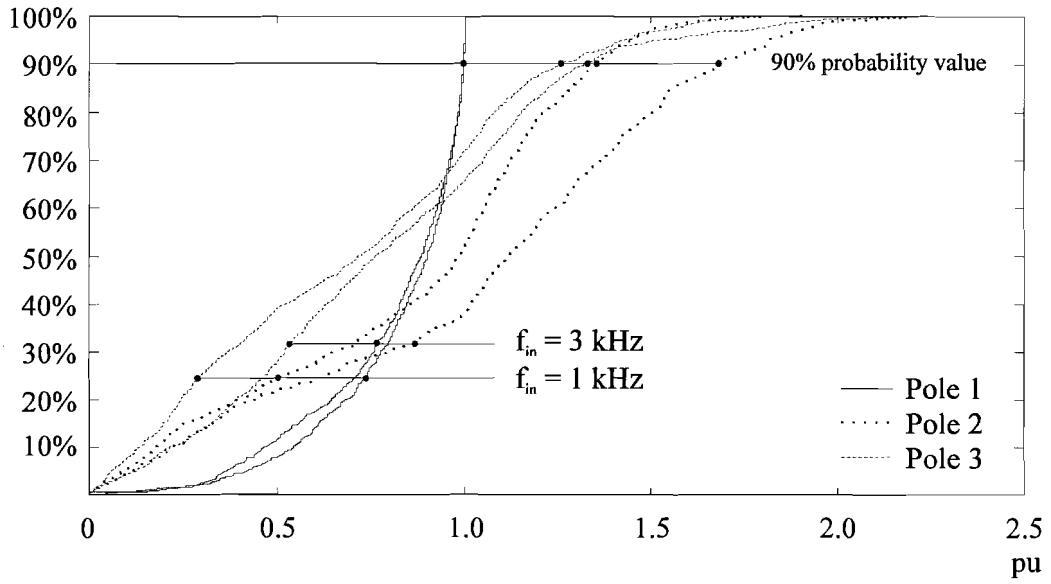

Fig 2.9: Probability of the height of the wavefronts for two different f_{in}'s

As can be seen there is little change in the probability of pole 1, since this is not related to the transient frequency (f_{in} or ω_{in}). The right shift of the other two poles can be explained with figure 2.10. Increasing f_{in} results in a higher overvoltage in a shorter time and thus reaching the higher breakdown value of the other pole, and for the other way around the breakdown value will have more time to decrease with lower f_{in}. Figure 2.10 with it's values is only valid with the closing speed of the circuit breaker is 1 m/s (F_k = 10) and the pole delay time is 200 µs, other values will produce another probability graph. The crosses resembles the value at which the second pole would breakdown.

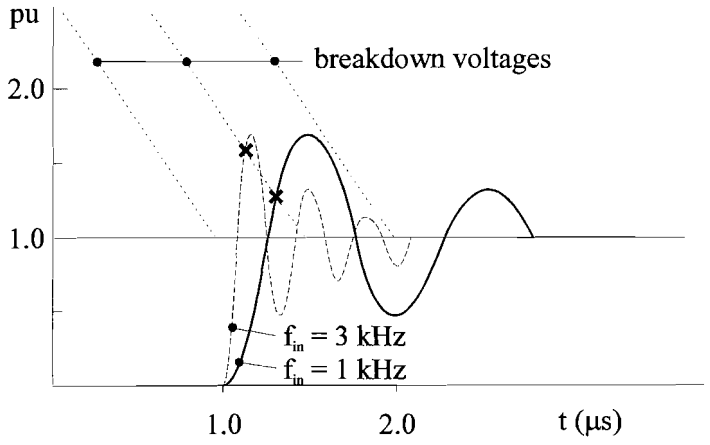

Fig 2.10: Influence of the transient frequency on the height of the switching surges

For the determination of the severity of steep wavefront when switching in, the 90% probability value will be taken as the value to consider. To investigate the influences (with f_{in} = 1kHz) of the different parameters the 90% probability value was taken when varying one of the parameters, t_{d1}, F_k and σ.

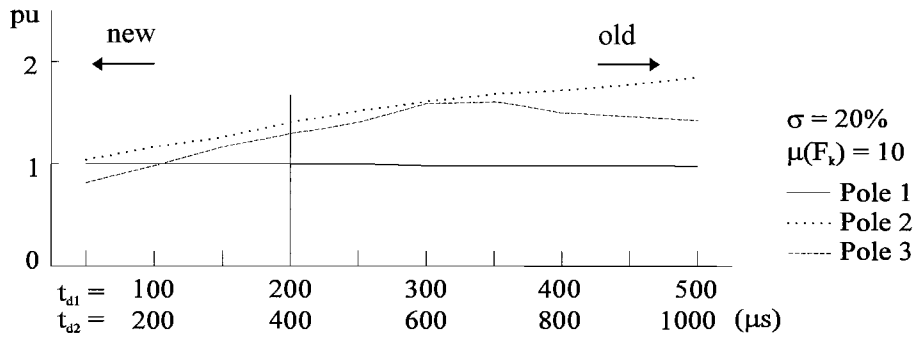

Fig 2.11: 90% probability values for $t_{d1} \in (50,500)$ μs

When increasing the pole delay time one can see an increase in the 90% probability value for pole 2 and in less extend also for pole 3. This corresponds to ageing of the mechanical part (looser mechanism) of the circuit breaker.

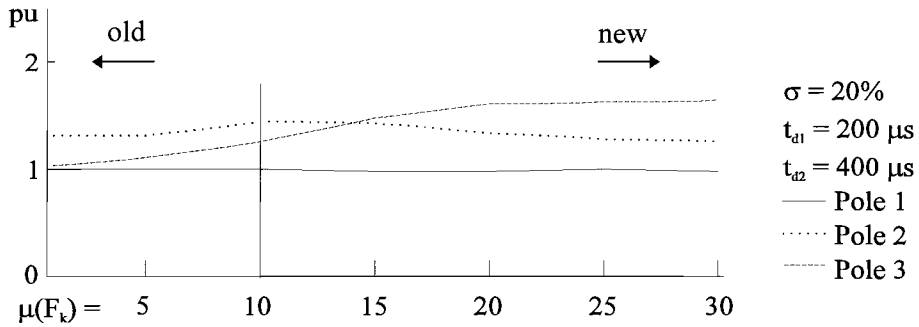

Fig 2.12: 90% probability values for $\mu(F_k) \in (1,30)$

The fact that theoretically the second pole is the one with the highest possible voltage jump, doesn't mean that this happens for all real problems, as can be witnessed in figure 2.12. The factor F_k corresponds to the behaviour of the insulating mechanism.

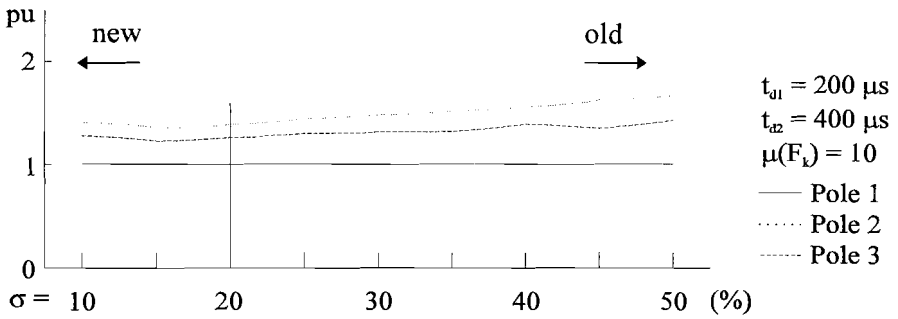

Fig 2.13: 90% probability values for σ ∈ (10,50) %

A greater variance has little influence on the 90% probability value for the three poles.

In the program each motor will be calculated with the Monte Carlo method to determine the probability of the height of the wavefront. In the advanced input menu one can change the parameters for fine tuning of the calculations.

2.2 Switching off

The influence of switching off a motor on the electric stress of the motor windings has been found minor compared to switching in. This is due to the fact that the steep wavefronts needed for the electric stress have, however potentially higher, a probability of occurrence that is much less than the (lower) making transients [2.3 , 2.4]. Especially when not switching off locked motors. Therefore only a compact explanation is given of the phenomena caused by switching off.

When switching off a motor there are three different states a motor can be in. The difference for the height of the transient recovery voltage can be found in the value of the current and the cos φ of the three different states:

- starting state: $\cos \varphi \approx 0.1$ $I \approx 6\ I_{nom}$ worst case
- no-load state: $\cos \varphi \approx 0.1$ $I \ll I_{nom}$
- full-load state: $\cos \varphi \approx 0.9$ $I \approx I_{nom}$ most common case

After opening phase 1 and interruption of the current, the remaining energy in the circuit will be transferred between the inductance and the capacitors, thus creating a transient phenomenon. Besides the overshoot of this transient recovery voltage (TRV), the voltage on the starpoint of the motor will become -0.5 u_1 (the sum of u_2 and u_3), this will result in an increased static voltage across the switch of 1.5 u_1.
To explain the TRV over the switch we will use a single phase circuit with a supply voltage u_n. This circuit is an equivalent of the single phase circuit in figure 2.3 were the surge is replaced by a supply voltage with an opening switch [2.5].

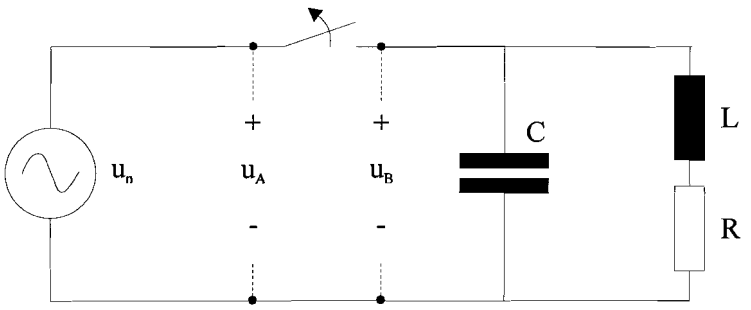

Fig 2.14: Single phase circuit

With : u_n = 1.5 times single phase supply voltage (See figure 2.3)
L = 1.5 times single phase motor inductance
R = 1.5 times single phase motor resistance
C = 2/3 times phase to phase cable cap. + 2 times phase to ground cable capacitance

For the theoretical consideration of the switching off in chapter 2.2.1 till 2.2.3, figure 2.14 with it's definitions will be mandatory.

The energy transfer creating the TRV is given by the static energy relation:

$$\tfrac{1}{2}LI^2 = \tfrac{1}{2}CU^2 \tag{2.15}$$

The transfer of magnetic energy in the coil to electric energy in the capacitor happens both on the supply side of the circuit-breaker as on the load side. This results in a TRV containing three frequencies; one defined by the load side and one defined by the supply side and the 50 Hz of the supply voltage. The 50 Hz is considered constant compared to the other frequency. The influence of the supply side is negligible since this transient amplitude in worst case is only 10% of the load side transient amplitude as stated in motor-switching test circuit of IEC 17A(S). Calculation with the laplacian method gives the $TRV(t) = u_A(t) - u_B(t)$ (see Appendix I).

The TRV itself is not the main cause for stress on the first turns of the motor, since the front is not steep enough and the TRV will distribute homogeneously over the motor windings. The height of the TRV can cause a breakdown and thus creating the steep wavefront which is the cause for the stress encountered on the insulation when switching off a motor.

The TRV consists of an energy flow between the motor inductance and the capacitor back and forth with an overshoot created by a voltage jump in a R,L,C-circuit. To include the latter the transient recovery voltage has to be calculated with the laplacian method. For the approximation of the height of the TRV when switching off a motor we will only consider the energy method. With the energy method we can calculate the height of the TRV without damping. For the time dependent TRV we refer to appendix I.

For the estimation of the height of the overvoltage (the first peak of the transient phenomenon) with the energy method we make the following assumptions:

- everything is calculated per unit unless otherwise mentioned
- damping of the transient phenomenon of the energy flow is not considered

With both assumptions the overvoltage over the switch is calculated (TRV) and the overvoltage over the motor for all three states.

2.2.1 Starting state

- $\cos\varphi \approx 0.1$
- the arc has enough energy to sustain itself

When opening the switch there will be an arc between the contacts, for the first current zero's an immediate reignition will occur. When the gap is large enough to withstand the TRV, a transient phenomenon will begin near the current zero. The current value on the moment of withstanding the voltage over the gap is called the chopping current (I_{chop}). Together with the energy relation in equation 2.15 we can calculate the overvoltage over the load side (u_B) as a result from the energy left in the load side:

$$\begin{aligned} &\tfrac{1}{2}C\,\hat{u}_B{}^2 = \tfrac{1}{2}LI_{chop}{}^2 + \tfrac{1}{2}C\left(u_n(0)\right)^2 \quad \Rightarrow \\ &\hat{u}_B = \sqrt{U^2 + I_{chop}{}^2 Z_0{}^2} \end{aligned} \tag{2.16}$$

and:

$U = u_n(0)$

Z_0 = characteristic impedance

Since the frequency of this transient phenomenon is much higher as the frequency of the supply voltage the maximum overvoltage over the circuit breaker (U_{TRV}) is:

$$\hat{u}_{TRV} = u_A - \left(-\hat{u}_B\right) = U + \sqrt{U^2 + I_{chop}{}^2 Z_0{}^2} \tag{2.17}$$

And the maximum overvoltage over the motor is:

$$\hat{u}_B = \sqrt{U^2 + I_{chop}{}^2 Z_0{}^2} \tag{2.18}$$

2.2.2 No-load state

- $\cos\varphi \approx 0.1$
- the arc hasn't enough energy to sustain itself

Since the arc can not sustain itself, the breakdown doesn't need to be near the current zero and thus $u_B(0)$ can be high. Instead of the I_{chop} we will have $i(0)=I_0$. The power factor being the same one would expect the same overvoltage as in the starting state. However the motor is running at its nominal number of revolution and will induce a induction voltage to counter-act the descending flux in the motor. This results in keeping u_B at u_A, making the TRV:

$$\hat{u}_{TRV} = I_0 Z_0 \tag{2.19}$$

And the maximum overvoltage over the motor is:

$$\hat{u}_B = u_B(0) + I_0 Z_0 \tag{2.20}$$

2.2.3 Full-load state

- $\cos\varphi \approx 0.9$
- the arc has enough energy to sustain itself

Both the voltage and the current will break near the current zero and only the energy in the coil is a factor of importance, making the u_{TRV} and the $\hat{u}_B$ the same as in the no-load state:

$$\hat{u}_{TRV} = I_0 Z_0 \tag{2.21}$$

$$\hat{u}_B = u_B(0) + I_0 Z_0 \tag{2.22}$$

Making the difference between the no-load and the full-load state the powerfactor, the value of the current at interruption and thus the low value $u_B(0)$ will have.

2.2.4 Breaking current and the characteristic impedance

The multiplication of the breaking current and the characteristic impedance gives the I_0Z_0. We will calculate the characteristic impedance (Z_0) as function of the power of the motor with the next parameters (per unit). The calculated resistance and inductance will be the single phase values. For transforming them into the single phase circuit components a multiplication factor as defined with figure 2.14 has to be used.

- $S = \sqrt{3} \cdot U_{line} \cdot I_{line}$; $I_{line} = I_{phase}$
- $U_{line} = \sqrt{3} \cdot U_{phase}$; $I_{phase} = S / \sqrt{3} \cdot U_{line}$
- $P = S \cdot \cos\varphi$

Depending only on the used supply voltage and the power of the motor and its power factor we can calculate the resistance and inductance of the motors:

$$\left.\begin{aligned} \cos\varphi &= \frac{R}{\sqrt{R^2 + \omega^2 L^2}} \\ I_{phase} &= \frac{U_{phase}}{\sqrt{R^2 + \omega^2 L^2}} \end{aligned}\right\} \quad \cos\varphi = \frac{R \cdot I_{phase}}{U_{phase}} = \frac{R \cdot S}{U_{line}^2} \qquad R = \frac{U_{line}^2 \cos\varphi}{S} = \frac{X}{S} \tag{2.23}$$

$$\left.\begin{aligned} \sin\varphi &= \frac{\omega L}{\sqrt{R^2 + \omega^2 L^2}} \\ \sqrt{R^2 + \omega^2 L^2} &= \frac{U_{phase}}{I_{phase}} = Z_{motor} \end{aligned}\right\} \quad \omega L = \sin\varphi \cdot \frac{U_{phase}}{I_{phase}} \qquad L = \frac{U_{line}^2 \sqrt{1 - \cos^2\varphi}}{\omega S} = \frac{X'}{S} \tag{2.24}$$

For a 3 kV motor one can calculate the characteristic impedance for the 50Hz as a function of the power of the motor according to [2.6], which is illustrated in appendix II, and with equation 2.24 obtaining the internal capacitance C_i.

$$Z_i = \sqrt{\frac{L}{C_i}} = \sqrt{\frac{X'}{S \cdot C_i}} = 8.27 \cdot 10^5 \, S^{-1/2} \quad \Rightarrow \quad C_i = \frac{X'}{Z_i^2} \tag{2.25}$$

The internal capacitance (C_i) calculated with equation 2.25 will be added with the total cable capacitance (C_C) for the single phase circuit. Including the multiplication factors the characteristic impedance is:

$$Z_0 = \sqrt{\frac{1\frac{1}{2}L}{1\frac{1}{2}C_i + C_C}} = \sqrt{\frac{1\frac{1}{2}X'}{S \cdot \left(1\frac{1}{2}C_i + \ell \cdot (\frac{2}{3}C_{phase} + 2C_{ground})\right)}} \tag{2.26}$$

The prospective overvoltages at load side are calculated as a function of the length of the cable and the power of the motor in full load state for $I_0 = 2A$ and $U_{line} = 3kV$. The value of I_0 is considered a common value, but can be higher. In the program, under the advanced input menu, this value can be changed.

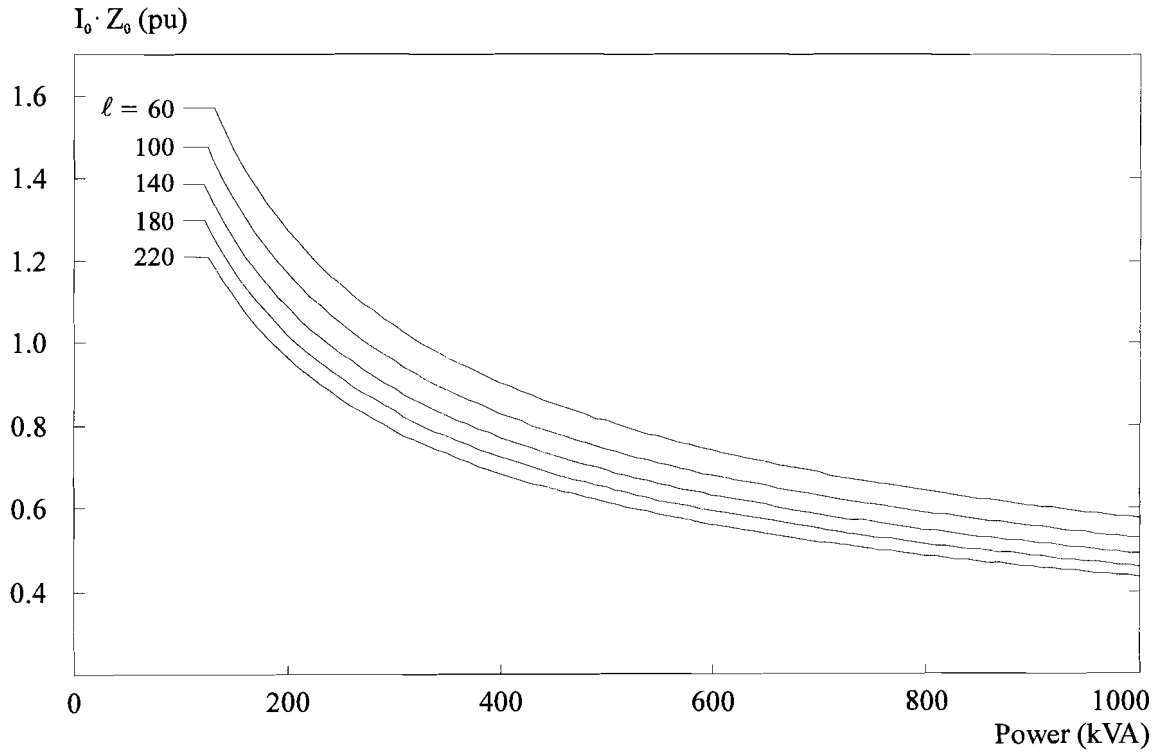

Fig 2.15: Overvoltages caused by the chopping of the circuit-breaker in the coil for different cable lengths.

If the prospective overvoltage exceeds the breakdown value of the gap a reignition will occur with a steep wavefront and causing stress on the interturn insulation of the motor. For a statistical examination of this stress one has to consider the probability of reignition, included with the state the motor is in. For the real value of the height of the surge, $\hat{u}_{TRV}$ has to be considered. As can be seen the worst case with $I_0 \cdot Z_0$ is found with small motors (larger Z_0) and short cables (smaller C_C). For the actual value of the transient recovery voltage one should use the equations given in the sections keeping in mind the definitions stated in figure 2.14.

3 Propagation of the wavefronts

We know that a steep wavefront is created when switching. In this section the behaviour of this wavefront will be discussed in an single phase version of the electrical system [3.1].

3.1 Reflections of the wavefronts

Characteristic impedance variations are essential in wavefront propagation in electrical systems. For the theory on reflections in loss free transmission lines there are two parts to consider.

- Injection of a wavefront.
- Reflection and refraction of a wavefront.

Injection of a wavefront.

When switching on a voltage jump there will be an injection of a wavefront. This will result into two wavefronts; one going to the left and one going to the right. With an impedance of Z_1 on the left and an impedance of Z_2 on the right, the ratio of both wavefronts can be obtained according to equation 3.1.

$$U_L = \frac{Z_1}{Z_1 + Z_2} U_F \quad ; \quad U_R = \frac{Z_2}{Z_1 + Z_2} U_F \tag{3.1}$$

U_L = height wavefront to the left
U_R = height wavefront to the right
U_F = height wavefront

Reflection and refraction of a wavefront

When a wavefront is approaching a jump in the impedance a part of the wavefront will continue into the transmission line (refraction) and the rest will reflect back into the transmission line (reflection). For a wavefront traveling from Z_1 to Z_2 the coefficient for the reflection (r) is given by:

$$r = \frac{Z_2 - Z_1}{Z_1 + Z_2} \tag{3.2}$$

For a wavefront with a height of U_F the reflection and the refraction are given by:

$$\begin{aligned} &\text{reflection:} \quad u'' = r \cdot U_F \\ &\text{refraction:} \quad u' = (1 + r) \cdot U_F \end{aligned} \tag{3.3}$$

With these formulas we can construct the reflections witnessed when switching. We will simplify the electrical system according to figure 3.1 for a better understanding.

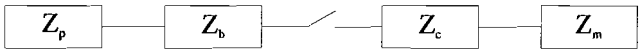

Fig 3.1: Simplified impedance circuit.

With : Z_p = impedance of parallel cables Z_b = impedance of the busbar
Z_c = impedance of the cable Z_m = impedance of the motor

For the simplified circuit the following construction of the reflecting wavefronts is made. This is done for the busbar side and for the behaviour at the motor side. With figure 3.2 we will simulate the closing of pole 2 (supplied from u_2 = 1pu) when the motorvoltage is already energized from u_1 = -0.5 pu.

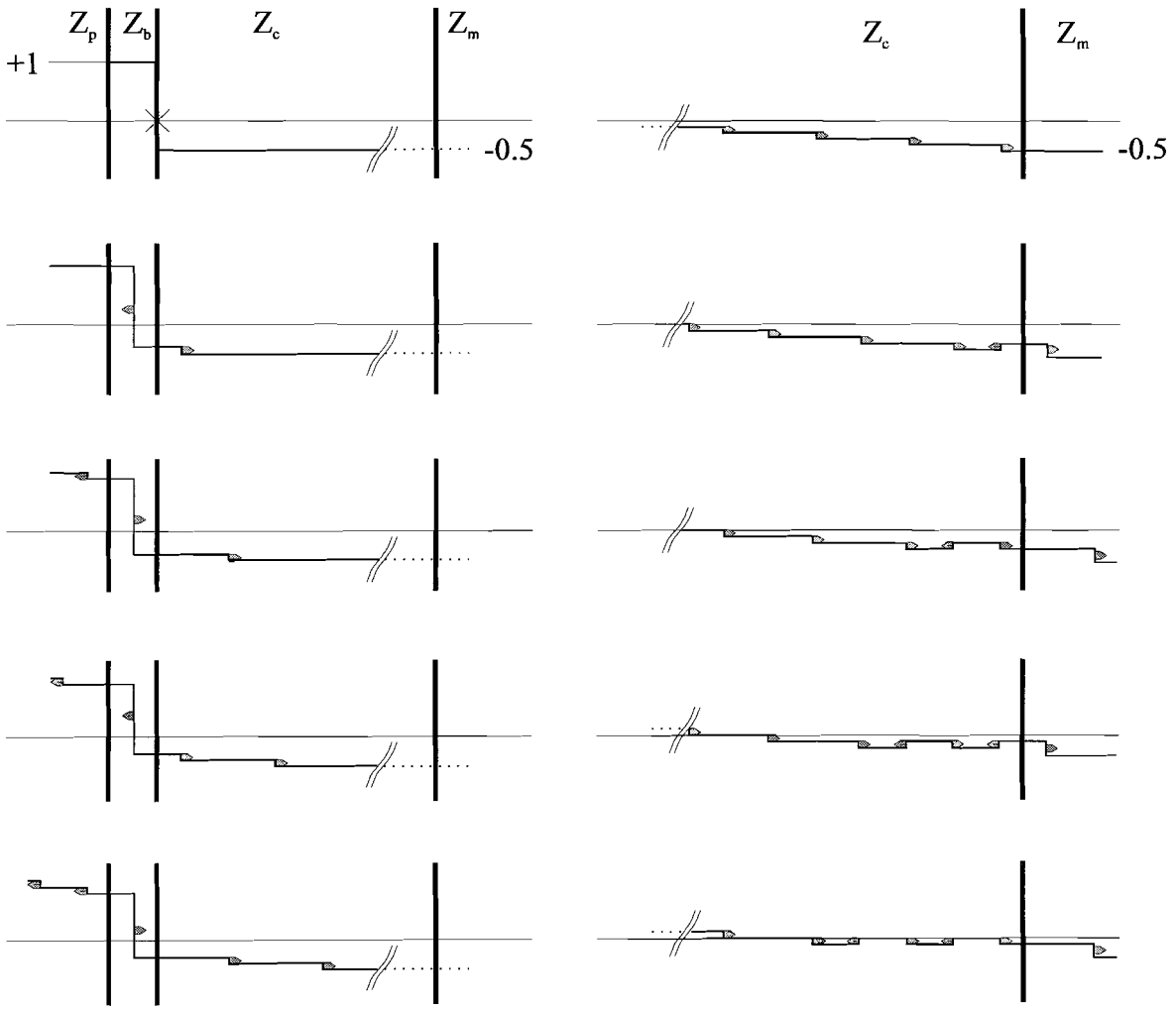

busbar side *motor side*

Fig 3.2: Construction of the wavefronts when switching

At the busbar side we can clearly see the effect of varying impedance's that results in the height of the wavefronts going into the cable and the loss of wavefront into the parallel cables. These effects will have a great influence in the resulting wavefront at the motor side.

At the motor side we can see the effect of a wavefront reflecting at an open end and doubling its voltage jump. (In this drawing the impedance of the motor is taken as an open end, $Z_0 = \infty$. With a motor some refraction will occur thus limiting the doubling of the voltage on the motor side.)

We can construct the wavefront on the motor side with these phenomena. By using the formulas for each impedance variation, with the following definitions :

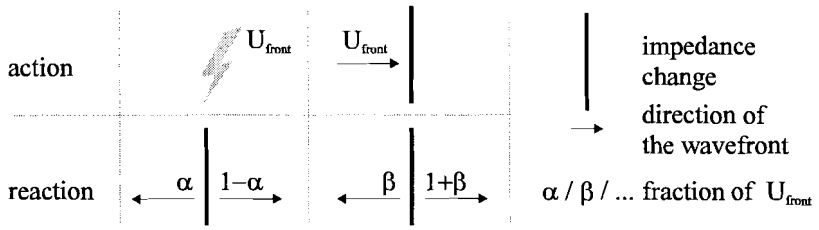

Fig 3.3: Definitions used for calculating the wavefront at the motor side

By constructing the equations for each reflection and refraction (Eq. 3.3) of the wavefronts we will get a mathematical series.

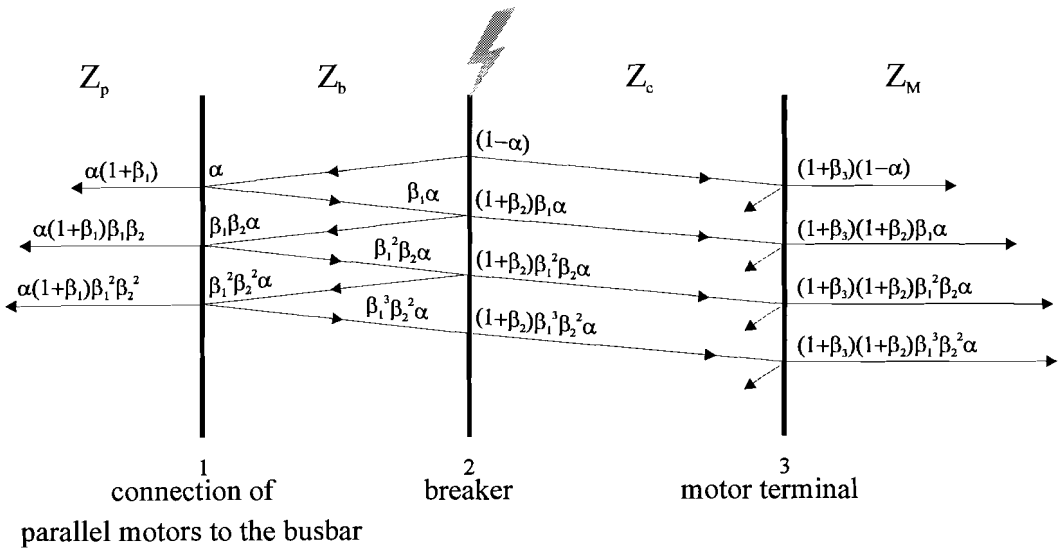

Taking into consideration the travel time τ_b of the busbar and τ_c of the cable, the voltage with the influence of the reflections in the transmission lines at the motor terminal (U_m) is given by the mathematical series (with a wavefront of U_F):

$$U_m(\tau_c + 2n\tau_b) = U_m(\tau_c) + \alpha \cdot (1+\beta_2) \cdot (1+\beta_3) \cdot \left[\frac{\beta_1 \left(1 - (\beta_1\beta_2)^n\right)}{1-\beta_1\beta_2} \right] \cdot U_F \qquad (3.4)$$

And: $U_m(\tau_c) = U_m(0) - (1-\alpha)(1+\beta_3) U_F$

A simulation has been made for equation 3.4 with the following impedance's: $Z_p = 30$; $Z_b = 300$; $Z_c = 30$ and $Z_m = 3000\ \Omega$ and $U_{m0} = -0.5$ pu.

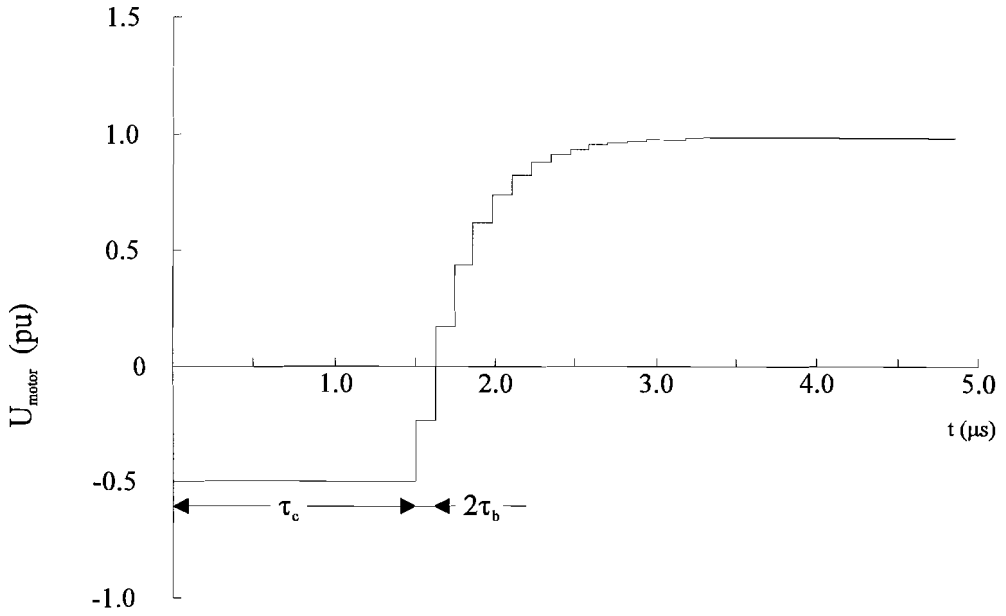

Fig 3.4: Simulation of the overvoltage over the motor

If the voltage jump of 1.5 pu went only to the motor side and had a total reflection there (r = 1; Eq 3.2) the voltage over the motor would have changed from -0.5 to (-0.5 + 2 x 1.5) = 2.5 pu (Eq 3.3) causing a voltage jump of 3 pu over the motor. Due to losses in the parallel circuit this is reduced to a voltage jump of 1.5 pu (with these impedance's). The steep value of this voltage jump is also flattened by the reflections in the bus. The effect of the voltage jump on the distribution over the turns of the coil is thus reduced, without taking into account the effects of the cable.

3.2 Propagation in cables

Calculations on cables were done with the PC-version of the electromagnetic transient program (EMTP), known as ATP. For the calculations on propagation in cables we used a NEN 3172-GPLK / 10 kV 3 x 16 cable. Measurements for this cable were done [3.2] so our calculations could be checked.

In order to use ATP for cables, we had to determine the cable constants needed for calculations. These constants can be calculated from the cable dimensions and knowledge on the materials used. Since the frequency witnessed when switching was in the same order as lightning surges (from a mathematical point of view) we used the CABLE CONSTANTS procedure within ATP [3.3].

From table 8 of NEN 3172 the following dimensions were offered for a 3 phase 16 mm^2 cable:

- isolation thickness 5.5 mm (core - core) paper/oil
  5.5 mm (core - pipe)
- pipe thickness 1.9 mm lead

Converting these dimensions for ATP use gave us the schematic drawing of the cable (figure 3.5), which we used for the CABLE CONSTANTS procedure (Appendix III).

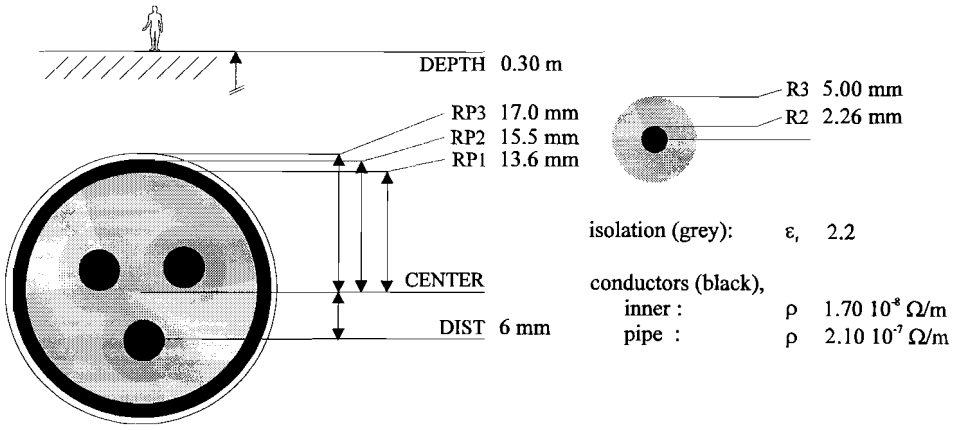

Fig 3.5: Cable dimensions used for ATP.

After obtaining the cable-constants for ATP, we connected a ramp source to one phase. To prevent ungrounded ends, or loose circuits, all other cable ends were connected to ground with a resistor of 1 MΩ. Results of the calculation with ATP (source code in appendix III) are given in figure 3.6.

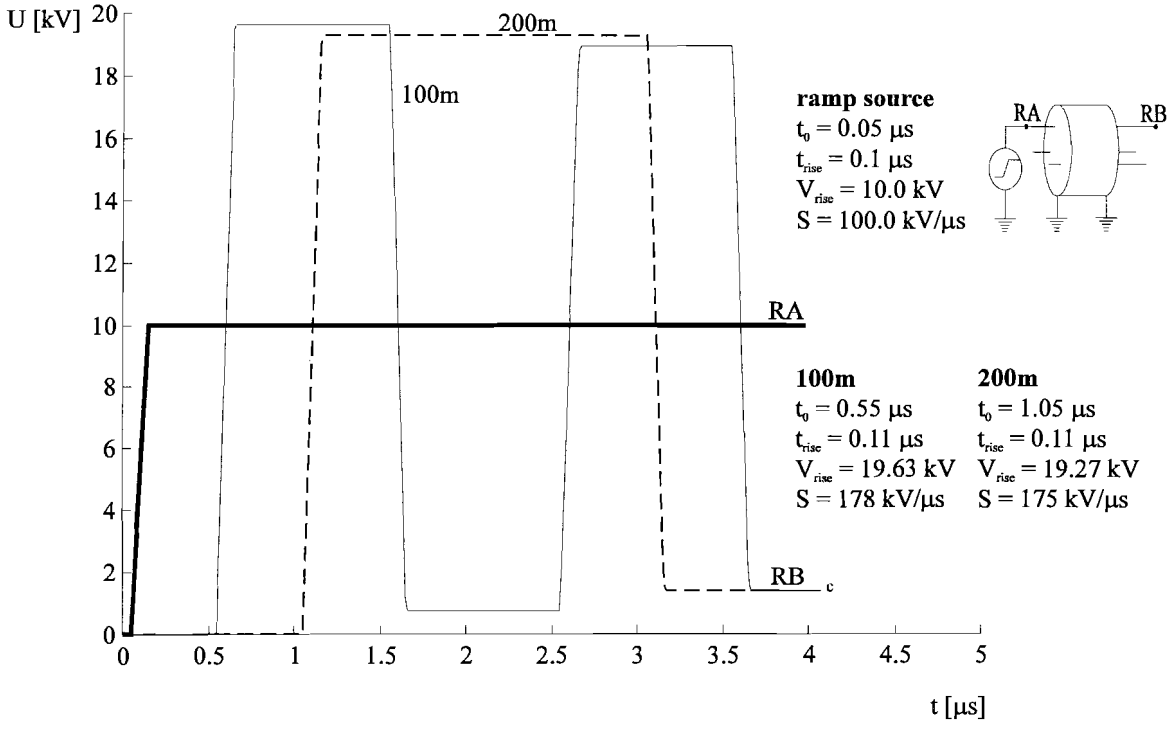

Fig 3.6: Results of the ATP calculation for cables

For both the calculations and the measurements [3.2] on GPLK-cables with a 10 kV ramp-source the results show little influence of the cable on the first wavefronts. One can conclude that the cable will only have an influence on the overvoltages with the cable-capacitance in the transient phenomena. The cable capacitance will vary according to the type of cable used; either paper-oil or XLPE cables.

3.3 NMA-method

For calculations of the transient phenomenon a dedicated program is developed, following the NMA method, as used eg. for EMTP. Doing this in Turbo Pascal 7.0 will result in increased flexibility for our electric setup possibilities and decreased computation time. Also the use of only one environment for programming has been a main factor.

The "Nodal Mode Admittance"-method can only be used with discrete network elements. The used formulas for the different network elements will be mentioned here [3.4].

Loss free transmission lines

Since the influence of the cable can be simulated by a loss free transmission line we can use the Bergeron-Schneider model for simulation.

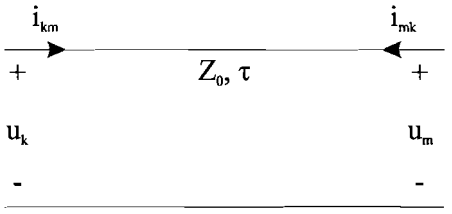

Fig 3.7: Bergeron-Schneider model for loss free transmission lines

With:

$$i_{km}(t) = \frac{1}{Z_0}\left[u_k(t) - u_m(t-\tau)\right] - i_{mk}(t-\tau)$$
$$i_{mk}(t) = \frac{1}{Z_0}\left[u_m(t) - u_k(t-\tau)\right] - i_{km}(t-\tau) \qquad (3.5)$$

Z_0 = characteristic impedance of the transmission line
τ = travel time

Concentrated coil

By using the trapezium rule for integration we can rewrite the differential equation for the current through a coil and thus obtain the lineair equations needed.

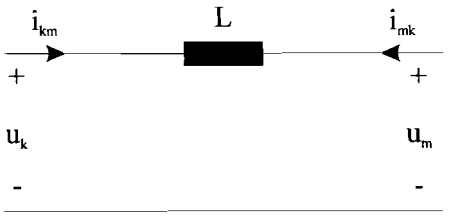

Fig 3.8: Concentrated coil

Differential equation:

$$u_k - u_m = L\frac{di_{km}}{dt} \quad \Rightarrow \quad i_{km} = i_{km}(t-\Delta t) + \frac{1}{L}\int_{t-\Delta t}^{t}(u_k - u_m)dt \tag{3.6}$$

Trapezoidrule:

$$\int_{t-\Delta t}^{t} f(t)dt = \tfrac{1}{2}\Delta t\left[f(t-\Delta t) + f(t)\right] \tag{3.7}$$

Combining equation 3.6 and 3.7 gives:

$$\begin{aligned} i_{km}(t) &= \frac{\Delta t}{2L}\left[u_k(t) - u_m(t)\right] + i_{km}(t-\Delta t) + \frac{\Delta t}{2L}\left[u_k(t-\Delta t) - u_m(t-\Delta t)\right] \\ i_{mk}(t) &= \frac{\Delta t}{2L}\left[u_m(t) - u_k(t)\right] + i_{mk}(t-\Delta t) + \frac{\Delta t}{2L}\left[u_m(t-\Delta t) - u_k(t-\Delta t)\right] \end{aligned} \tag{3.8}$$

Concentrated capacitance

Combining the trapezoid rule for integration and the differential equation for the capacitor we can obtain the equations needed with a capacitance.

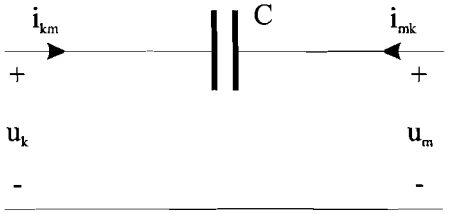

Fig 3.9: Concentrated capacitance

Differential equation for the capacitor:

$$i_{km} = C\frac{du}{dt} \quad \Rightarrow \quad u_k(t) - u_m(t) = \frac{1}{C}\int_{t-\Delta t}^{t} i_{km}(t)dt + u_k(t-\Delta t) - u_m(t-\Delta t) \tag{3.9}$$

By combining equation 3.9 and using the trapezium rule we can obtain the following equations:

$$\begin{aligned} i_{km}(t) &= \frac{2C}{\Delta t}\left[u_k(t) - u_m(t)\right] - i_{km}(t-\Delta t) - \frac{2C}{\Delta t}\left[u_k(t-\Delta t) - u_m(t-\Delta t)\right] \\ i_{mk}(t) &= \frac{2C}{\Delta t}\left[u_m(t) - u_k(t)\right] - i_{mk}(t-\Delta t) - \frac{2C}{\Delta t}\left[u_m(t-\Delta t) - u_k(t-\Delta t)\right] \end{aligned} \tag{3.10}$$

Concentrated resistor

For a resistor the lineair equations are:

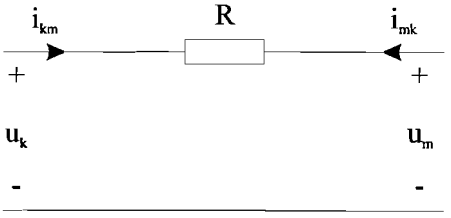

Fig 3.10: Concentrated resistor

$$i_{km}(t) = \frac{1}{R}\left[u_k(t) - u_m(t)\right]$$
$$i_{mk}(t) = \frac{1}{R}\left[u_m(t) - u_k(t)\right] \qquad (3.11)$$

3.4 Circuit model

By using the formulas for the currents every network can be calculated with Kirchoff's law. This results in a n x n matrix (A) and a vector containing the node voltages ($\underline{x}$) on a time t, which are calculated from the values of past voltages and currents ($u_m(t-\tau)$ and $i_{mk}(t-\tau)$).

$$A \cdot \underline{x} = \underline{b} \qquad (3.12)$$

This vector is solved with a numerical procedure in Turbo Pascal 7.0 (SLEGSY) obtained from [3.5].

Some simplifications were made in our circuit to improve calculation time. These simplifications consists of:

- Surge is modeled by a ramp source between cable and busbar circuit.
- Cables to the left and right of the motor under consideration are replaced by a resistor, this will give the same result on the wavefront on the motor. The reflection of those cables is neglected.
- Other parallel cables to the left and right are replaced by one resistor with the same value as all parallel cables would give. This can be done since the refraction coefficient in each busbar section connected to a cable is ca. 0.17 (see equation 3.3). After two or three refraction's the influence of the other parallel cables on the waveform going to the motor terminal is drastically decreased.
- The motor is replaced with a resistor, representing the motor impedance. This is done to split the calculation into two pieces. Later the motor model will be implemented into the program.
- Only left to the motor there is a possibility to insert a compensation capacitor.

Simulations with MicroCap IV were done to confirm these simplifications.

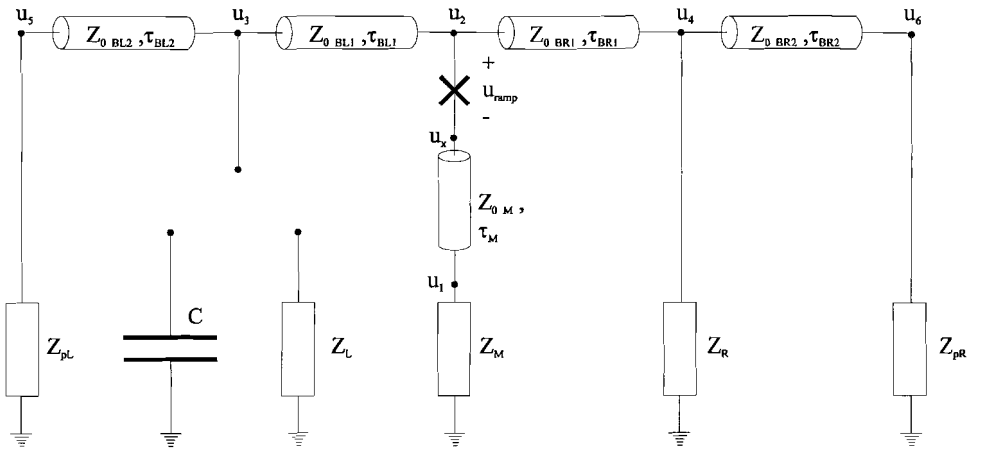

Fig 3.11: Circuit used for calculation with the NMA-method.

Equation 3.12 is now constructed on the following manner:

Node 1: $i_{1x} + i_{10} = 0$ (3.13)

$$\left.\begin{aligned} i_{1x}(t) &= \frac{1}{Z_{0M}}\left[u_1(t) - u_x(t-\tau_M)\right] - i_{x1}(t-\tau_M) \\ i_{10}(t) &= \frac{1}{Z_M}\left[u_1(t)\right] \\ u_x(t) &= u_2(t) - U_{ramp}(t) \end{aligned}\right\} \quad \left[\frac{1}{Z_{0M}} + \frac{1}{Z_M}\right]\cdot u_1(t) = \frac{1}{Z_{0M}}\left[u_2(t-\tau_M) - U_{ramp}(t-\tau_M)\right] + i_{x1}(t-\tau_M)$$

Node 2: $i_{x1} + i_{23} + i_{24} = 0$ (3.14)

$$\left.\begin{aligned} i_{x1}(t) &= \frac{1}{Z_{0M}}\left[u_x(t) - u_1(t-\tau_M)\right] - i_{1x}(t-\tau_M) \\ i_{23}(t) &= \frac{1}{Z_{0_{BL1}}}\left[u_2(t) - u_3(t-\tau_{BL2})\right] - i_{32}(t-\tau_{BL2}) \\ i_{24}(t) &= \frac{1}{Z_{0_{BR1}}}\left[u_2(t) - u_4(t-\tau_{BR2})\right] - i_{42}(t-\tau_{BR2}) \end{aligned}\right\} \quad \left[\frac{1}{Z_{0_{BL1}}} + \frac{1}{Z_{0_{BR1}}} + \frac{1}{Z_{0M}}\right]\cdot u_2(t) = \frac{1}{Z_{0M}}\left[u_{ramp}(t) + u_2(t-\tau_M)\right] + i_{1x}(t-\tau_M) + \frac{1}{Z_{0_{BL1}}} u_3(t-\tau_{BL1}) + i_{32}(t-\tau_{BL1}) + \frac{1}{Z_{0_{BR1}}} u_4(t-\tau_{BR1}) + i_{42}(t-\tau_{BR1})$$

By doing this for all nodes we can create the following matrix to solve equation 3.12.

$$A = \begin{bmatrix} \frac{1}{Z_{0_M}} + \frac{1}{Z_M} & 0 & 0 & 0 & 0 & 0 \\ 0 & \frac{1}{Z_{0_{BL1}}} + \frac{1}{Z_{0_{BR1}}} + \frac{1}{Z_{0_M}} & 0 & 0 & 0 & 0 \\ 0 & 0 & \frac{1}{Z_{0_{BL1}}} + \frac{1}{Z_{0_{BL2}}} + (1-\alpha)\frac{1}{Z_L} + \alpha\frac{2C}{\Delta t} & 0 & 0 & 0 \\ 0 & 0 & 0 & \frac{1}{Z_{0_{BR1}}} + \frac{1}{Z_{0_{BR2}}} + \frac{1}{Z_R} & 0 & 0 \\ 0 & 0 & 0 & 0 & \frac{1}{Z_{0_{BL2}}} + \frac{1}{Z_{pL}} & 0 \\ 0 & 0 & 0 & 0 & 0 & \frac{1}{Z_{0_{BR2}}} + \frac{1}{Z_{pR}} \end{bmatrix} \quad (3.15)$$

$$x = [\, u_1\ u_2\ u_3\ u_4\ u_5\ u_6 \,] \quad (3.16)$$

and,

$$b = \begin{bmatrix} \frac{1}{Z_{0_M}}\left[u_2(t-\tau_M) - U_{ramp}(t-\tau_M)\right] + i_{x1}(t-\tau_M) \\ \frac{1}{Z_{0_M}}\left[U_{ramp}(t) + u_1(t-\tau_M)\right] + i_{1x}(t-\tau_M) + \frac{1}{Z_{0_{BL1}}}u_3(t-\tau_{BL1}) + i_{32}(t-\tau_{BL1}) + \frac{1}{Z_{0_{BR1}}}u_4(t-\tau_{BR1}) + i_{42}(t-\tau_{BR1}) \\ \frac{1}{Z_{0_{BL1}}}u_2(t-\tau_{BL1}) + i_{23}(t-\tau_{BL1}) + \frac{1}{Z_{0_{BL2}}}u_5(t-\tau_{BL2}) + i_{53}(t-\tau_{BL2}) + \alpha\left(\frac{2C}{\Delta t}u_3(t-\Delta t) + i_{30}(t-\Delta t)\right) \\ \frac{1}{Z_{0_{BR1}}}u_2(t-\tau_{BR1}) + i_{24}(t-\tau_{BR1}) + \frac{1}{Z_{0_{BR2}}}u_6(t-\tau_{BR2}) + i_{64}(t-\tau_{BR2}) \\ \frac{1}{Z_{0_{BL2}}}u_3(t-\tau_{BL2}) + i_{35}(t-\tau_{BL2}) \\ \frac{1}{Z_{0_{BR2}}}u_4(t-\tau_{BR2}) + i_{46}(t-\tau_{BR2}) \end{bmatrix} \quad (3.17)$$

In equation 3.15 and 3.17, α indicates the use of a cable to the left ($\alpha = 0$) or the use of a compensation capacitor to the left ($\alpha = 1$)

3.5 Influences of the setup of the electrical system on the wavefront.

In this section some results of calculations with the NMA-method on different setups will be presented. All calculations were done with two different rise times for the ramp source. The t_{rise}=10 ns represents a vacuum switch and the t_{rise}=0.1μs represents a oilbreaker (see Appendix IV).

The standard configuration used is:

- busbar section length of 1 m
- cable length of 40 m
- cable impedance of 30 Ω
- busbar impedance of 300 Ω
- parallel cable impedance of 30 Ω
- motor impedance of 3000 Ω
- amplitude of ramp source from 0 on t = 0 to 1 on t = t_{rise}

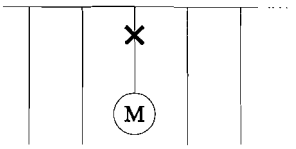

The influence of the busbar section length.

Since the greatest part of the wavefront will first go into the busbar, the length and thus the travel time of the busbar has great importance on the wavefront on the motor side.

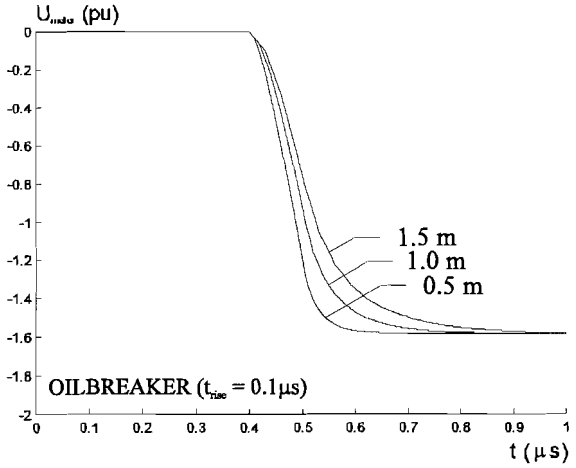

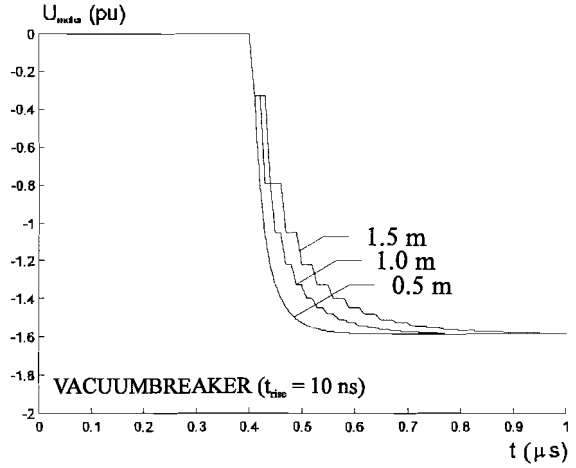

On can see that not the rise time of the ramp source is the main factor, but the busbar section length, on determing the rise time of the wavefront on the motor side. The only difference is that the 10ns rise time is faster than the travel time if one busbar section is 1m or longer. This results in a discrete type of wavefront.

The influence of the busbar configuration.

Depending on where the motor is situated on the rail of the busbar, there will be another wavefront on the motor side.

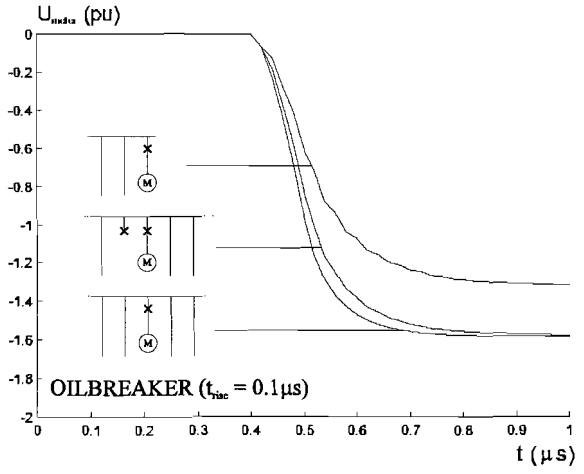

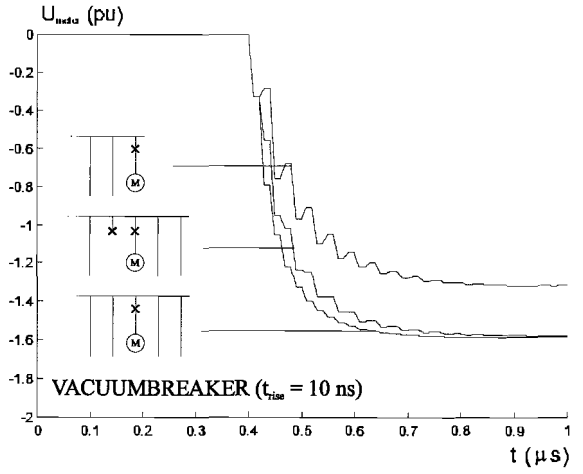

When the cable to the left is not used we see only a little difference in the signal. However if the motor is on the end of the busbar a lot of the wavefront of the ramp source is lost. With the vacuumbreaker one can see the influence of a non-symmetrical busbar setup (busbar end is 0.5 m).

The influence of parallel cables.

To further check the influence of the busbar configuration we also calculated the wavefronts for different number of parallel cables to the left and right.

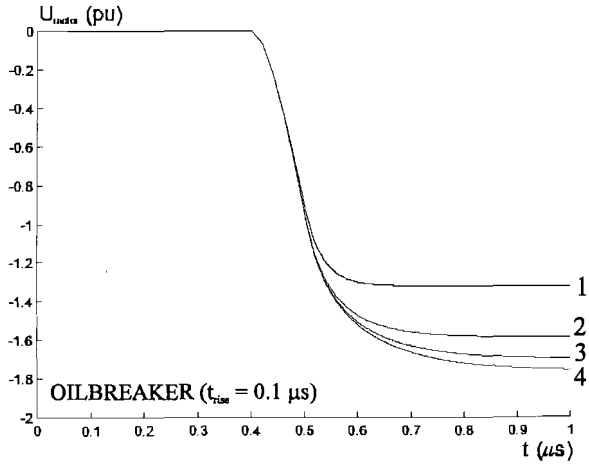

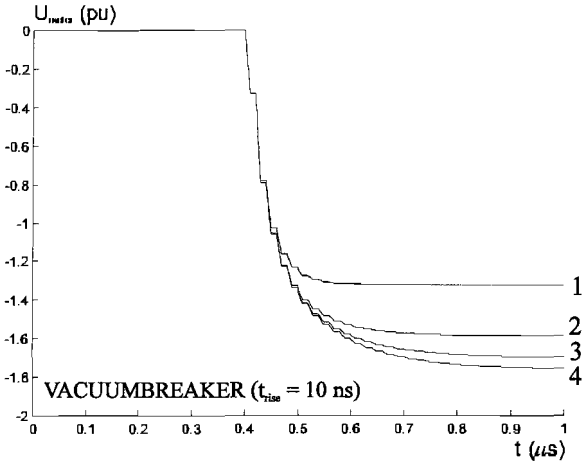

The less parallel cables the more will be lost of the wavefront. This agrees with the results found when connecting a motor to the end of a busbar. When we would extend the number of parallel cables to infinite this would result in an open end on the end of the second busbarsection. However the simplification made is not valid to this extend. To overcome this fault, only a choice between none, one, two or three parallel cables is given in the program.

The influence of the impedance of the motor

Because we decided not to insert the motor model into this part of the calculations, we have to determine the effect of the motor impedance on the wavefront.

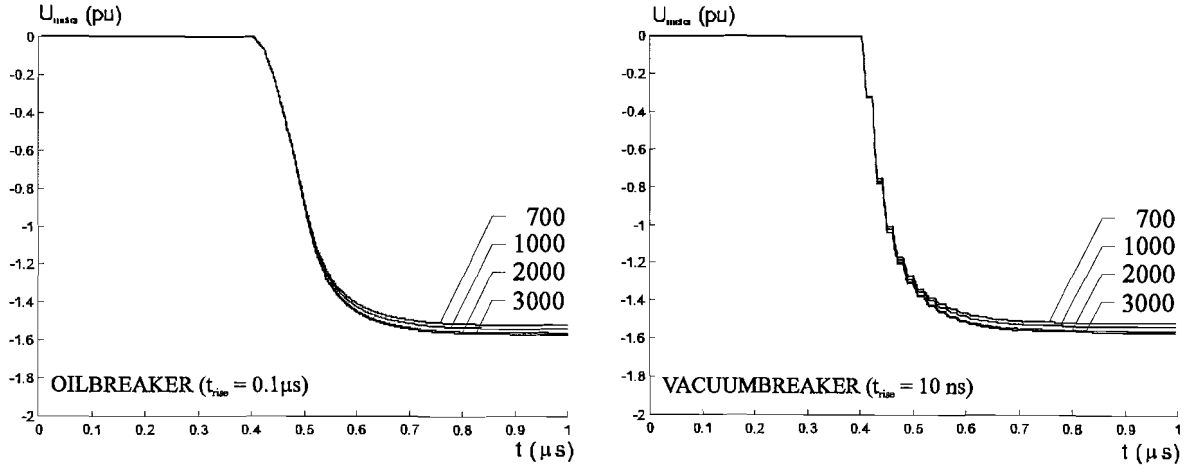

One can see that the maximum voltage doesn't vary much (1.53 - 1.58 pu). The values of the internal impedance's resembles motors between 110 kW (2700 Ω) till 1MW (760 Ω) [2.6]. These calculations show that the previously made assumption of replacing a motor model with a resistor is allowed.

The influence of a capacitor.

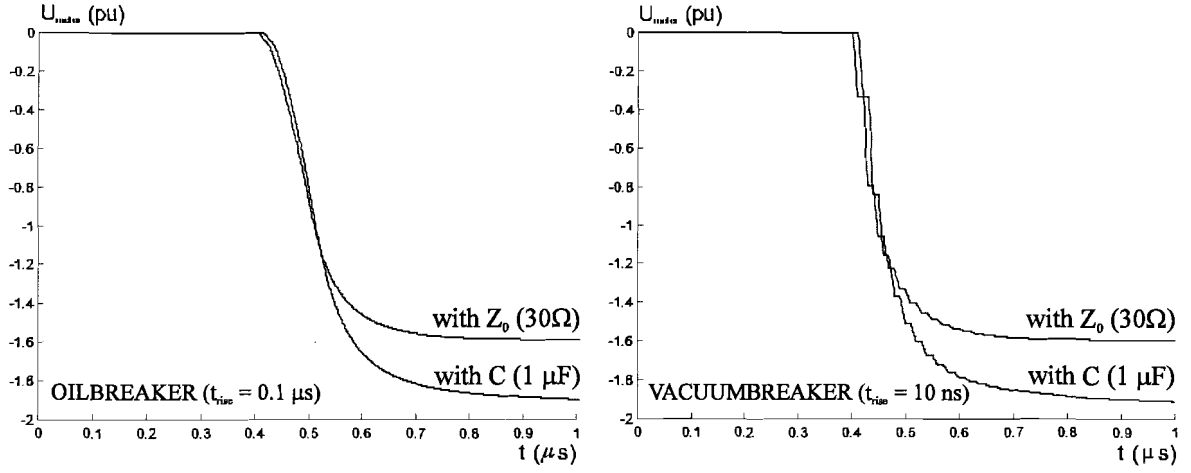

When a capacitor is placed in the neighborhood a low impedance is witnessed by the steep wavefront (high frequency) and thus influencing the wavefront on the motor side in a negative manner. This setup results into the highest overvoltage on the motor side.

4 Electric stress on the motor

To determine the extend of the electric stress in the motor a literature study was conducted to obtain a motor model and some modifications were made to the calculation program to import the data obtained from the busbar configuration calculations.

Motor model

Three types of models were encountered in the literature:

- EMTP-models, fully described as transmission lines with different mutual inductance's in the slots and the motor ends.[4.1]
- Finite Element Method-models used for determining the electric stress on the isolation.[4.2]
- Lumped components-model, with a coil or with a turn as smallest motor element. [4.3 , 4.4 , 4.5 , 4.6]

Since we cannot use the exact dimensions of the motors in the models, due to the lack of data supplied by ISLA, we have to restrict ourselves in the use of the lumped components model. (Even if we had the exact dimensions of the motors, it would be difficult to implement this in a computation program using all kinds of different motors within the restricted time of the research).

For a rise time of 0.2 μs or greater, one can calculate with a coil as smallest motor element and consider a linear voltage distribution over the turns. This is caused by the existence of high mutual inductance's between turns and a small mutual inductance between coils. For rise times up to 280 ns a model consisting of two to three coils will be adequate to calculate overvoltages in the first coil. The dielectric losses in the isolation material can be modeled by using a resistor over the capacitors.

The model with three coils terminated with a characteristic impedance was used from Adjaye and Cornick [4.3]. The choice was made for this model, since it gave the best option to fill in realistic values for the lumped components and it was very thoroughly explained in the article and it could be easily implemented in the program. Choosing a coil as smallest motor element may cause a small variance in the linearity of the voltage distribution across the turns in the coil, but this would be less than the variance created by the values postulated for the turn-model.

Program modifications

In the calculation of the influence of the busbar setup on the waveform of the surge we replaced the motor with an impedance due to memory limitations of Turbo Pascal 7.0. This has been corrected by saving the current flowing into the motor cable and the voltage on the motorcable. Because we can neglect the influence of the reflection at the end of the motor cable on the beginning of the motor cable in our time span this was permitted. Also the fact that we are using the Bergeron-Schneider model for loss free transmission lines allowed us to modify and improve the calculating section of the program.

A RC nudge absorber has been added at the end of the motor cable to calculate the effect of filtering on the switching surges. When calculating without filter the value of the resistor is 1 MΩ thus simulating no existence of the filter. This was done since we are restricted to the matrix dimensions (9x9nodes).

4.1 Circuit model

The circuit consists of the arriving motor cable, the filter and the three coils of the motor terminated by the characteristic impedance [4.3].

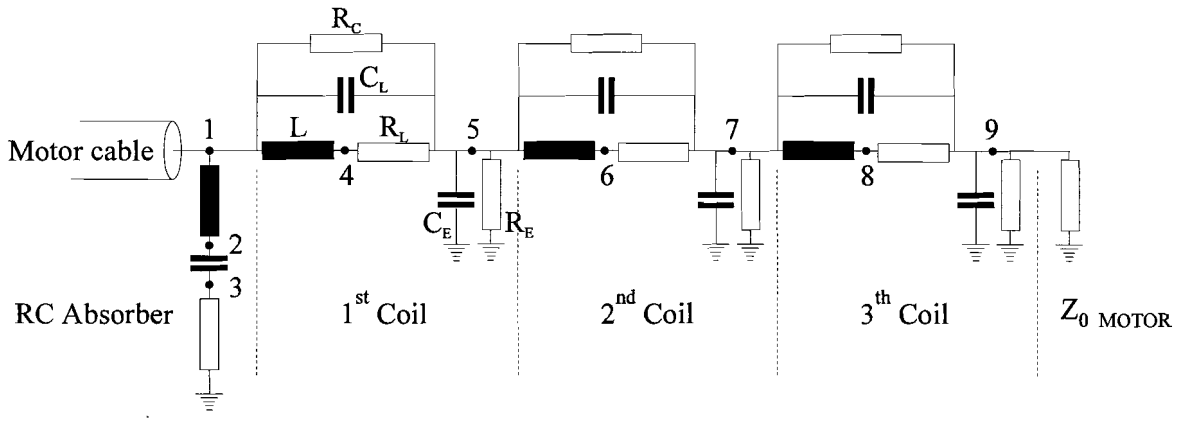

Fig 4.1: One phase circuit model of a motor

The circuit model consists of :

- Motor cable with: $-Z_0$ characteristic impedance of the motor cable
  $-\tau_m$ delay time of the motor cable (in the program this is avoided by using the saved values of the beginning of the motor cable in the busbar section).
- RC absorber with: $-L_F$ line inductance of the connecting cable
  $-C_F$ filter capacitance
  $-R_F$ filter resistance
- Coils with $-L$ one phase stator leakage inductance of the coil
  $-R_L$ one phase coil resistance
  $-C_L$ capacitance over the coil
  $-R_C$ dielectric losses of C_L
  $-C_E$ coil capacitance to ground
  $-R_E$ dielectric losses of C_E
- $Z_{0\ MOTOR}$ $-Z_{0\ M}$ characteristic impedance for termination of the circuit.

With this circuit model we can create in a similar way as explained with the busbar section in chapter 3.4 the NMA-matrix:

$$A \cdot \underline{x} = \underline{b} \tag{4.1}$$

The matrices to solve equation 4.1 are :

$$A = \begin{bmatrix}
\frac{1}{Z_0}+\frac{\Delta t}{2L_F}+\frac{1}{R_C}+\frac{2C_L}{\Delta t}+\frac{\Delta t}{2L} & -\frac{\Delta t}{2L_F} & 0 & -\frac{\Delta t}{2L} & -\frac{1}{R_C}-\frac{2C_L}{\Delta t} \\
-\frac{\Delta t}{2L_F} & \frac{\Delta t}{2L_F}+\frac{2C_F}{\Delta t} & -\frac{2C_F}{\Delta t} & 0 & 0 \\
0 & -\frac{2C_F}{\Delta t} & \frac{2C_F}{\Delta t}+\frac{1}{R_F} & 0 & 0 \\
-\frac{\Delta t}{2L} & 0 & 0 & \frac{\Delta t}{2L}+\frac{1}{R_L} & -\frac{1}{R_L} \\
-\frac{1}{R_C}-\frac{2C_L}{\Delta t} & 0 & -\frac{1}{R_L} & 0 & 2\cdot\frac{1}{R_C}+2\cdot\frac{2C_L}{\Delta t}+\frac{1}{R_L}+\frac{1}{R_E}+\frac{2C_E}{\Delta t}+\frac{\Delta t}{2L} \\
0 & 0 & 0 & 0 & -\frac{\Delta t}{2L} \\
0 & 0 & 0 & 0 & -\frac{1}{R_C}-\frac{2C_L}{\Delta t} \\
0 & 0 & 0 & 0 & 0 \\
0 & 0 & 0 & 0 & 0
\end{bmatrix}$$

$$\begin{bmatrix}
0 & 0 & 0 & 0 \\
0 & 0 & 0 & 0 \\
0 & 0 & 0 & 0 \\
0 & 0 & 0 & 0 \\
-\frac{\Delta t}{2L} & -\frac{1}{R_C}-\frac{2C_L}{\Delta t} & 0 & 0 \\
\frac{\Delta t}{2L}+\frac{1}{R_L} & -\frac{1}{R_L} & 0 & 0 \\
-\frac{1}{R_L} & 2\cdot\frac{1}{R_C}+2\cdot\frac{2C_L}{\Delta t}+\frac{1}{R_L}+\frac{1}{R_E}+\frac{2C_E}{\Delta t}+\frac{\Delta t}{2L} & -\frac{\Delta t}{2L} & -\frac{1}{R_C}-\frac{2C_L}{\Delta t} \\
0 & -\frac{\Delta t}{2L} & \frac{\Delta t}{2L}+\frac{1}{R_L} & -\frac{1}{R_L} \\
0 & -\frac{1}{R_C}-\frac{2C_L}{\Delta t} & -\frac{1}{R_L} & \frac{1}{R_C}+\frac{2C_L}{\Delta t}+\frac{1}{R_L}+\frac{1}{R_E}+\frac{2C_E}{\Delta t}+\frac{1}{Z_{0M}}
\end{bmatrix} \tag{4.2}$$

The x-vector is:

$$x = [\, u_1\ u_2\ u_3\ u_4\ u_5\ u_6\ u_7\ u_8\ u_9\,] \tag{4.3}$$

And the b-vector is:

$$b = \begin{bmatrix}
\frac{1}{Z_{0M}}\cdot u_{cable|saved}+i_{cable|saved}-i_{12}(t-\Delta t)-\frac{\Delta t}{2L_F}\cdot\left(u_1(t-\Delta t)-u_2(t-\Delta t)\right)+i_{15}(t-\Delta t)+\ldots \\
\quad\ldots-\frac{2C_L}{\Delta t}\cdot\left(u_1(t-\Delta t)-u_5(t-\Delta t)\right)-i_{14}(t-\Delta t)-\frac{\Delta t}{2L}\cdot\left(u_1(t-\Delta t)-u_4(t-\Delta t)\right) \\
i_{23}(t-\Delta t)+\frac{2C_F}{\Delta t}\cdot\left(u_2(t-\Delta t)-u_3(t-\Delta t)\right)-i_{21}(t-\Delta t)-\frac{\Delta t}{2L_F}\cdot\left(u_2(t-\Delta t)-u_1(t-\Delta t)\right) \\
i_{32}(t-\Delta t)+\frac{2C_F}{\Delta t}\cdot\left(u_3(t-\Delta t)-u_2(t-\Delta t)\right) \\
-i_{41}(t-\Delta t)-\frac{\Delta t}{2L}\cdot\left(u_4(t-\Delta t)-u_1(t-\Delta t)\right) \\
i_{51}(t-\Delta t)+\frac{2C_L}{\Delta t}\cdot\left(u_5(t-\Delta t)-u_1(t-\Delta t)\right)+i_{50}(t-\Delta t)+\frac{2C_E}{\Delta t}\cdot u_5(t-\Delta t)+i_{57}(t-\Delta t)+\ldots \\
\quad\ldots-\frac{2C_L}{\Delta t}\cdot\left(u_5(t-\Delta t)-u_7(t-\Delta t)\right)-i_{56}(t-\Delta t)-\frac{\Delta t}{2L}\cdot\left(u_5(t-\Delta t)-u_6(t-\Delta t)\right) \\
-i_{65}(t-\Delta t)-\frac{\Delta t}{2L}\cdot\left(u_6(t-\Delta t)-u_5(t-\Delta t)\right) \\
i_{75}(t-\Delta t)+\frac{2C_L}{\Delta t}\cdot\left(u_7(t-\Delta t)-u_5(t-\Delta t)\right)+i_{70}(t-\Delta t)+\frac{2C_E}{\Delta t}\cdot u_7(t-\Delta t)+i_{79}(t-\Delta t)+\ldots \\
\quad\ldots-\frac{2C_L}{\Delta t}\cdot\left(u_7(t-\Delta t)-u_9(t-\Delta t)\right)-i_{78}(t-\Delta t)-\frac{\Delta t}{2L}\cdot\left(u_7(t-\Delta t)-u_8(t-\Delta t)\right) \\
-i_{87}(t-\Delta t)-\frac{\Delta t}{2L}\cdot\left(u_8(t-\Delta t)-u_7(t-\Delta t)\right) \\
i_{97}(t-\Delta t)+\frac{2C_L}{\Delta t}\cdot\left(u_9(t-\Delta t)-u_7(t-\Delta t)\right)+i_{90}(t-\Delta t)+\frac{2C_E}{\Delta t}\cdot u_9(t-\Delta t)
\end{bmatrix} \tag{4.4}$$

For the value of L in figure 4.1 we have to take the leakage inductance of the one phase coilgroup. Due to the high frequent character of our signal, the signal will only see the leakage inductance in the stator. Eddy currents will prevent the surge to contribute to the main magnetic field in the motor.

An estimation of the values of L and C_E was given by Kerkenaar of which a English summary; see appendix V.

Method of estimation

Determining the capacity of a coil to ground and of the coil inductance seems to be impossible without design data. With design data for HOLEC-EMCOL motors some estimations were performed. Motor data were requested by ISLA from other manufactures, but were not received to date.

Isolated coils are inserted in rectangle grooves of more or less the same dimensions (except for the length of the coil). The estimated relative permitivity of the isolation material is five (ε_r = 5). Together with the thickness of the isolation these data will determine the coil's capacitance.

The starting current of an induction machine is mainly determined by the total leakage inductance at 50 Hz. This is usually given in motorbrochures. To determine the number of coils one needs the (confidential) design data. The coils in a belt of high voltage motors are normally inductively coupled at 50 Hz. For the estimation of the coil inductance both the coupled values and uncoupled values were calculated. High frequent switching surges will cause relatively high eddy current and force the magnetic flux along air leakage paths. The value of the coil leakage inductance is therefore approximated by the stator leakage inductance at 50 Hz, circa half of the total calculated leakage inductance. This is expected to be the weakest point in the estimation.

Conclusion

Calculations of coil leakage inductance and capacitance to ground are not likely possible without design data. For the HOLEC-EMCOL motors around 1 MW it can be concluded that:
- the estimated capacity of a coil to the ground of the machine is 2.5 nF.
- the estimated stator leakage inductance of a coil (coupled at 50 Hz) is 20..60 μH (2 - 4 poles / 3kV machines)
- the estimated stator leakage inductance (uncoupled) is 0.4..0.6 mH (2 - 4 poles / 3kV machines)
- the estimated delay times in the coils for high frequent switching surges are between 0.3 and 0.6 μs. For uncoupled coils this value is between 1 and 2 μs.

Both capacity and leakage inductance, in the 300 - 2200 kW range, seems not to be strongly related to the power of the motor.

We used the average value found for the data set of the uncoupled values of the coil surge-inductance and the coil to ground capacitance for the 3kV motors in the calculation program. In the program the choice for the values of the model is made with the number of poles in the advanced input menu as written in table 4.1. The option for neither 2 or 4 poles will give the values found in Adjaye & Cornick's article[4.3].

Table 4.1

# poles	L (mH)	R_L (Ω)	C_L (pF)	R_C (kΩ)	C_E (nF)	R_E (kΩ)
2	0.53	0.1	60	2.0	2.89	10
4	0.48	0.1	60	2.0	2.72	10
not 2 or 4	0.34	0.1	60	2.0	0.91	10

4.2 Results of calculations

The overvoltages over the first coils of the motor were calculated with a standard configuration for the busbar as written in chapter 3.5 (with cable length > 60m) . For the motor model we used the 2 pole option.

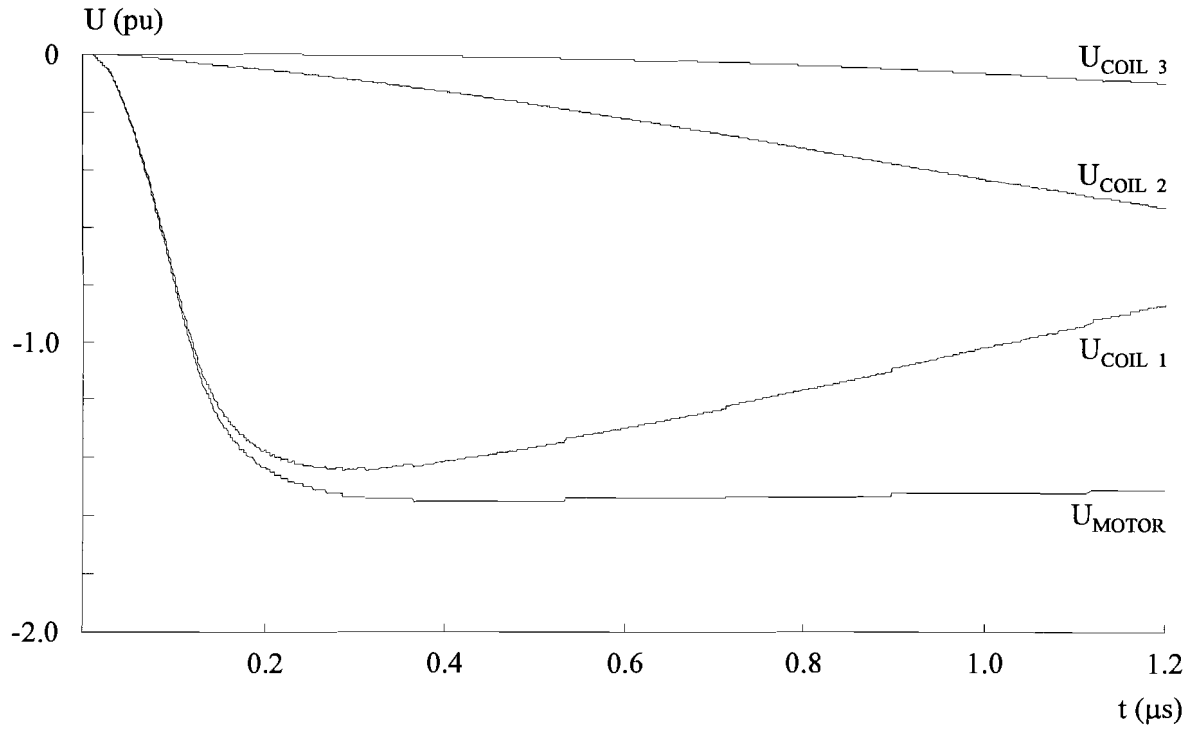

Fig 4.2: Overvoltage over the motor coils

We can see that the voltage over the first coil is almost identical to the surge arriving at the motor. In the program we restricted ourselves to displaying only the voltage over the first coil and till 0.6 μs. This reduces the computation time and gives enough information of the overvoltage over the coil. It also shows that the rise time of the voltage over the first coil is smaller than the delay time of the coils. This means the simplifications (three coils terminated with a characteristic impedance) made to the motor model will not influence the results in this time domain.

In appendix V one can see that there is little variation in the high frequent motor model parameters. The influence of the variation on the height of the overvoltage over the first motor coil was calculated by using the maximum and the minimum values for L and C_E. This is done since no values were found for motors in the unusual 100 - 500 kW range.

Maximum values used for L = 1mH and C_E = 4.5 pF
Minimum values used for L = 0.4mH and C_E = 1 pF

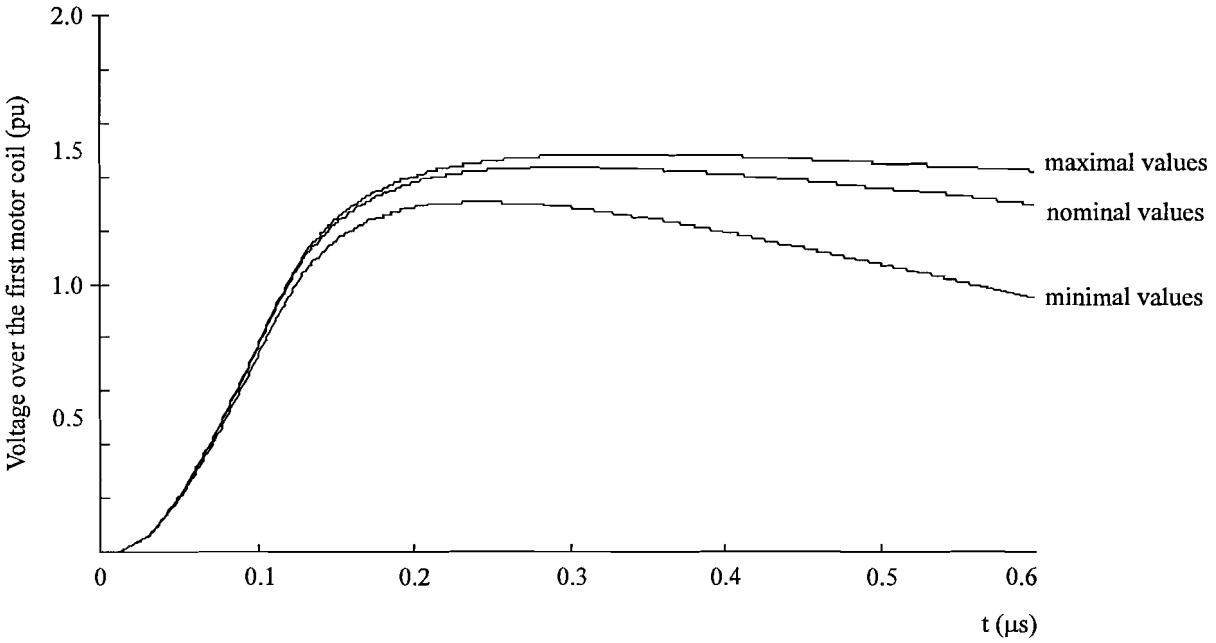

Fig 4.3: Influence of the high frequent motor model parameters

The result of 10% variation in overvoltage over the first coil shows that the values of the motor model parameters are not of great influence on the top of the resulting overvoltage over the first coil. The busbar setup will have a greater influence as will the low frequent motor parameters.

5 Insulation degradation

For the insulation degradation during the years of motor operation a summary will be given of the mechanism of degradation [5.1]. Further a study was conducted in transforming the mechanisms of deterioration into a function dependent of the years of operation and / or the number of starts. In figure 5.1 a cross section of a coil is given, in this figure the structure of a coil consisting of a number of turns can be seen. Each turn will be insulated with one or two layers, impregnated or not and tied together and filled with insulation material. This results in many possibilities for the insulation system of a motor. The main conclusion that can be given is that it is not possible to give a mathematical function that is reliable for all the motortypes present at ISLA refinery, even if a given type of statistical distribution is assumed a priori, it must be verified. Very often a formula is used which will only be valid for *that type of motor* with *that type of insulation* under *those conditions*. The following will be a summary of the theory and the solutions found in the literature.

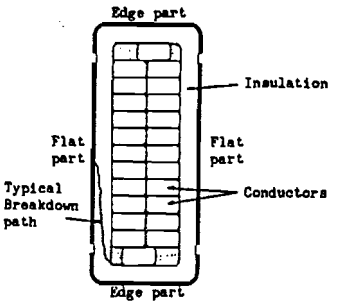

Fig 5.1: Cross section of a coil [5.5]

5.1 Mechanism of degradation

The mechanical stress is responsible for cracks or voids in the insulation system and will have a negative influence on the withstand capability of the insulating system. Under usual operation the motors will vibrate, causing mechanical stress. And sudden changes of the torque on the axis will certainly induce forces on the leads.
A motor in a normal state will be heated and the metal will expand. If there is a non-symmetric heating going on this will cause a tension on the materials causing mechanical stress.
Mechanical stress can also be a result of the many electromagnetic forces on the leads. When a sudden high current is flowing through the machine (starting motor) or a sudden change of the torque on the axis (blocked motor), the motor will experience unusual forces that lead to mechanical stress on the insulation system.

Thermal stress is obtained when the motor's nominal current is exceeded. The temperature rise (related to I^2) can not be cooled sufficiently and will deteriorate the insulation system and weaken the withstand capability. The insulation materials are classified in temperature groups. Figure 5.2 gives a typical voltage withstand capability as a result of thermal stress as a function of time.

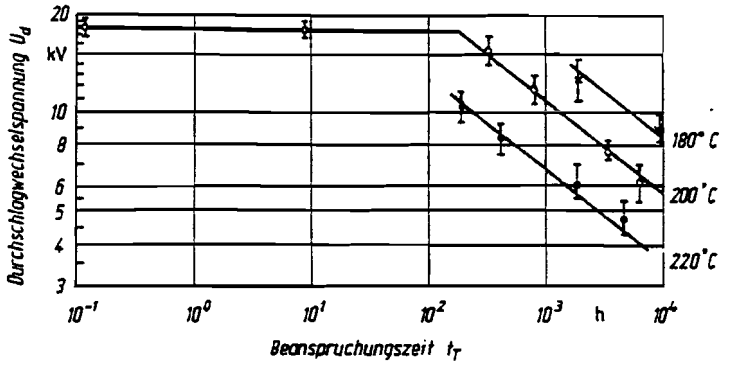

Fig 5.2: Model for a thermal degradation of winding insulation [5.1]

A threshold in time is witnessed, before the withstand capability decreases. A common numerical relation for the lifetime of insulation material as a function of time and absolute temperature (K) is given by the Arrhenius relation in equation 5.1 (see also [5.2]).

$$L_T = k_T \cdot e^{(-b/T)} \tag{5.1}$$

Electric stress on the insulation system is divided into stress by a constant supply voltage and stress from surges. The first is related to long-term operation of the motors and the second to the number of surges and thus the number of switching.

Partial discharge and treeing are phenomena caused by electric stress. The result of these phenomena will cause eventually a breakdown of the insulation system. When such electric phenomena are present it is also possible that chemical reactions will occur thus deteriorating the insulation material further. To determine the lifetime of the insulation it is crucial to know the type and dimensions of the insulation material used. Often a two layer insulation is used for motor windings were the layers do not react the same on electric stress. And if once a void is created in the first layer, surges will stress the second layer with an inhomogeneous field distribution (like a needle - plane geometry) having other consequences. Due to these factors it seems that in order to obtain reliable relations to determine the insulation degradation, measurements are essential to determine the parameters in the relations.

The result of the three types of stress will have a negative influence on the withstand capability of the insulating system. The highest risk for mechanical stress is found at the end terminal, because no slot is present to hold the leads and when assembling the motor the chance of pulling and pushing of the leads is high. The highest risk for thermal stress is where the worst cooling is experienced. For the electric stress, the highest risk is at the end windings. This is because of the highest voltage distribution over the insulation with surges and the high probability of voids and cracks (thus weakening the insulation withstand capability).

5.2 Evaluation of the references

In this section an evaluation of the references will be given, summarizing the methods and the practical experiences of the authors.

Three types of relations have been found in the literature for the electric stress and can be used separately or combined with each other:

- inverse power model
- Weibull distribution (2 or 3 parameters)
- empirical relations

The inverse power model is given by:

$$L_E = k_E \cdot E^{-n} \tag{5.2}$$

This relation is often used for the constant electric stress of the supply system. The lifetime of the insulation material (L_E) can be determined after the parameters have been extracted from measurements for the same type of insulation.

The Weibull distribution is a sophistication and can be used together with the inverse power model:

$$F(t) = 1 - e^{\left(\frac{-(t-\gamma)}{\alpha}\right)^{\beta}} \tag{5.3}$$

γ = third parameter
α = time to failure for 63.2% probability
F = probabilistic life model

With the inverse power model α can be calculated. If the parameters are being related to the electric field and temperature, equation 5.3 becomes the probabilistic life model for combined stresses. In Montanari [5.3] equation 5.3 is even sophisticated by implementing an electric threshold in the inverse power model. Over the past few years the Weibull probability distribution has gained wide acceptance in the statistical treatment of breakdown times of solid dielectrics. This distribution is used since it seems to fit experimental life data better than do most other distributions. The only problem is that there is no simple technique to determine α, β and γ.

The third type of relation is the empirical one. The Japanese [5.4 , 5.5] have come up with two types of empirical relations. The first one is only related to the number of working years (TOSHIBA [5.4]) and the second article has also included the number of start-stops. These two empirical relations have been compared in figure 5.3, and are given by:

$$V_R(\%) = 100 \cdot (1 - 0.02)^{Y} \tag{5.4}$$

$$V_R(\%) = 100 \cdot (1 - 8.75 \cdot 10^{-3} \cdot Y) \cdot (1 - 6.4 \cdot 10^{-5} \cdot N) \tag{5.5}$$

$V_R(\%)$ = withstand capability in percentage of the nominal value
Y = number of working years
N = number of start-stops

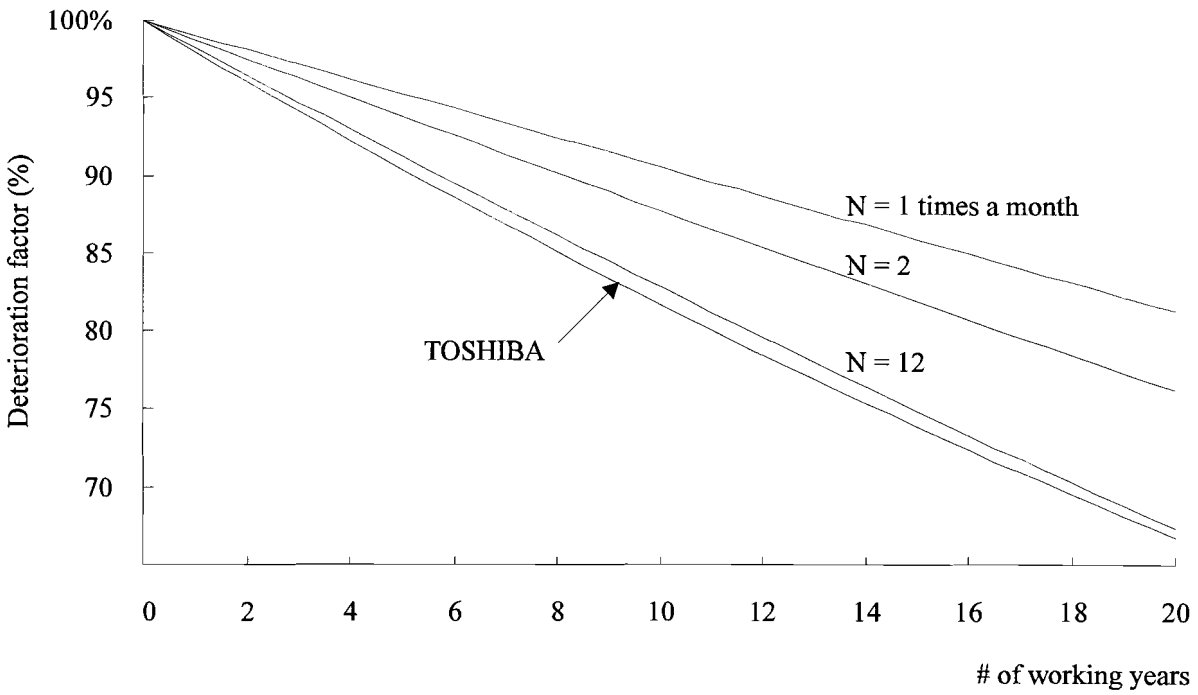

Fig 5.3: Empirical relations for insulation degradation

The nominal number of start-stops was not mentioned in the TOSHIBA report, but vacuum circuit breakers were used. A common phenomenon with vacuum switchgear is multiple reignitions, this could be one of the reasons why the number of start-stops in the second relation (eq. 5.5) had to be about 12 times a month to have the same degradation curve. Since we are working with mostly oil circuit breakers we will use equation 5.5 in the program. One has to keep in mind that this empirical relation does not make a difference between circuits with the different probabilities of height of surges.

The improvement of the probabilistic life model can only be done if the parameters are known for the different types of insulation systems. This makes the use of relations difficult for our purposes.
Equation 5.5 is deducted from measurements of varnish (solvent-type thermosetting resin) and mica splittings insulated 3.3 kV induction motor stator windings used for 15 years or more. And since the motors at ISLA are rated for 3 kV and also of age, eq. 5.5 has been used to determine the degradation (or ageing) factor in the program.

In Stone [5.6] tests have been performed on an unfilled epoxy. This paper presents the results of the testing, and discussed their implication for practical equipment. The parameters for the Weibull distribution (2 parameters) have been determined. The measurements showed a tremendous variation in failure times. Their experience is that the invers power model, together with the Weibull probability distribution, produces a better fit when compared to an exponential model and either a Weibull or LogNormal distribution.

Further from a statistical point of view they found that, surge ageing behaves much the same as ageing under alternating voltage. For their research on pure epoxy they found that more than 60.000 surges or so at a stress level higher than about 7 MV/cm is likely to be subject to failure by surge ageing. Including the fact that an average of 150 surges occur per switching event from the vacuum breaker, users should be concerned about ageing of the turn insulation by voltage surges if such high stress level is present.

The investigation in Gupta [5.7] contains results of tests conducted on 216 coils in three different motor stators. The results showed that a threshold voltage may exist, similar to high voltage cables, for surge aging of turn insulation. This hypothesis is supported by the fact that, with more uniform distribution of the "unaged" and "aged" coils, no significant ageing of the turn insulation was detected up to 8000 surges at 7.8 pu in the third stator. "Unaged" meaning no surge ageing was applied by the authors on the stators. Gupta limits the use of this hypothesis due to the scope of his study. The insulation consisted of mica-paper tape and is less prone to surge ageing as other common forms of turn insulation, e.g. varnishes, polyimides and dacron-glass. His results concluded that surge magnitudes that may cause surge ageing for mica-paper insulation is rare for normally operating utility motors.

In Walker [5.8] experiences with turn insulation failures are discussed (13.2 kV motors). The motors showed early insulation failures in the end turn region. It showed that in every case there was a catastrophic failure of the ground wall. In his case the main cause were large voids in the end turn region of the stator coils. This part of the coil must retain a degree of flexibility to allow the build of the stator winding. During the insertion of the coils, the end turn sections are twisted in a fashion that tends to displace the ground wall insulation immediately adjacent to the conductor insulation and this mechanical stress creates a large void. The partial discharge in this void can reach the relatively thin conductor insulation and create an interturn failure and extend to a turn to ground failure.

The literature makes it clear that there are many processes going on which results in insulation degradation. Each research clarifies one aspect and at the mean time brings up other questions. This makes it very difficult to predict insulation failure without measurement and even with measurements.

6.1 Purpose and design

A dedicated program was written to compute the overvoltage on the first winding of the motor. The overvoltage over the winding will also be a measure for the interturn electric stress.
The program should be able to compute the overvoltage for different types of motors (power, age, etc.) in different surroundings (different neighbours) as there are present at the refinery of ISLA. The only constant for all motors will be the global parameters (supply voltage and power frequency).

Since there are about 200 motors, the program has been organized to keep all motors connected to one busbar in one record file. The maximum of 60 record files can each contain up to 60 motors. For all motors specific parameters will be calculated and stored in an ASCII motor.cal file. In this file also the waveform at the motor end and the waveform over the first winding will be saved. This data will be used for the graphical output, but can be used by the user if wanted. *All motors should have unique names*, if this is not the case a calculation of a motor with the equal name will overwrite the previous file even if it is not connected to the same busbar.

A choice was made to separate the input, calculation and the output into menu items. This allows the user to insert the data without having to wait for the calculations and the graphical output each time. The possibility to delete a motor, or a busbar record file were also implemented as was the option to change the global parameters. This will all be explained in the user guide.

The input parameters have been divided into two types, one necessary for each motor without standard values and one with advanced options to experiment or for fine tuning. Standard values are given for the advanced parameters. These parameters will be explained in the next paragraph with their restrictions and their consequences.

6.2 Input parameters

The input fields of the parameters are divided into three groups:

- characters (char) : All characters (A..Z) are valid as are the numbers (0..9) as are underscores and hyphens. The lowercase characters will be automatically converted to uppercase.
- numbers (num) : All numbers (0..9) including the "E,+,-" for scientific notation. The metric measurement has a point as decimal separator.
- choice : A choice is given with highlighted characters.

Entering a non valid character, number or choice will cause a beep. The program will give a message in the help line that a non valid input has been made. The help line is always the lowest line of the screen. To insure the program's functioning all standard parameters have strict ranges to which the input has to comply. Exceeding the range (upward or downward) will cause an error beep and the valid range is displayed in the help line. If advanced is mentioned in table 6.1 the value can be entered in the advanced menu. With the input one has to keep in mind the dimensions the program is computing with. (e.g. m or dm)

Table 6.1: Standard motor parameters.

Name	Input	Range	Comments / consequences
ID	char	1 to 8 char	This unique name is used to create the calculation file. If the ID is the same as another one in the same busbar record file, the program will ask to overwrite the previous data.
Year	num	1900 - now	The year of installment of the motor is used to calculate the ageing factor. 'Now' is taken from the computers system date. See chapter 5.
Power	num	100 - 1200 kW	Used to calculate the low frequent inductance of the motor.
Cable length	num	30 - 300 m	Together with the capacitance of the cable (F/m) this gives the total cable capacitance. The greater the capacitance the lower the transient frequency. See chapter 2.1.2. (Advanced)
Cable type	choice	O X	Used to choose between the values for the OIP- or XLPE-cable capacitance. (Advanced)
Switch type	choice	O V	Used to choose between the rise time of a Oil circuit breaker or a Vacuum circuit breaker. (Advanced)
Switch freq.	num	0 - 3E5 /month	Used for the calculation of the ageing factor. Switching more times a month will cause more electric stress over the years resulting in a weaker insulation system. See chapter 5.
Length 1st left till 2nd right	num	0 - 40 dm	The length of the busbar to the first/second connected cable to the left/right of the motor under consideration. The influences of the busbar is essential on the resulting waveform arriving at the motor end terminal. See chapter 3.5.
Left neighbour Right neighbour	choice choice	N O X C N O X	None means the motor is situated at the busbar end. O or X will choose between the characteristic impedance's of the OIP- or XLPE-cable left to the motor. (Advanced) C indicates that there is a compensation condensator left to the motor. (Advanced)
# par. cables	choice	N O T	For the rest of the cables attached to the busbar left of the motor there are three options: None : characteristic impedance is put at 1 MΩ. One: characteristic impedance is put at 15 Ω. Two or more: char. impedance is put at 30 Ω. The influences of the parallel cables is given in chapter 3.5

All advanced motor parameters can be changed for each motor. The parameters are displayed in scientific notation, only the motor characteristics are integers and thus displayed. The dimensions (if any) are displayed behind the input field. If the resistor in the RC-absorber is 1 MW, no input fields for the rest of the absorber will be displayed. All values used in the NMA-matrix cannot be zero, this would cause a division by zero in the program. Instead one should enter a small value keeping in mind the numerical precision of the computer. Entering a zero resets the advanced parameter to its standard value. The standard values for the advanced motor parameters can be changed in the source code of the program. The source code can be found in the unit ISLA_PAR.pas under constants.

Table 6.2: Advanced motor parameters.

Name	Standard values		Comments / consequences
Busbar	3.00E+02	Ω	The characteristic impedance of the busbar is important for the reflection and refraction coefficient. This will influence the steepness of the wavefront
OIP-cable XLPE-cable	3.00E+01	Ω Ω	The value of the OIP- and XLPE-cable characteristic impedance, which the program uses as selected with the standard motor parameters.
# of turns # of poles			*Will be changed to allow full parameter input if necessary.* *Alan.*
Pole delay pole 1 - 2 pole 1 - 3	2.00E-04 4.00E-04	s s	With the value of the pole delay times one can simulate the age of the circuitbreaker. Increasing these resembles an older breaker (looser contacts). The values are used in the probability calculation. See chapter 2.1.1 fig 2.5 and chapter 2.1.2 fig 2.11 for the consequences.
closing speed	1.00E+00	m/s	With the closing speed the factor F_k is calculated, decreasing this value resembles ageing of the medium of the circuit breaker and this has influences on the probability calculations. See chapter 2.1.1 fig 2.4 and 2.1.2. fig 2.12 for the consequences.
t_{rise} oil breaker t_{rise} vacuum breaker	1.00E-07 1.00E-08	s s	The rise time of the front when breaking down of a circuit breaker. This has influence on the shape of the wavefront arriving at the motor terminal. See chapter 3.5.

Table 6.2: Advanced motor parameters. (continued)

Name	Standard values	Comments / consequences
chopping current	2.00E+00 A	The value of the chopping current when switching off. Increasing this value will result in a linear increase in the maximum of the height of the surge when switching off. See chapter 2.2.4.
overshoot factor	1.70E+00	The overshoot factor of the transient used to simplify the calculations and increase the calculation speed. See chapter 2.1.1, fig 2.2 for consequences.
normal distribution factor	2.00E-01	This factor is the related to the variance in the normal distribution of the closing speed (F_k). See chapter 2.1.2 fig 2.13 for the consequences.
capacitor	1.00E-06 F	The value of the compensation condensator. This value is only used by the program if in the standard option the 'C' of the left neighbour is selected
$C_{phase\ to\ phase}$ OIP-cable XLPE-cable $C_{phase\ to\ ground}$ OIP-cable XLPE-cable	2.55E-11 F/m F/m 8.20E-11 F/m F/m	The cable capacitance. These values are used to calculate the transient frequency. See chapter 2.1.1 equation 2.3.
filter resistance capacitance line inductance	1.00E+06 Ω 1.00E-06 F 1.00E-08 H	The RC absorber is selected with the value of the filter resistance. Smaller than 1 M Ω will activate input for the filter capacitance and the line inductance. The inductance of the cable connecting the absorber to the motor terminal has great influence and should be kept small. A value of ca. 0.5 μH/m is usually used.

6.3 User guide

The user guide will gives the requirments needed for the program and will explain the usage of the program. The program is written in Pascal and compiled to an executable with the Borland Turbo Pascal 7.0 program. Both executable and source code files are supplied to ISLA.

Requirements

- IBM compatible computer
- numerical processor
- EGA / VGA colorscreen
- 80486 33 Mhz gives a computation time of ca. 15 seconds/motor.
- 200 kB for the executable files, for each motor about 20kB is needed for the calculation file and the storage in the record file.

The program needs isla.exe and global.dat in the same directory to start. The program isla_res.exe is an utility program supplied to collect results from all calculated motors.

The following styles were used : < > key to be pressed
bold option to be chosen
italic option to be entered by keyboard

MAIN MENU
When using isla.exe the program will start in the main menu.

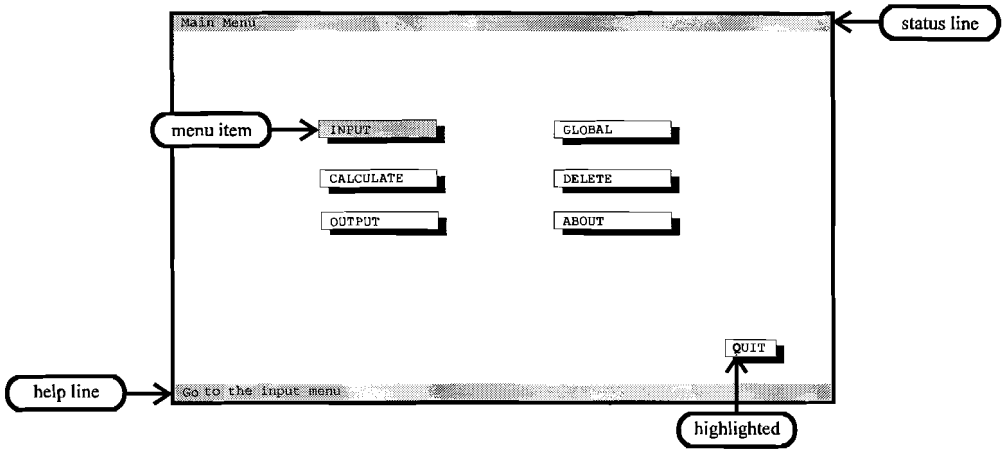

Moving from menu item forward is done with <TAB> and backward with <SHIFT-TAB>. Confirming a menu item is done with <ENTER>. The status line will give information about the menu item and if needed the busbar record file and/or motor ID. The help line will display information about the options at the selected field or will give the information about the error if an error occurs. At all times a menu item with a highlighted letter can be reached by pressing <ALT-*letter*> (in this case <ALT-Q>).

The main menu consists of seven items:
- **input** input of the motor parameters, stored in *.rec files, each file corresponds to a busbar
- **calculate** calculates of the overvoltage for one motor saved in motor.cal file
- **output** graphical output on screen for one calculated motor, a hardcopy can be made
- **global** option to change the global parameters in global.dat.
- **delete** option to delete a motor or remove a busbar record file when empty.
- **about** summary of the menu options
- **quit** returns to DOS.

The first five menu items will now be discussed.

INPUT

Before entering the motorparameters the busbar record file has to be chosen.

- **new** entering a new record file, the options are:
  - *input* maximum of 8 char., after <ENTER> the user goes to the **ok** option.
  - **ok** if the file exists one can edit it or return to the **new** option, a new name will create a new record file and directly go to the standard input screen
  - **quit** returns to the main menu
- **select** selects an existing busbar (maximum of 60)
- **quit** returns to the main menu

If there are motors in the selected record file a motor can be chosen.

- **new** goes directly to the standard input menu
- **select** selects an existing motor (maximum of 60) and goes to the standard input screen
- **quit** returns to the main menu

Standard input menu

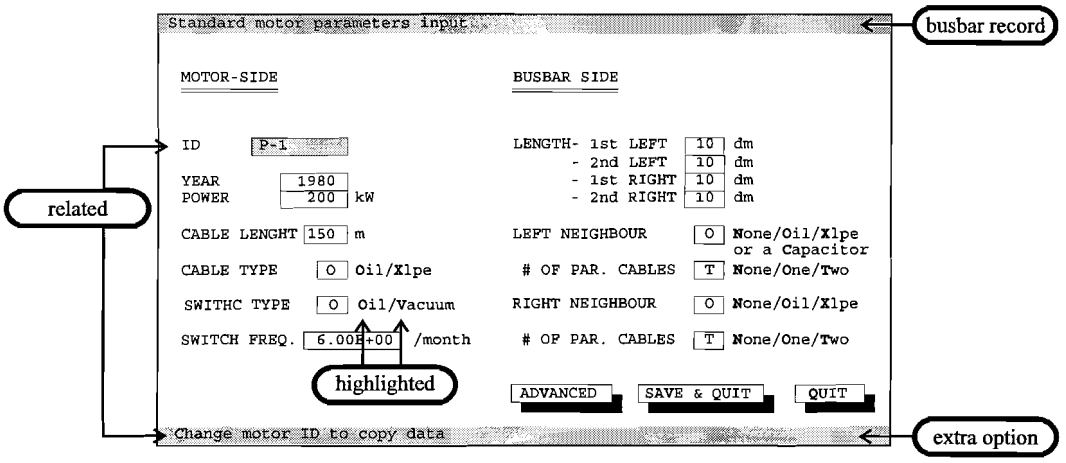

The busbar record file used is written in the statusline. The help line displays field related information. If it is an existing motor, all old values are displayed and the user can go directly to the **advanced** menu item with <ALT-A>. Highlighted characters display the valid choices. Entering none for the left or right neighbour causes the program to skip the question of the other parallel cables to the left or right. In both the standard and the advanced input menu pressing <ENTER> or <TAB> in a field has the same results.

The options in the standard input menu are:

- **advanced** goes to the advanced input menu
- **save & quit** saves the motor parameters and returns to the main menu, if the motor already exists in the busbar record file one can overwrite it or return to the main menu.
- **quit** returns to the main menu

Advanced input menu

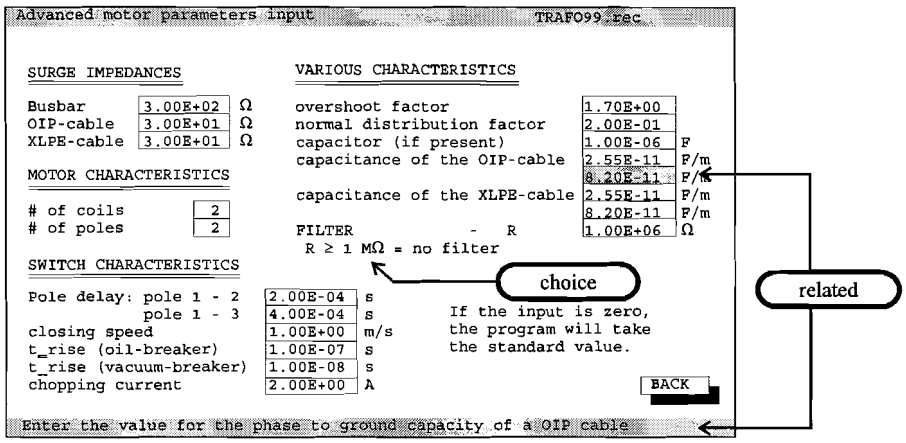

In the advanced motor parameters input all values are already entered with the standard values. When changing these the user has to save the motor parameters in the standard input menu (**save & exit**). The help line still offers field related information. With a resistance smaller than 1 MΩ the RC-absorber is used and the capacitance and line inductance fields will be displayed. <ALT-B> goes to the option **back** which allows the user to go back to the standard input menu.

If one selects an existing motor in the record file and changes the motor name, one can copy all the parameters to a new motor. For a hardcopy <PRINTSCREEN> can be used.

CALCULATE

When calculating the user has to choose a motor in a busbar record file. And the progress of the motor being calculated is shown. If there is no motor present; a message will appear and after confirming this the user returns to the main menu. The subroutine creates a ASCII motor calculation file with the following configuration:

CALCULATED MOTOR PARAMETERS : *identifcation*

L (H)	R_L (Ω)	C_L (F)	} motor model
R_C (Ω)	C_E (F)	R_E (Ω)	} (fig 4.1)
$C_{phase\ to\ phase}$ (F)	$C_{phase\ to\ ground}$ (F)	WITH/NO FILTER	
Motor cable (Ω)	Left cable (Ω)	Right cable (Ω)	} characteristic
Par. cables left (Ω)	Par. cables right (Ω)	rise time breaker (s)	} impedances
transient frequency (rad/s)	ageing factor	alpha (see eq. 3.15 and 3.17)	

maximum overvoltage when switching off (pu)

CALCULATED PROBABILITIES (10 - 50 - 90% of Pole 1 - 2 - 3)

10% pole 1	50% pole 1	90% pole 1
10% pole 2	50% pole 2	90% pole 2
10% pole 3	50% pole 3	90% pole 3

CALCULATED INTERTURN OVERVOLTAGE (1pu-surge)

time (s)	U_{MOTOR} (pu)	U_{COIL1} (pu)

OUTPUT

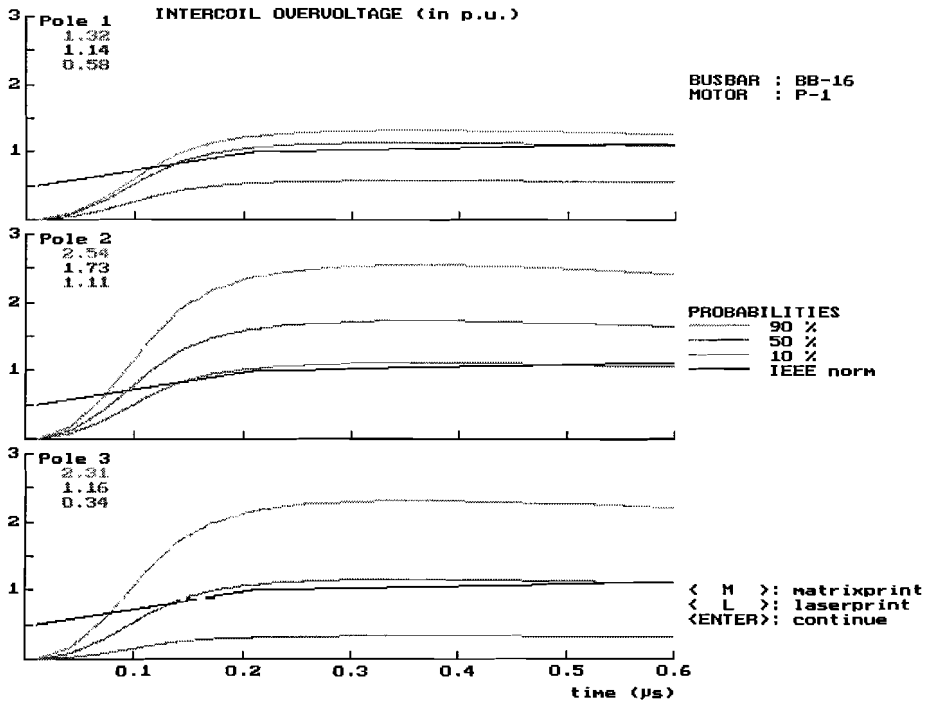

The graphical color output contains the waveform over the first coil at the motor end for three different probabilities of the height of the surge. In each graph in the top left corner the maximum values of the waveforms are displayed. The fourth line in each graph is the IEEE norm multiplied with the aging factor for this motor displayed. A black and white bitmapped hardcopy can be made on IBM compatible matrix printer (9 pins) and on a HP Laserjet. All graphs can be reproduced with own graphical programs using the ASCII motor calculation file.

GLOBAL

The global input screen shows the global parameters and allows them to be changed. After changing them there are the following options:

- **save & quit** saves the new global options after reconfirmation
- **quit** returns to the main menu

Also in this menu item the help line is field related.

DELETE

This menu item allows the user to select a motor to delete. After selection the program reconfirms the users choice and deletes the calculation file and removes the motor from the record file. When selecting a motor the user can return to the main menu by pressing <ESC> as is written on the help line. If a busbar record file is empty the user has a choice to delete the record file.

ISLA Utility program

The purpose of the utility program isla_res.exe is to read all motor calculation files and extract the results into one ASCII file for further examination.

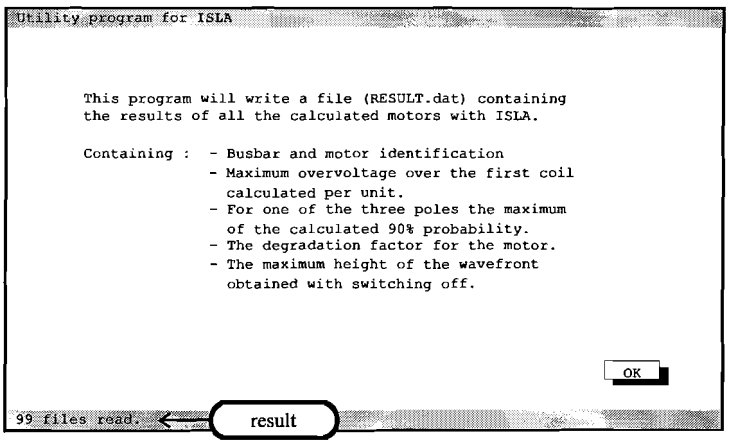

A summary is given of the calculated items that are extracted. In the help line the motor files that are opened are displayed and at the end the total number of files read is displayed. The user can, with an additional program, extract the results in the ASCII file for comparison. An example of a results.dat file is given in chapter 6.4.

6.4 Test case

In the test case the link between an existing industrial surrounding and the program is made. It will be made clear how to enter the data for each motor. In this test case all advanced parameters won't be changed. After using the program the utility program isla_res.exe will be used to gather the maxima of the calculations, and the listing will be discussed.

Circuit

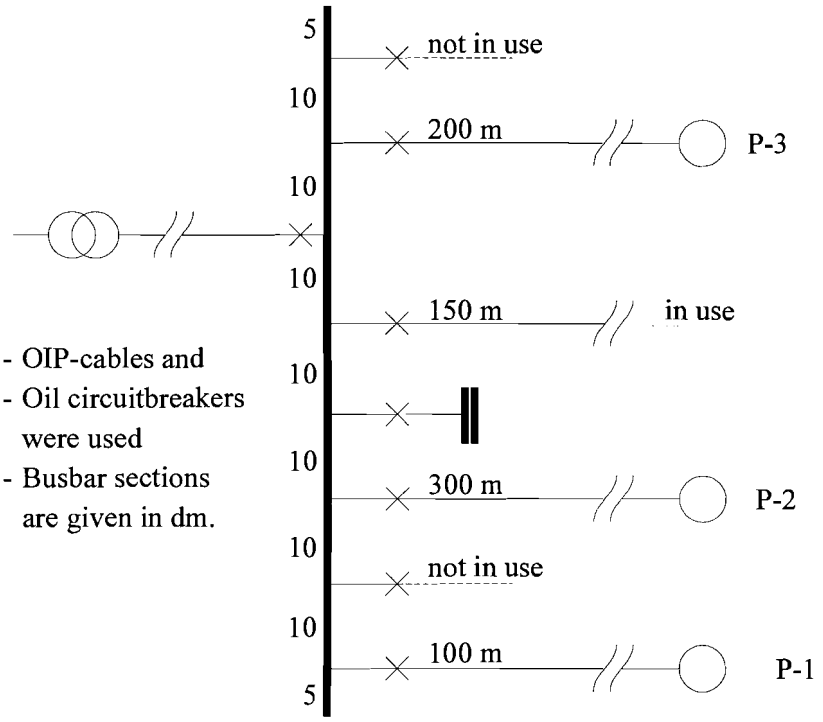

Fig 6.1: Schematic drawing

Input

Three motors are connected to this busbar. The length of each busbar section is dependant of the use of the cables (with a maximum of 40 dm) to the left and the right of the motor under consideration. In this test case it is assumed that the motors are in operation at the same time. For the motor P-2 we changed left and right, because of the compensation capacitor at the right. The program only allows those to the left of the motor. In table 6.3 the input is shown according to the dimensions of table 6.1.

Table 6.3

ID	Year	Power	length	cable	breaker	freq.	length busbar sections				left	#par	right	#par
P-1	1980	200	100	O	O	4	5	0	20	10	N	N	O	T
P-2	1970	1000	300	O	O	4	10	10	20	5	C	T	O	N
P-3	1990	500	200	O	O	4	10	10	15	0	O	T	N	N

Result

The grahpical output of the three motors for the second pole is given below. This result will give an indication of the severity of overvoltages for all three motors. The IEEE norm is multiplied by the ageing factor, and gives an indication of the withstand capability of the motor in relation to the overvoltage.

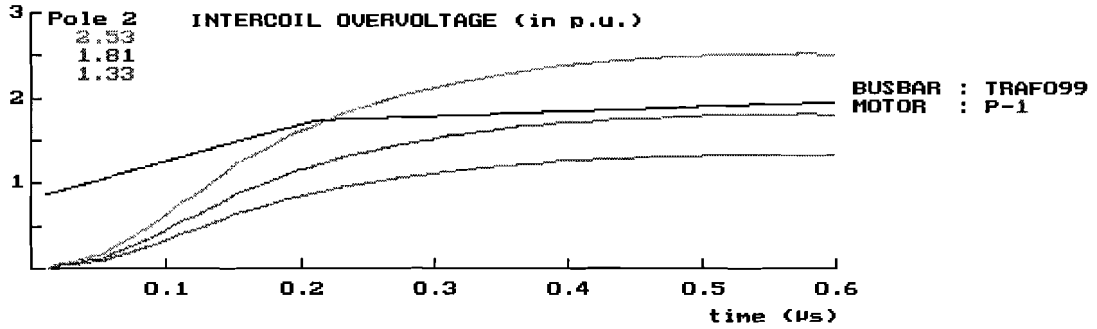

Fig 6.2: Graphical output of P-1.

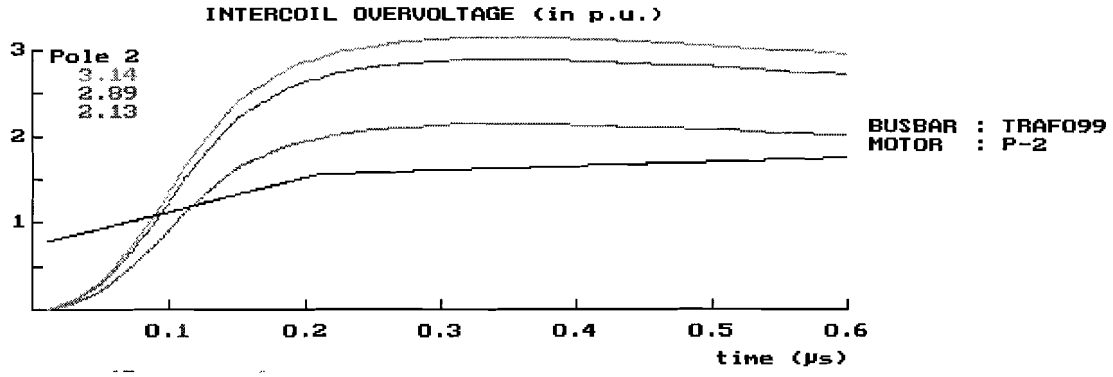

Fig 6.3: Graphical output of P-2.

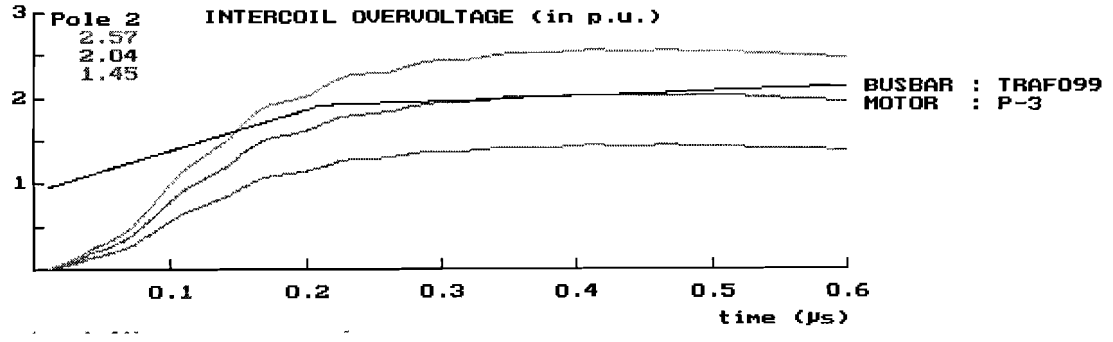

Fig 6.4: Graphical output of P-3.

ISLA_RES.exe

The result of the utility program is given below. This listing can be used in another application (e.g. spreadsheet) to construct a sorted list of the calculated motors. This can be done with the one of the results or with a multiplication of different calculated results. One can see that all influences are taken into account and this can give unsuspected results. For example P-1 (small motor and short cable) is not the worst case. P-2 with a compensation capacitor next to it, hasn't the highest surges (1.86pu) nevertheless P-2 will have the highest overvoltage over the first coil with a 1pu surge (1.68pu). This means one cannot predict all the worst cases with a mnemonic.

ID-string		Ucoil_max	Max_90%	Degradation	I0_Z0
TRAFO99	P-1	1.20E+00	2.22E+00	8.69E-01	1.12E+00
TRAFO99	P-2	1.68E+00	1.86E+00	7.81E-01	3.76E-01
TRAFO99	P-3	1.27E+00	2.26E+00	9.56E-01	6.01E-01

The overvoltage over the first coil as drawn in the graphical output is constructed by multiplying the 90% probability value with the overvoltage over the coil. The 90% probability value given here is the maximum of the three poles. The ageing factor is multiplied with the IEEE norm so the withstand value of the insulation system can be compared with the appearing surges.
The maximum of the overvoltage at the motor terminal indicates the severence of the busbar setup of a surge (1pu). The theoretical maximum of a surge when switching off is also given. One should keep in mind that the probability of occurrence of:

- the surge when breaking down is low
- the maximum height when breaking down is low.

This is the reason of not using the value, of the surges when switching off, within the program for degradation purposes.

7 Conclusions and recommendations

7.1 Conclusions

The study on electric stress due to switching resulted in an investigation on steep-fronted switching surges. The surges which are steep enough will be inhomogeneously distributed over the motor coils. This results in the first coil being stressed by almost the whole surge and not partially. Since the mutual inductance of the turns in a coil is big, the surge over the coil will be linear distributed over the turns. This directed the study to the origin of the surges, the circuit breaker, the construction of the first wavefront on the motor terminal, the industrial surrounding, and the distribution over the motor coils.

By transforming the three phase circuit behind the circuit breaker into a single phase circuit it was possible to introduce several parameters. The influence of each parameter (transient frequency, pole delay times, closing speed and variation in the normal distribution) was researched in our model, and the link to a practical situation was made. A higher resonance frequency of the transient phenomenon resulted in more severe surges with given closing speed, pole delay times, etc. In the program each time all parameters entered will be used to determine the probability of the height of the surges. The assumption seen in many references, that the closing of the second pole is always the most severe, is disputed. The steeper the breakdown voltage decreases (newer insulating mechanism) the higher the third pole surge will become. This can result in a higher third pole surge than the second pole surge, again with the other parameters kept constant. The effect of variation in the breakdown field strength can be neglected, however a greater pole delay time will show an increase of the height of the surge.

When switching off, the theoretical height of the transient recovery voltage is calculated. When there would be a reignition, a steep-fronted surge will arise. For three different states in which the motor can be, a derivation was made. The common factor in all three was the product of the breaking current and the characteristic impedance. The relation of the cable length and the motor power was calculated and resulted that the heighest theoretical overvoltage occur with small motors connected to short cables. For the actual value of the transient recovery voltage for each of the three phases' equations 2.17, 2.19 and 2.21 should be used (keep in mind the definitions stated in figure 2.14).

The propagation of the wavefront created with the surge at the circuit breaker is characterized by reflections in the busbar. To determine if the cables and the busbar sections will damp the wavefront, first the cable was examined. The result from calculations and measurements indicated that in the range of 30 to 200m all effects could be neglected, no further investigation into the busbarsections was conducted.

The busbar circuit was divided into sections and several setups were investigated. The smaller the length of the busbar sections, the steeper the final wavefront at the motor terminal. If a motor was connected to the end of a busbar section almost a reduction of 20% was witnessed on the maximum of the overvoltage, connecting more parallel cables increases the maximum overvoltage. If however a compensation condensator is connected next to the motor under consideration, a drastic increase of the overvoltage was witnessed. The motor itself (varying from 700Ω to 3000Ω) had little influence on the final wavefront at the motor terminal.

From the different models a lumped components-model, with a coil as smallest motor element, was chosen. This model could be implemented in the software and realistic values could be gathered for this model. With the rise time of our surges (ca. 0.2 μs) the distribution over the turns in a single phase motor coil can be approximated with a linear distribution. And the motor model can be simplified by using only the three first coils and a characteristic impedance for the rest of the coils. This simplification is valid due to larger coil propagation time than surge rise time (see figure 4.2). An estimation was made for the components by R. Kerkenaar in appendix V from confidential design data. It illustrated that it is very hard to have the right motor parameters for each motor which are at ISLA. To achieve this, one should know design data for each type of motor on the premises, this is also necessary for the determination of a realistic deterioration factor for the insulation material. An option to attach a RC absorber at the motor terminal was introduced, with a possibility to enter the line inductance for the connecting cable.

The main reason for interturn insulation failure is found due to switching surges, extreme thermal or mechanical stress omitted. In chapter 5 a summary is given of the theory and numerical possibilities for calculating a degradation factor. An empirical relation is found which is related to the number of years of operation and the number of start-stops and was compared with one related to only the number of years of operation. They related to each other if there were about 12 start-stops a month.

The software program in Turbo Pascal 7.0 was made and the NMA-calculations were tested with MicroCap IV and showed no faults. A user guide with all parameters explained is written in chapter 6. The listing of the source code will be separately enclosed together with the program.

7.2 Recommendations

To improve the results of the calculations, in relation to the overvoltage over the coil, given with the isla.exe program measurements should be made on the motors at ISLA. This will allow the user to fill in the right advanced options for the motor.

For the insulation deterioration of the motor windings, a lot depends on the used layers of the insulation, the thickness, the material, etc. It is not possible, without proper knowledge off the motor under consideration, to predict with a reasonable accuracy the withstand capability of the insulation. Measurements should fill in the gap between the motors in the field and the model.

The theoretical work can be enhanced if there is more knowledge on the subject. This can improve the results of the predictions, but always a probability is introduced. If a motor is on the wrong end of the 90% probability value for a few surges in a row, still an insulation failure will occur without being predicted.

Testcases showed that motors connected to the busbar-end have lower overvoltages over the first motor coil. The severest case was found with a compensation capacitor connected next to the motor. The small motors with short cables have a higher transient frequency, resulting in higher overvoltages. Also breakdown surges, when switching off, is the worst with small motors.

References

[1.1] Gupta, B.K. and B.A. Lloyd, G.C. Stone, S.R. Campbell, D.K. Sharma, N.E. Nilsson
TURN INSULATION CAPABILITY OF LARGE AC MOTORS. Part 1: Surge Monitoring.
IEEE Trans. on Energy Conversion, Vol. EC-2 (1987), No. 4, p. 658-665.

[1.2] Gupta, B.K. and B.A. Lloyd, G.C. Stone, D.K. Sharma, J.P. Fitzgerald
TURN INSULATION CAPABILITY OF LARGE AC MOTORS. Part 2: Impulse Strength.
IEEE Trans. on Energy Conversion, Vol. EC-2 (1987), No. 4, p. 666-673.

[1.3] Gupta, B.K. and B.A. Lloyd, G.C. Stone, D.K. Sharma, N.E. Nilsson, J.P. Fitzgerald
TURN INSULATION CAPABILITY OF LARGE AC MOTORS. Part 3: Insulation Coordination.
IEEE Trans. on Energy Conversion, Vol. EC-2 (1987), No. 4, p. 674-679.

[1.4] Gupta, B.K. and D.K. Sharma, D.C. Bacvarov
MEASURED PROPAGATION OF SURGES IN THE WINDING OF A LARGE A-C MOTOR.
IEEE Trans. on Energy Conversion, Vol. EC-1 (1986), No. 1, p. 122-129.

[1.5] Cornick, K.J. and A.N.D. Tleis
FACTORS GOVERNING THE SEVERITY OF PRESTRIKING TRANSIENTS IN MOTOR SYSTEMS.
IEE Proc. B Electric Power Applications, Vol. 137 (1990), No. 1, p. 14-24.

[1.6] Cornick, K.J. and T.R. Thompson
STEEP-FRONTED SWITCHING VOLTAGE TRANSIENTS AND THEIR DISTRIBUTION IN MOTOR WINDINGS. Part 1: System measurements of steep-fronted switching voltage transients.
IEE Proc. B (Electric Power Applications), Vol. 129 (1982), No. 2, p. 45-55

[1.7] Cornick, K.J. and T.R. Thompson
STEEP-FRONTED SWITCHING VOLTAGE TRANSIENTS AND THEIR DISTRIBUTION IN MOTOR WINDINGS. Part 2: Distribution of steep-fronted switching voltage transients in motor windings.
IEE Proc. B (Electric Power Applications), Vol. 129 (1982), No. 2, p. 56-63.

[1.8] Nassar, O.M.
MOTOR INSULATION DEGRADATION DUE TO SWITCHING SURGES AND SURGE PROTECTION REQUIREMENTS.
IEEE Trans. on Energy Conversion, Vol. EC-1 (1986), No. 3, p. 182-189.

[2.1] Kardos, R.C.M.
BEREKENINGEN AAN OVERSPANNINGEN BIJ HET SCHAKELEN IN EEN MOTOR TESTCIRCUIT MET VACUÜMSCHAKELAARS.
Eindhoven, Technische Universiteit Eindhoven, 1992. Afstudeerverslag EG/92/639.

[2.2] Gradshteyn, I.S.
TABLE OF INTEGRALS, SERIES AND PRODUCTS
London: Academic Press 1994, 5TH ed.

[2.3] Colombo, E. and G. Costa, L. Piccarreta
RESULTS OF AN INVESTIGATION ON THE OVERVOLTAGES DUE TO A VACUUM CIRCUIT-BREAKER WHEN SWITCHING AN H.V. MOTOR.
IEEE Trans. on Power Delivery, Vol. 3 (1988), No. 1, p. 205-212.

[2.4] Zotos, P.A.
MOTOR FAILURES DUE TO STEEP FRONTED SWITCHING SURGES: THE NEED FOR SURGE PROTECTION - USER'S EXPERIENCE
IEEE Trans. on Industry Applications, Vol. 30 (1994), No. 6, p. 1514-1524.

[2.5] Smeets, R.P.P.
VERMOGENSSCHAKELAARS IN DE ELEKTRICITEITSNETTEN
Eindhoven: Technische Universiteit Eindhoven, 1994.
Dictaatnr. 5764

[2.6] Slamecka, M.E.
COUPURE DES FAIBLES COURANTS INDUCTIFS. Chapitre 3, Partie A.
le Groupe de Travail 13.02 du Comité d'Etudes No. 13 (Appareillage de Coupure).
Electra, Vol. 75 (1981), p. 5-30.

[3.1] Overbeek, H.H.
ELEKTRICITEITSOPWEKKING, -TRANSPORT EN -DISTRIBUTIE. Deel 2.
Eindhoven: Technische Universiteit Eindhoven, 1992.
Dictaatnr. 5633.

[3.2] Akker, W.F. van den
DEMPING VAN SCHAKELOVERSPANNINGSTRANSIENTEN IN ENERGIEKABELS
Eindhoven, Technische Universiteit Eindhoven, 1995. Stageverslag EG/95/762.S.

[3.3] Ametani, A.
FREQUENCY DEPENDENT PARAMETERS OF OVERHEAD LINES
EMPT Summer Course at EMTP Center Leuven, Belgium (1989), 24-28 July.

[3.4] Oostveen, J.P. van
BEREKENINGEN AAN OVERSPANNINGEN BIJ HET SCHAKELEN IN EEN MOTOR TESTCIRCUIT MET VACUUMSCHAKELAARS. Toepassingen van de Nodal Matrix Admittance methode.
Eindhoven, Technische Universiteit Eindhoven, 1992. Afstudeerverslag EG/92/640.

[3.5] Ginneken, K. e.a.
DOCUMENTATIE EN PROGRAMMA BIJ DE NUMERIEKE TURBO PASCAL BIBLIOTHEEK TPNUMLIB.
Eindhoven, versie 1, November 1991

[4.1] Bacvarov, D.C. and D.K. Sharma
RISK OF WINDING INSULATION BREAKDOWN IN LARGE AC MOTORS CAUSED BY STEEP SWITCHING SURGES. Part 1. Computed Switching Surges.
IEEE Trans. on Energy Conversion, Vol. EC-1 (1986), No. 1, p. 130-139.

[4.2] Bacvarov, D.C. and D.K. Sharma
RISK OF WINDING INSULATION BREAKDOWN IN LARGE AC MOTORS CAUSED BY STEEP SWITCHING SURGES. Part 2. Probalistic Risk Assessment.
IEEE Trans. on Energy Conversion, Vol. EC-1 (1986), No. 1, p. 140-151.

[4.3] Adjaye, R.E. and K.J. Cornick
DISTRIBUTION OF SWITCHING SURGES IN THE LINE-END COILS OF CABLE-CONNECTED MOTORS.
Electric Power Applications, Vol. 2 (1979), No. 1, p. 11-21.

[4.4] Gurardado, J.L. and K.J. Cornick
A COMPUTER MODEL FOR CALCULATIONG STEEP-FRONTED SURGE DISTRIBUTION IN MACHINE WINDINGS
IEEE Trans. on Energy Conversion, Vol 4 (1989), No.1, p. 95-101.

[4.5] Reckleff, J.G. and J.K. Nelson, R.J. Musil, S. Wenger
CHARACTERIZATION OF FAST RISE-TIME TRANSIENTS WHEN ENERGIZING LARGE 13.2 kV MOTORS.
IEEE Trans. on Power Delivery, Vol. 3 (1988), No. 2, p. 627-636.

[4.6] Wright, M.T. and S.J. Yang, K. McLeay
GENERAL THEORY OF FAST-FRONTED INTERTURN VOLTAGE DISTRIBUTION IN ELECTRICAL MACHINE WINDINGS.
IEE Proc. B Electric Power Applications, Vol. 130 (1983), No. 4, p. 245-256.

[5.1] Rüffer, K.
SCHALTEN VON ELEKTROMOTOREN
Berlin: VEB Verlag Technik, 1990.

[5.2] Paloniemi, P. and A. Ristola
BASICS OF MULTI-STRESS AGING TESTS: SURVEY OF ACTUAL OPERATING CONDITION OF LARGE INDUSTRIAL MOTORS.
In: Conference Record of the 1990 IEEE Int. Symp. on Electrical Insulation. Toronto, 3-6 June 1990.
New York: IEEE, 1990, Vol. 11, p. 4-7.

[5.3] Montanari, G.C. and M. Cacciari
A PROBALISTIC LIFE MODEL FOR INSULATING MATERIALS SHOWING ELECTRICAL THRESHOLDS.
IEEE Trans. on Electrical Insulation, Vol. 24 (1989), No. 1, p. 127-134.

[5.4] SWITCHING SURGE IN VACUUM CIRCUIT BREAKERS AND VACUUM CONTACTORS. Chapter 3: Insulation coordination.
TOSHIBA Internal Report

[5.5] Matsunobu, K. and F. Aki, K. Kadotani
AN ANALYSIS OF INSULATION AGEING OF GENERATOR STATOR WINDINGS
In: Conference Record of the 1984 Int. Symp. on Electrical Insulation. Montreal, 11-13 June, 1984
New York: IEEE, 1984, Vol. 5, p.258-261

[5.6] Stone, G.C. and R.G. van Heeswijk, R. Bartnikas
INVESTIGATION OF THE EFFECT OF REPETITIVE VOLTAGE SURGES ON EPOXY INSULATION.
IEEE Trans. on Energy Conversion, Vol. 7 (1992), No. 4, p. 754-759.

[5.7] Gupta, B.K. and B.A. Lloyd, D.K. Sharma
DEGRADATION OF TURN INSULATION IN MOTOR COILS UNDER REPETITIVE SURGES.
IEEE Trans. on Energy Conversion, Vol. 5 (1990), No. 2, p. 320-326.

[5.8] Walker, P. and J.N. Champion
EXPERIENCE WITH TURN INSULATION FAILURES IN LARGE 13.2 KV SYNCHRONOUS MOTORS.
IEEE Trans. on Energy Conversion, Vol. 6 (1991), No. 4, p. 670-676.

With the laplacian method the solution for the differential problem of figure I.1 can be calculated in the s-domain and transformed back into the time domain. This appendix shows how to solve the problem presented in figure I.1.

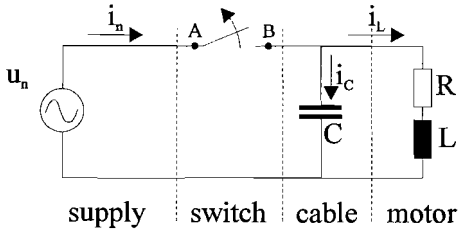

Fig I.1: One phase electric circuit of a motor

The inductance and capacitance of the load side (not drawn) will have two results on the transient recovery voltage (u_{TRV}) when opening the switch:

- the voltage loss over the supply inductance results $u_B < u_n$
- the transient phenomenon on the supply side (u_A) will influence the u_{TRV} ($u_{TRV} = u_A - u_B$)

These two influences will not exceed 10% of the $\hat{u}_B$ in the worst case situation. Since these minor influences cause a major increase in the calculations, the supply side is neglected in further calculations.

Before the switch is opened the following relations apply:

$$\begin{aligned} u_n &= \hat{U}\sin(\omega t + \varphi + \Phi) \\ i_n &= \hat{I}\sin(\omega t + \Phi) \end{aligned} \qquad \text{(I.1)}$$

with:

φ = atan($\omega L/R$)

Φ = opening angle

The initial situation per unit is characterized with the following changes:

$$\begin{aligned} u_A(0_-) &= u_n = \sin(\varphi + \Phi) \\ u_B(0_-) &= u_n = U_{B0} \\ i_n(0_-) &= i_n = I_{chop} \\ i_L &= i_n >> i_C \end{aligned} \quad \Rightarrow \quad \begin{aligned} u_A(0_+) &= u_n \\ u_{AB}(0_+) &= u_{TRV} \\ i_n(0_+) &= 0 \\ i_L &= -i_C \end{aligned} \qquad \text{(I.2)}$$

These changes define the differential equations on t = 0, written in the s-domain the equations to solve for the load side are:

$$\begin{aligned} R i_{Ls} + sL i_{Ls} - L I_{chop} &= u_{Bs} \\ u_{Bs} &= \frac{i_{Cs}}{sC} + \frac{U_{B0}}{s} \end{aligned} \qquad \text{(I.3)}$$

Since $i_C = -i_L$ we can eliminate the current in equation I.3 and find the solution for u_B in the s-domain.

$$-sRCu_{Bs} + RCU_{B0} - s^2LCu_{Bs} + sLCU_{B0} - LI_{chop} = u_{Bs} \quad \Rightarrow$$
$$u_{Bs} = \frac{U_{B0}(RC + sLC) - LI_{chop}}{s^2LC + sRC + 1} \tag{I.4}$$

For transformation into the time domain we have to rearrange the solution:

$$u_{Bs} = \frac{U_{B0}(RC + sLC) - LI_{chop}}{\left((s+\beta_t)^2 + \omega_{in}{}^2\right)LC} \tag{I.5}$$
$$\beta_t = \frac{R}{2L}$$
$$\omega_{in}{}^2 = \omega_0{}^2 - \beta_t{}^2 \quad ; \quad \omega_0 = \sqrt{\frac{1}{LC}}$$

into:

$$u_{Bs} = \left[\frac{U_{B0}C\beta_t - I_{chop}}{\omega_{in}C}\right] \cdot \frac{\omega_{in}}{(s+\beta_t)^2 + \omega_{in}{}^2} \quad + \quad U_{B0} \cdot \frac{s+\beta_t}{(s+\beta_t)^2 + \omega_{in}{}^2} \tag{I.6}$$

With equation I.6 and the standard transformations for the laplacian calculation method we can transform the equation into the time domain:

$$u_B(t) = \left[\frac{U_{B0}C\beta_t - I_{chop}}{\omega_{in}C}\right] \cdot e^{-\beta_t t} \cdot \sin(\omega_{in}t) \quad + \quad U_{B0} \cdot e^{-\beta_t t} \cdot \cos(\omega_{in}t) \tag{I.7}$$

By using goniometric calculations this can be written as:

$$u_B(t) = U^* \cdot e^{-\beta_t t} \cdot \cos(\omega_{in}t - \psi) \tag{I.8}$$

with:

$$U^* = \sqrt{\left[U_{B0} - \frac{I_{chop}}{C\beta_t}\right]^2 \cdot \frac{\beta_t{}^2}{\omega_{in}{}^2} + U_{B0}{}^2}$$
$$\psi = \operatorname{atan}\left[\frac{\beta_t}{\omega_{in}} - \frac{I_{chop}}{\omega_{in}CU_{B0}}\right]$$

A simulation is done for a single phase motor circuit with these parameters:

- 3 kV supply voltage
- power factor of 0.1
- $I_{chop} = 2$ A
- $\hat{I} = 50$ A
- $R = 6\ \Omega$
- $L = 187$ mH
- $C = 80$ nF

Giving :

- transient recovery voltage over the switch : $u_{TRV} = u_A - u_B$
- prospective overvoltage over the motor : u_B

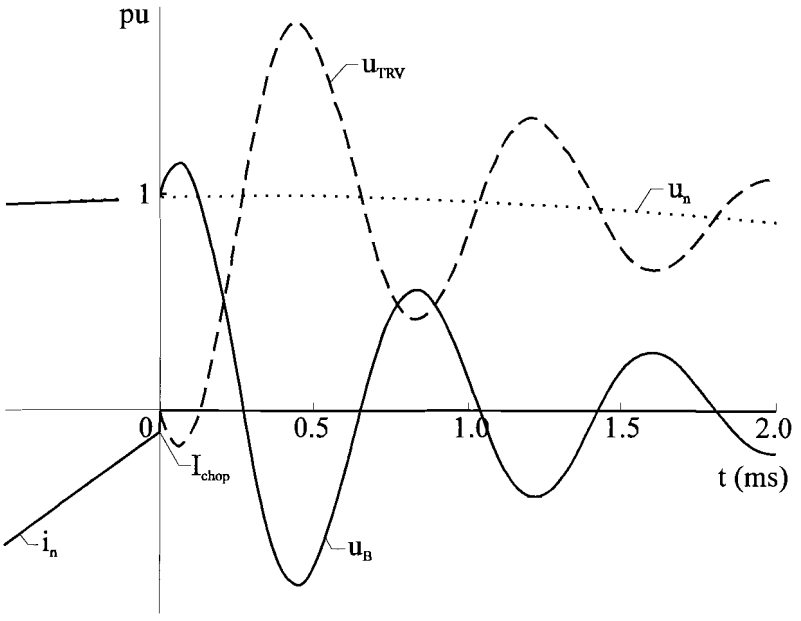

Fig I.2: Transient voltages when opening.

In this case the prospective overvoltage does not exceed the TRV and both overvoltages are not the main cause for stress on the first turns of the motor. However if the TRV has a reignition, a much steeper wavefront will enter the cable and cause the stress on the motor.

The internal characteristic impedance (Z_i) of a motor is given by:

$$Z_i = \sqrt{\frac{L_i}{C_i}} \qquad \text{(II.1)}$$

where:

L_i = inductance of the motor (L)
C_i = internal capacitance

In a CIGRE-report [Elektra 75] the Z_i is measured for motors. A graphical impression of the Z_i as a function of the power of the moter is given in fig II.1 for different supply voltages.

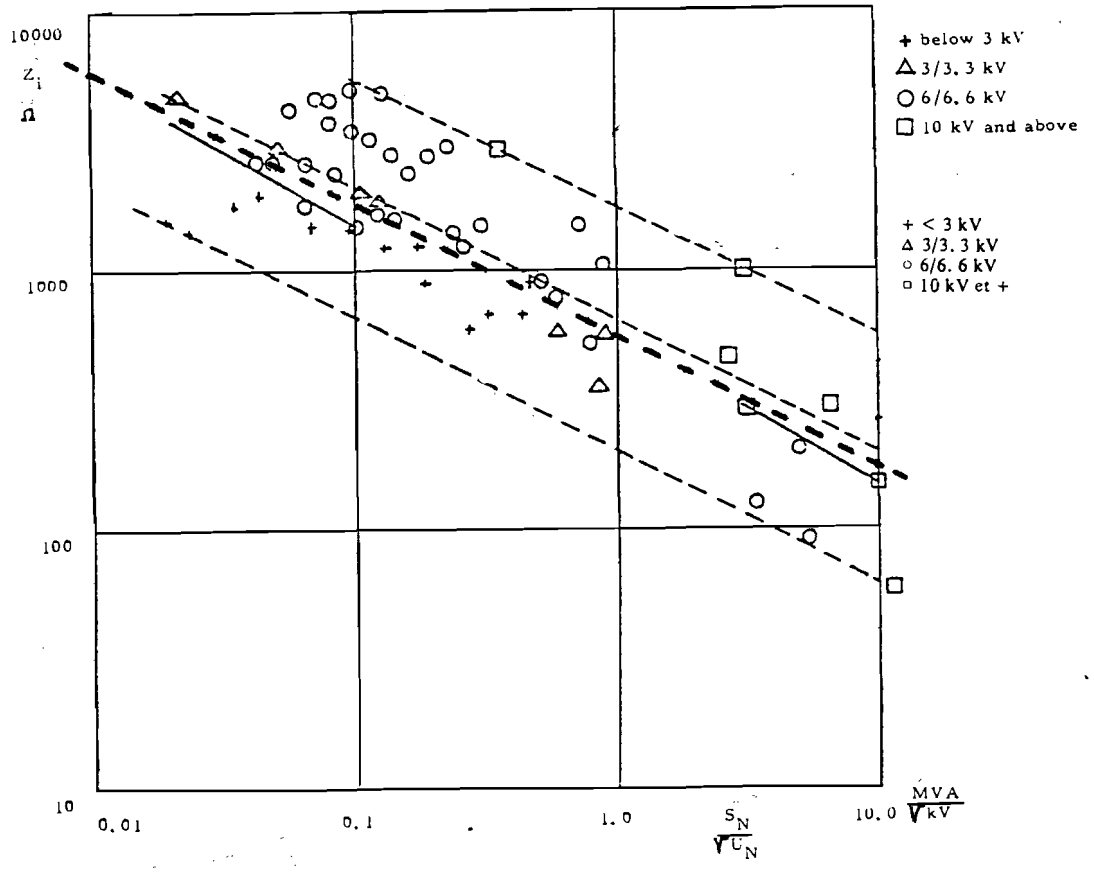

Fig II.1: Surge impedance of rotating machines

In our case, with a supply voltage of 3 kV, the thick dotted line is of importance. By exctracting the function for this line the Z_i can be determined.

With $(x_1,y_1) = (1.73\ 10^3, 5910)$
$(x_2,y_2) = (1.73\ 10^7, 174)$
we can determine the slope of the line:

$$m = \frac{\Delta \log(Z_i)}{\Delta \log(S)} = \frac{\log(5910) - \log(174)}{\log(1.73\ 10^7) - \log(1.73\ 10^3)} \approx -0.5 \tag{II.2}$$

From equation II.2 we can determine Z_i as function of S for a supply voltage of 3 kV:

$$\Delta \log(Z_i) = -0.5 \log(S) \quad \Rightarrow \quad Z_i = 8.27\ 10^5\ S^{-\frac{1}{2}} \tag{II.3}$$

In chapter 2.2.4 we have calculated L as a function of S^{-1}:

$$L = \frac{3U^2\sqrt{1-\cos^2\varphi}}{\omega S} = \frac{X'}{S} \tag{II.4}$$

Combining equations II.1, II.3 and II.4 we get:

$$Z_i = \sqrt{\frac{L}{C_i}} = \sqrt{\frac{X'}{SC_i}} = 8.27\ 10^5\ S^{-\frac{1}{2}} \quad \Rightarrow \quad C_i = \frac{X'}{\left(8.27 \cdot 10^5\right)^2} \tag{II.5}$$

For a motor supplied with a 3 kV, 50 Hz supply voltage system we get:

$$C_i = 18\ \text{nF} \tag{II.6}$$

Source code for calculating the cable constants.

```
begin new data case
cable constants
c UNDERGROUND CLASS B CABLE WITH 3 CONDUCTORS, PIPE UNGROUNDED IN HOMOG. EARTH
branch       RA    RB    YA    YB    BA    BB    PI    PO
    3   -1    3     0     1     1     1     1     0
c PIPE PARAMETERS
   13.6E-3   15.5E-3   17.0E-3    2.10E-7       1.0        2.2        2.2
c LOCATION OF THE MIDDLE OF THE INNER CONDUCTORS
    6.0E-3        0.0     6.0E-3      120.0     6.0E-3      240.0
c INNER CONDUCTOR HAS: CORE / + SHEATH / + ARMOR = 1 / 2 / 3
    1     1     1
c INNER CONDUCTOR PARAMETERS
   0.00E+0   2.26E-3   5.00E-3
   1.70E-8        1.0        1.0        2.2
   0.00E+0   2.26E-3   5.00E-3
   1.70E-8        1.0        1.0        2.2
   0.00E+0   2.26E-3   5.00E-3
   1.70E-8        1.0        1.0        2.2
c PIPE LOCATION INTO THE GROUND
   3.00E-1
c FREQ CARDS          ┌──── freq used for high transient simulations
          100.0  5.0E5              100.00 1
c                                     └──── length of the cable
blank card ending frequency cards
blank card ending cable constants
$punch, ca_105.pch  { ca_[length of cable/power of freq used].pch }
begin new data case
blank card ending session
```

Source code for calculating the propagation in cables

```
begin new data case
exact phasor equivalent              {not lumped R
c MISC. DATA CARDS
   1.E-8   5.E-6    5.E5    5.E5     {freq = 5E5
     100       1               1                                  1
$INCLUDE ca_105.pch
blank card ending branch cards
c SWITCHES
c      PI   -4.E-3     5.E-3          {PIPE GROUNDED
c      PO   -4.E-3     5.E-3
blank card ending switch cards
12     RA 0     10.0E3               0.1E-6   {0.1 us Trise}        5.0E-8
blank card ending source cards
       RA     RB
blank card ending output request
blank card ending plot cards
begin new data case
blank card ending session
```

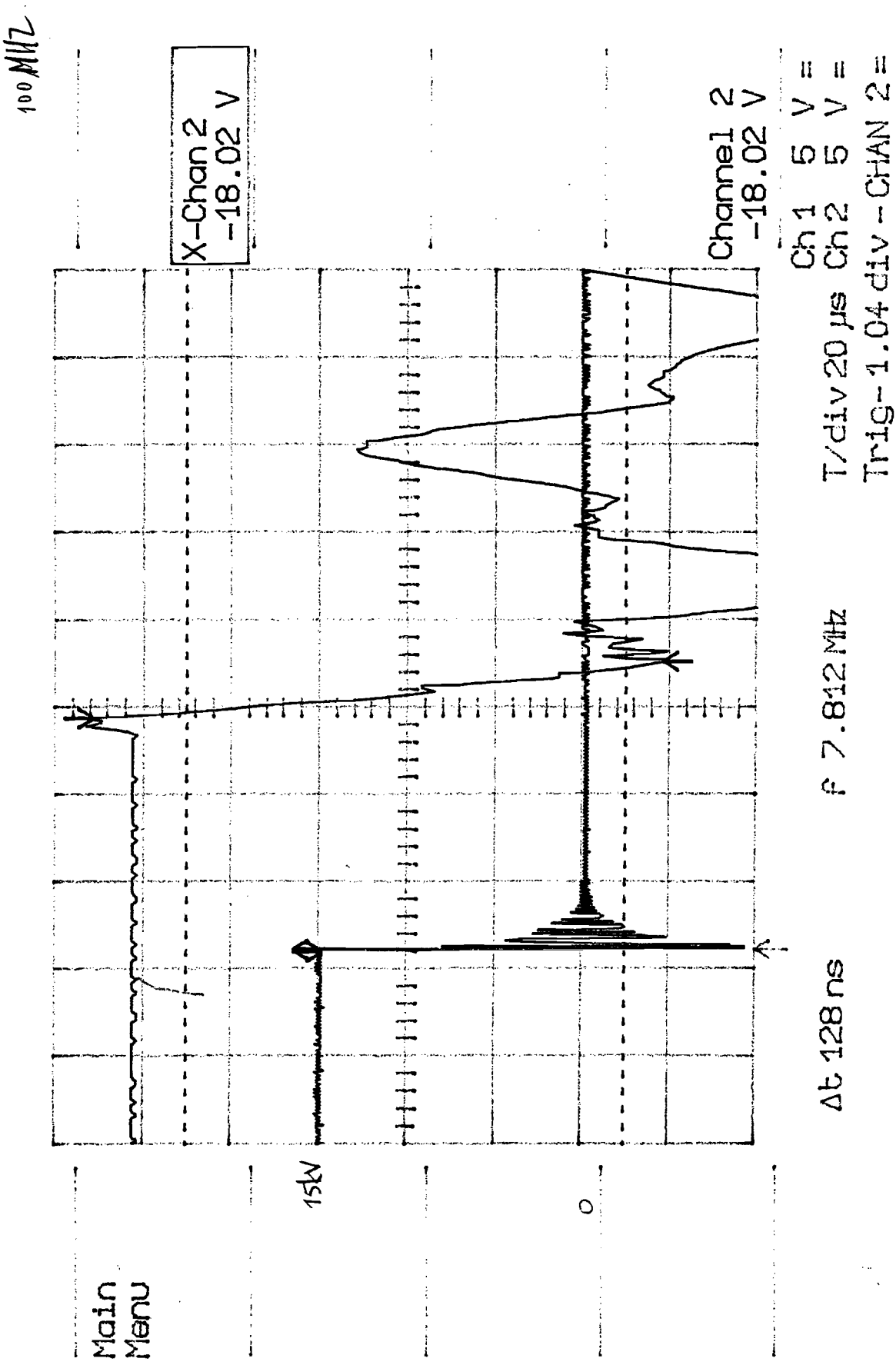
100 MHz
X-Chan 2
-18.02 V
Channel 2
-18.02 V
Ch1 5 V =
Ch2 5 V =
T/div 20 µs
Trig- 1.04 div - CHAN 2 =
f 7.812 MHz
Δt 128 ns
15W
0
Main
Menu

Schatting van spoelinductiviteiten en -capaciteiten, bepalend voor het stootspanningsgedrag bij hoogspanningsmotoren

EMV 95-10

Inleiding

Door dr. ir. R.P.P. Smeets van de vakgroep Elektrische Energiesystemen (EG) is mij [1] verzocht op korte termijn een schatting van de orde van grootte te maken van de inductiviteiten en capaciteiten van de spoelen waaruit de wikkelingen van elektrische kortsluitankermotoren bestaan. De waarden van die inductiviteiten en capaciteiten dienen voor de bepaling van het elektrisch gedrag van de motoren bij onderwerping aan zogenaamde stootspanningen. De beoogde motoren staan op de ISLA-raffinaderij [2] te Curaçao en hebben nominale vermogens rond 1 MW, zijn aangesloten op spanningen van 3 tot 6 kV bij 50 Hz en hebben verschillende pooltallen. Het verzoek is gedaan binnen het kader van een contract dat de Technische Universiteit Eindhoven heeft gesloten met ISLA en waarvan dr. Smeets projectleider is.

Werkwijze

Een berekening van de capaciteit van een spoel naar machinemassa/aarde en van de statorlekinductiviteit -die bepalend zijn voor het stootspanningsgedrag van een inductiemotor- lijkt zonder ontwerpgegevens van motoren van willekeurig fabrikaat niet goed mogelijk. Omdat ik nog beschikte over enkele confidentiële ontwerpgegevens [3] van HOLEC-hoogspanningsmotoren [4] uit de zogenaamde EMCOL-serie en daarnaast nog beschikte over een brochure betreffende twee- en vierpolige EMCOLs, heb ik deze motoren als uitgangspunt voor een eerste schatting genomen. De fabricage van EMCOLs is in het begin van de tachtiger jaren gestaakt. Het zal duidelijk zijn dat op deze basis niet zonder nader onderzoek harde uitspraken gemaakt kunnen worden over moderne hoogspanningsmotoren van HOLEC, noch over hoogspanningsmotoren van ander fabrikaten. Voor zes, acht en tienpolige motoren moet een extrapolatie gemaakt worden [5]; dit is hier niet uitgevoerd. Gezien de constuctiewijzen van hoogspanningsmotoren verwacht ik voor de motoren met pooltallen 2 en 4 echter geen afwijkingen van de hier gemaakte schattingen van de spoelcapaciteit met een factor 5 en van de spoelinductiviteit met een factor 10 of groter.

De spoelen van hoogspannings-kortsluitankermotoren zijn in het algemeen vormspoelen. Ze worden gewikkeld met geïsoleerde [6] rechthoekige draden, zodanig dat de doorsnede van de spoel ook weer rechthoekig is. Na het wikkelen worden ze in een gezet in een langgerekte zeskant vorm. Hierna

1 ir. R.W.P. Kerkenaar, vakgroep Elektromechanica en Vermogenselektronica (EMV), Techn. Univ. Eindhoven.

2 Refineria ISLA (Curazao) S.A., Affiliate of Petroleos de Venezuela S.A., verder hier aan te duiden met ISLA.

3 De gegevens hadden betrekking op isolatie-dikten, gleufcombinaties en gleufafmetingen van EMCOL-machines. Wegens het confidentiële karakter van die gegevens zullen ze niet zonder toestemming van HOLEC in dit rapport worden opgenomen. Omdat de EMCOL-serie allang uit productie is, bestaat de mogelijkheid dat HOLEC bereid is die ontwerpgegevens vrij te geven.

4 Bedoeld worden machines welke geschikt zijn voor spanningen tussen 1 en 11 kV (eventueel tot 22 kV bij generatoren); in verband met de bij distributienetten gebruikelijke nomenclatuur zou het minder verwarrend zijn indien men deze machines zou aanduiden als middenspanningsmachines. In dit rapport zullen de bedoelde machines als hoogspanningsmachines worden aangeduid.

5 Bij de opdracht is geen nadere aanduiding van het pooltal aangegeven.

6 Een draadisolatie bijvoorbeeld bestaande uit polyesterimide met een dubbele glasvezel-omspinning.

wordt de gleuf- en spoelkopisolatie -een samenstelling van epoxy en mica- - in niet- of semi-uitgeharde toestand aangebracht. Over het gedeelte van de spoel dat in de gleuven wordt geplaatst -het gleufdeel- wordt een halfgeleidend laag/folie aangebracht: deze dient de potentiaal te vereffenen dat ontstaat tussen geleider en de ruwe gleufwand. Deze halfgeleidende laag steekt in axiale richting enkele centimeters buiten het blikpakket uit. Afhankelijk van het toegepaste isolatiesysteem worden worden de isolaties daarna al of niet geïmpregneerd en uitgehard [7]. De spoelen hebben in het algemeen alle dezelfde afmetingen en worden in twee lagen in rechthoekige open gleuven aangebracht. De gleuven worden met niet- of halfmagnetische spieën afgesloten. Bij minder gangbare en duurdere systemen -voornamelijk in generatoren- worden voorgevormde spoelzijden, als staven, axiaal in halfgesloten gleuven geschoven en vervolgens aan de uiteinden gelast in een edelgas-omgeving. Voor dit rapport is de essentie van de voorgaande korte beschrijving dat de capaciteit van een spoel wordt gevormd door de geleider, de gleuf-isolatie en de halfgeleidende laag. De capaciteit wordt dan bepaald door:

- de relatieve permitiviteit van de gleuf-isolatie: deze is hier gesteld op een enigszins willekeurige waarde 5 [8];
- de dikte van de gleuf-isolatie [9];
- de axiale lengte van een spoel: deze is geschat uit de as-harthoogte van de machine [10].

De aanloopstroom/blokkeerstroom van een inductiemachine wordt voornamelijk bepaald door de (totale) lekreactantie bij 50 Hz. Deze is eenvoudig uit een machinebrochure te halen. Voor de bepaling van de lekinductiviteit per spoel is het noodzakelijk het aantal spoelen van een fase te weten: voor een driefasige machine met een tweelaagswikkeling is dit gelijk aan het aantal (stator)gleuven gedeeld door 3. Daarvan zijn de (2q) spoelen van een wikkeltak [11] bij 50 Hz vrijwel volledig inductief gekoppeld. Vanwege onduidelijkheid over de gevolgde weg van de flux is ook gerekend met niet inductief gekoppelde spoelen. Bij hoogspanningsmotoren zijn, vrijwel altijd, alle spoelen van een fase in serie geschakeld. Met de eerder genoemde confidentiële ontwerpgegevens waren de gleufcombinaties bekend. De frequentiecomponenten van stootspanningen zijn voor een aanzienlijk deel hoogfrequent; de hoogfrequente componenten veroorzaken relatief sterke wervelstromen in het blik. Hierdoor zullen de met de stootspanningen gekoppelde fluxen goeddeels over luchtwegen worden gedwongen; de mate waarin dit gebeurt en de frequentieafhankelijkheid daarvan is in dit korte onderzoek echter niet onderzocht. Vooralsnog is aangenomen dat slechts de statorlekinductiviteit en niet de lekinductiviteit van de rotor voornamelijk maatgevend is voor het stootspanningsgedrag [12]: hiervoor is de *helft* van de totale lekinductiviteit *bij 50 Hz* genomen. Dit is dan ook waarschijnlijk het meest zwakke punt in de schatting.

---

7 E: curing.

8 Nadere gegevens ontbreken; verwacht wordt dat de waarden van de relatieve diëlektrische permitiviteit van de gleufisolatie varieert tussen 3 en 5.

9 De islolatiedikte is gegeven in de bijlage met titel "Isolation thickness versus voltage for HOLEC high-voltage EMCOL cage motors".

10 Zie tabel 1: HOLEC EMCOL kortsluitankermotoren: huisgrootten (frame sizes H), *geschatte* blikpakketlengten en vermogens.

11 Gewoonlijk geeft men met q het aaltal gleuven per pool en fase aan; bij de gebruikelijke tweelaagswikkeling zijn er dan 2q (deel)spoelen per wikkeltak (of zo u wilt per poolpaar en fase). Voor de besproken tweepolige motoren bereikt 2q waarden van 16 en 20; voor de vierpolige machines is 2q gelijk aan 10. Voor motoren met hogere pooltallen kan men voor 2q waarden verwachten van 4 tot 8.

12 E: coil surge inductance

Conclusie

Een berekening van de capaciteit van een spoel naar machinemassa/aarde en van de statorlek-inductiviteit, beide bepalend voor het stootspanningsgedrag, lijkt zonder ontwerpgegevens van motoren van willekeurig fabrikaat niet mogelijk.

Voor de beschouwde HOLEC-motoren geldt bij een vermogens rond 1 MW dat:

- de geschatte capaciteit van een spoel naar machinemassa 2.5 nF [13] bedraagt;
- de geschatte statorlekinductiviteit (bij 50 Hz) -dat bepalend lijkt te zijn voor het stootspannings-gedrag- voor inductief gekoppelde spoelen in twee- en vierpolige 3 kV-motoren 20..60 μH is, voor tweepolige inductief gekoppelde spoelen in 6 kV-motoren 60..80 μH is en voor vierpolige inductief gekoppelde spoelen in 6 kV-motoren 80..100 μH is [14] (de geschatte statorlekinductiviteit bij niet inductief gekoppelde spoelen is : 2- en 4 polige 3 kV : 0.4..0.6 mH en voor de 2- en 4 polige 6 kV motoren : 0.9..1.2 mH[15]);
- de verwachte vertragingstijden van de stootspanningen voor alle beschouwde motoren tussen de 0.3 en 0.6 μs liggen. Voor de ongekoppelde spoelen geldt een vertragingstijd van 1 á 2 μs.

De schatting van de spoelinductiviteit en in het bijzonder het deel van die inductiviteit dat maat-gevend is voor het stootspanningsgedrag, is naar verwachting het meest zwakke punt in de schatting.

Er is (nog) geen extrapolatie gemaakt voor de waarden van spoelcapaciteit en -lekinductiviteit voor motoren met pooltallen 6 en hoger.

Zowel capaciteit als lekinductiviteit lijken binnen het beschouwde vermogensbereik, dat zich uitstrekt van 300 tot 2200 kW, vrijwel onafhankelijk van het machine-vermogen te zijn. Een relatie met de lengte van het blikpakket van de machine is vooralsnog alleen met betrekking tot de capaciteit, aannemelijk gemaakt [16].

Er is geen enkele ijkpunt beschikbaar zodat over de nauwkeurigheid van de schatting geen uitspraak gedaan wordt.

ir. R.W.P. Kerkenaar,
vakgroep Elektromechanica en Vermogenselektronica (EMV), Techn. Univ. Eindhoven.
95.07.04.

13 Zie de bijlagen getiteld: " Estimated coil to ground capacitance of HOLEC High Voltage EMCOL 2-pole cage motors " en " Estimated coil to ground capacitance of HOLEC High Voltage EMCOL 4-pole cage motors ".

14 Blijkens de brochure bedraagt de aanloopstroom van zowel 3 als 6 kV machines ongeveer 600 A: de lekinductiviteit van de 6 kV-motoren moet dus grofweg twee-maal groter dan die van de 3 kV-motoren zijn. De grotere lekreactantie kan constructief onder meer bereikt worden door toepassing van relatief smallere en diepere gleuven, door het aanbrengen van zogenaamde strooidammen en door het toepassen van half-magnetische spieën.

15 Zie de bijlagen getiteld: " Estimated coil surge-inductance of HOLEC High Voltage EMCOL 2-pole cage motors " en " Estimated coil surge-inductance of HOLEC High Voltage EMCOL 4-pole cage motors ".

16 Zie de bijlagen getiteld: " Estimated coil to ground capacitance of HOLEC 3 kV EMCOL 2- and 4-pole cage motors versus the estimated stack length " en " Estimated coil to ground capacitance of HOLEC 6 kV EMCOL 2- and 4-pole cage motors versus the estimated stack length ".

		R-20	R-10	2 polen	4 polen	6 polen	8 polen	2 polen	4 polen	6 polen
		ratio	estimated	50Hz	50Hz	50Hz	50Hz	50Hz	50Hz	50Hz
		1.12202		3..3.3 kV	3..3.3 kV	3..3.3 kV	3..3.3 kV	6..6.6 kV	6..6.6 kV	6..6.6 kV
type	huisgrootte	h	pakket-lengte	P	P	P	P	P	P	P
		m	m	kW	kW	kW	kW	kW	kW	kW
140KE	450M	0.450	0.450	400				315		
140KE	450L	0.450	0.560	450						
162KE	500VS	0.500	0.355		560					
162KE	500S	0.500	0.400	500	630					
162KE	500S	0.500	0.400	560	710					
162KE	500M	0.500	0.500	630	800			315	560	
162KE	500M	0.500	0.500	710				400	630	
162KE	500M	0.500	0.500					450		
162KE	500M	0.500	0.500					500		
162KE	500L	0.500	0.630	800	900			560	710	
162KE	500L	0.500	0.630					630		
180KE	560VS	0.560	0.400						800	
180KE	560VS	0.560	0.400						900	
180KE	560S	0.560	0.450	900				710	1000	
180KE	560S	0.560	0.450	1000				800		
180KE	560M	0.560	0.560	1120				900	1120	
180KE	560M	0.560	0.560					1000		
180KE	560L	0.560	0.710					1120	1250	
180KE	560L	0.560	0.710					1250		
206KE	630VS	0.630	0.450		1400				1400	
206KE	630VS	0.630	0.450		1600				1600	
206KE	630VS	0.630	0.450		1800					
206KE	630S	0.630	0.500		2000				1800	
206KE	630M	0.630	0.630					1400	2000	
206KE	630L	0.630	0.800					1600		
230KE	710S	0.710	0.710					2000		
260KE	710M	0.800	0.800					2200		

tabel 1 HOLEC EMCOL kortsluitankermotoren: huisgrootten (frame sizes), *geschatte* blikpakketlengten en vermogens[17]

Estimated coil surge-inductance of HOLEC High-Voltage EMCOL 2-pole cage motors

uncoupled

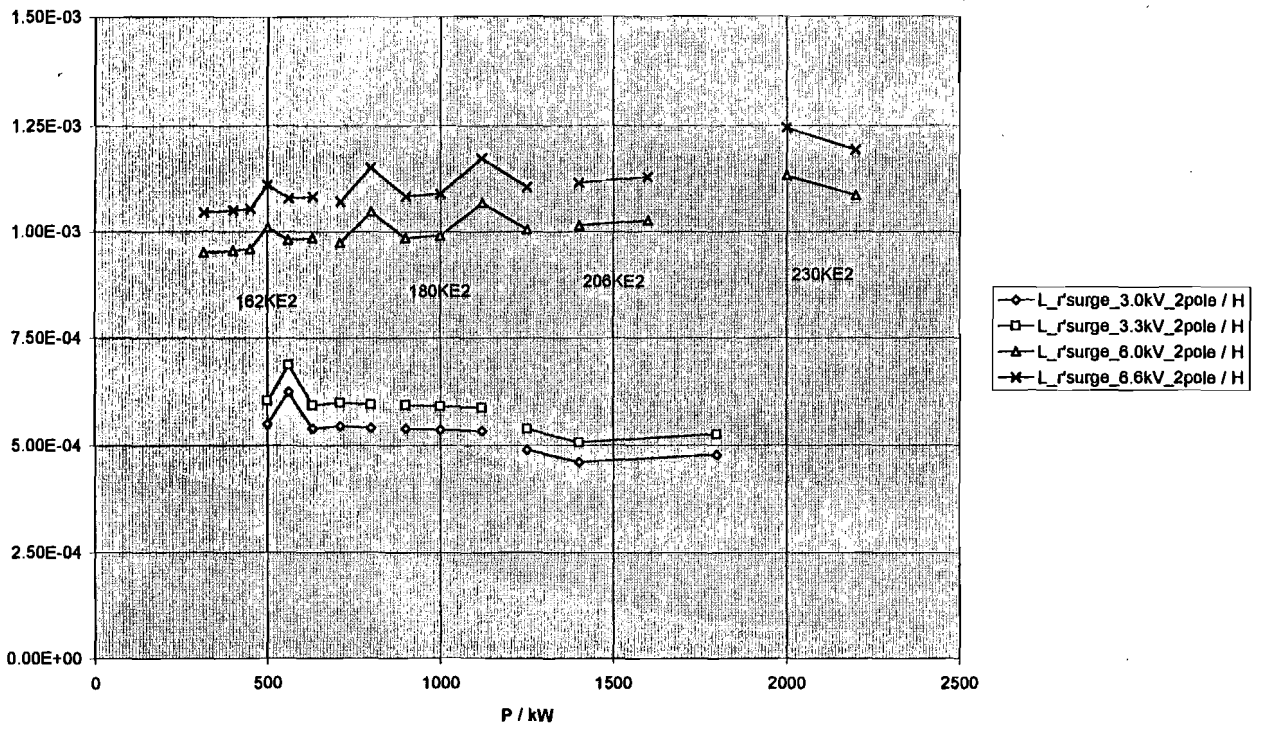

ISLA01J.XLS/EMV-rk/95.06.26-11:03

Estimated coil surge-inductance of HOLEC High-Voltage EMCOL 4-pole cage motors

uncoupled

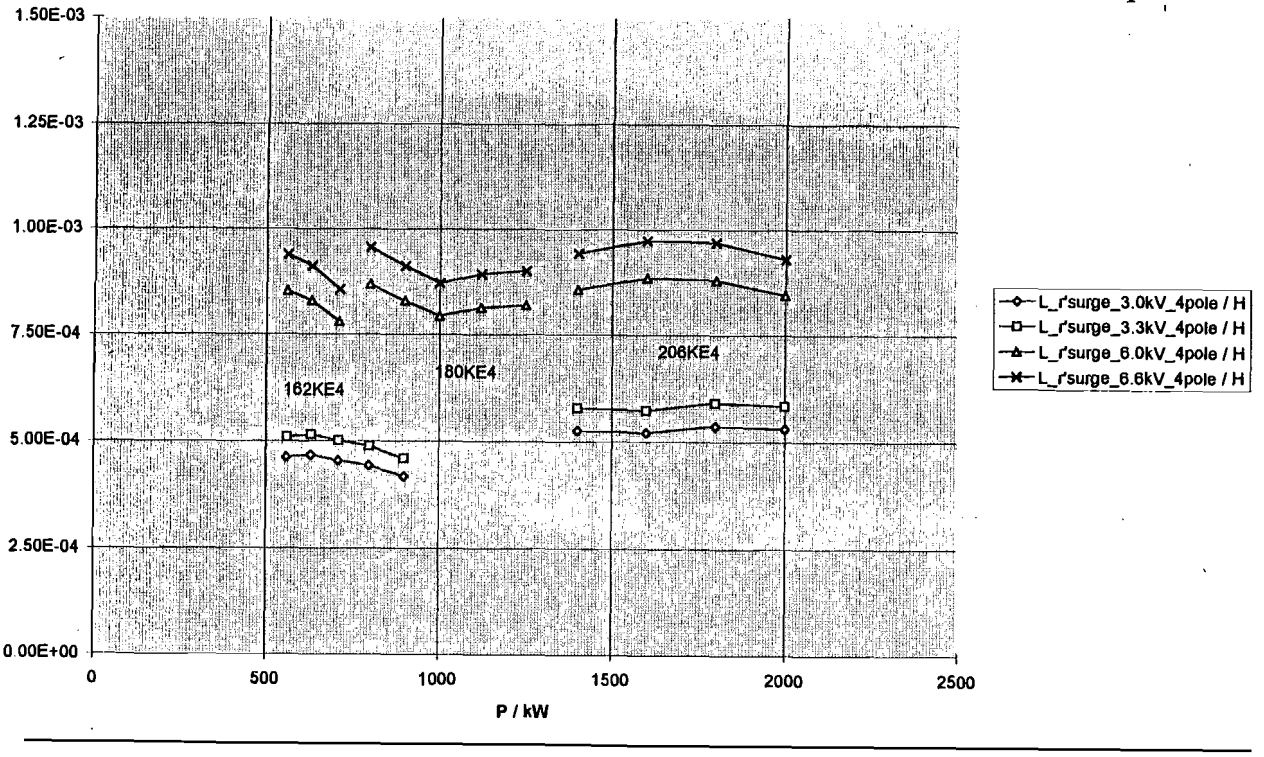

ISLA01J.XLS/EMV-rk/95.06.26-11:06

Estimated coil to ground capacitance of HOLEC High-Voltage EMCOL 2-pole cage motors

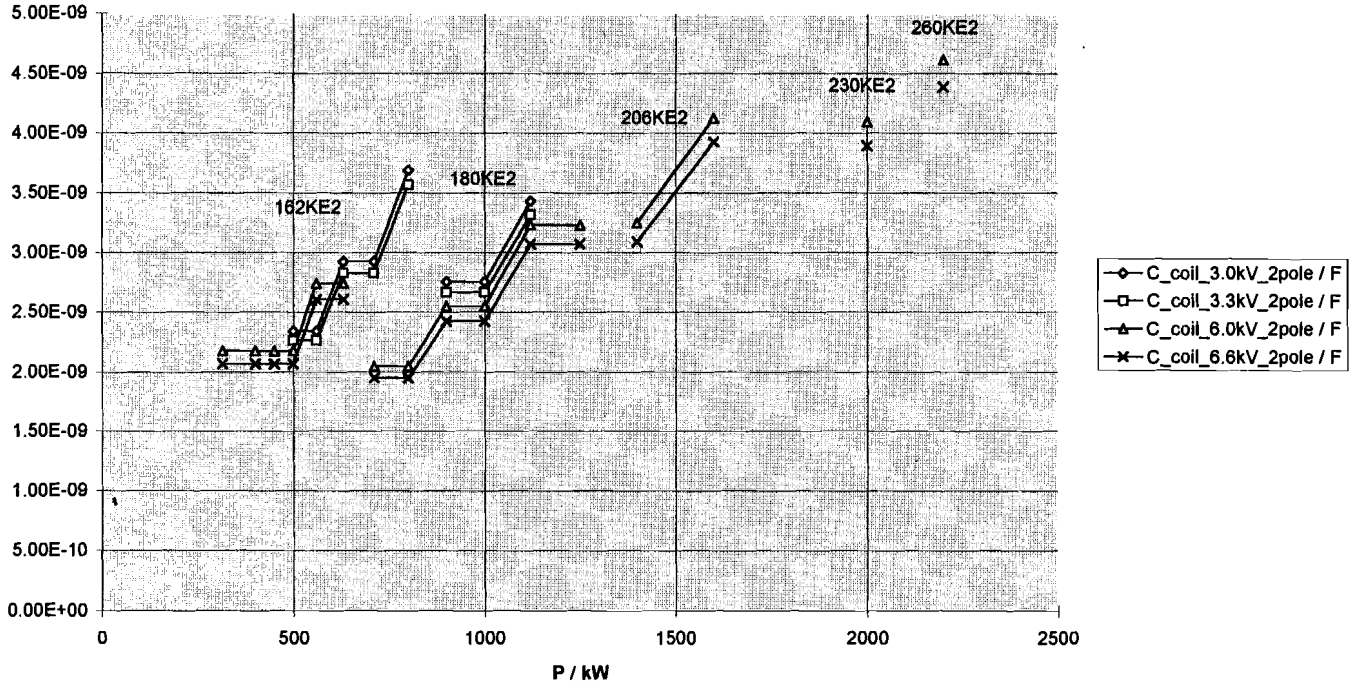

ISLA01J.XLS/EMV-rk/95 06.26-11:16

Estimated coil to ground capacitance of HOLEC High-Voltage EMCOL 4-pole cage motors

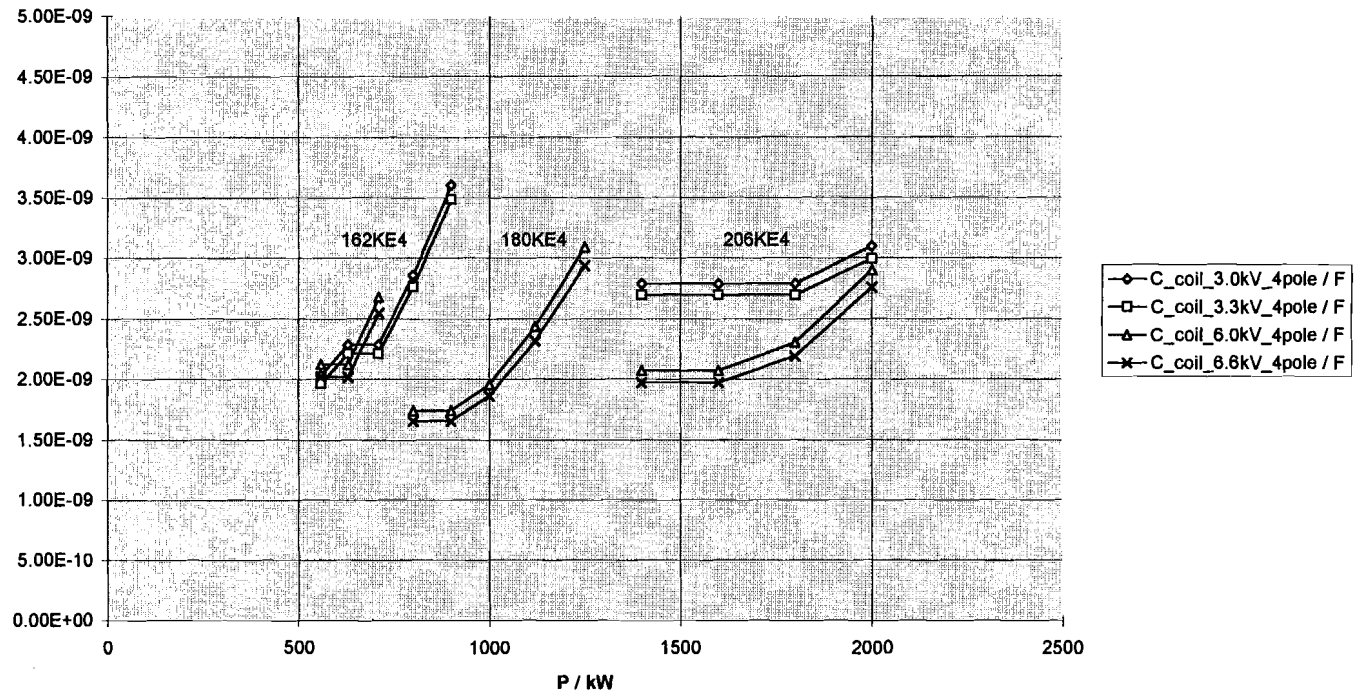

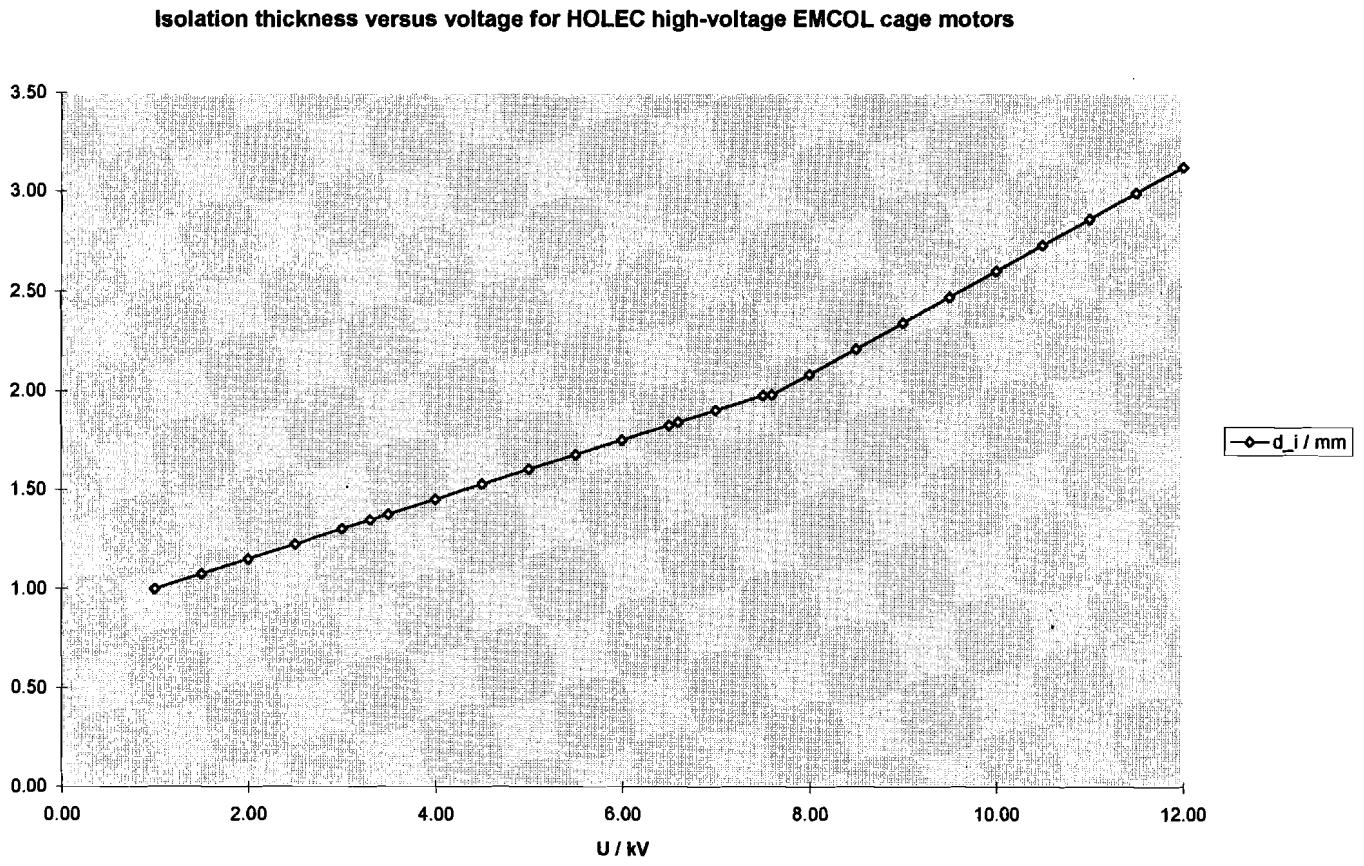
Isolation thickness versus voltage for HOLEC high-voltage EMCOL cage motors
3.50
3.00
2.50
2.00
1.50
1.00
0.50
0.00
0.00
2.00
4.00
6.00
8.00
10.00
12.00
U / kV
d_i / mm
ISLA01J.XLS/EMV-rk/95.08.26-22:23

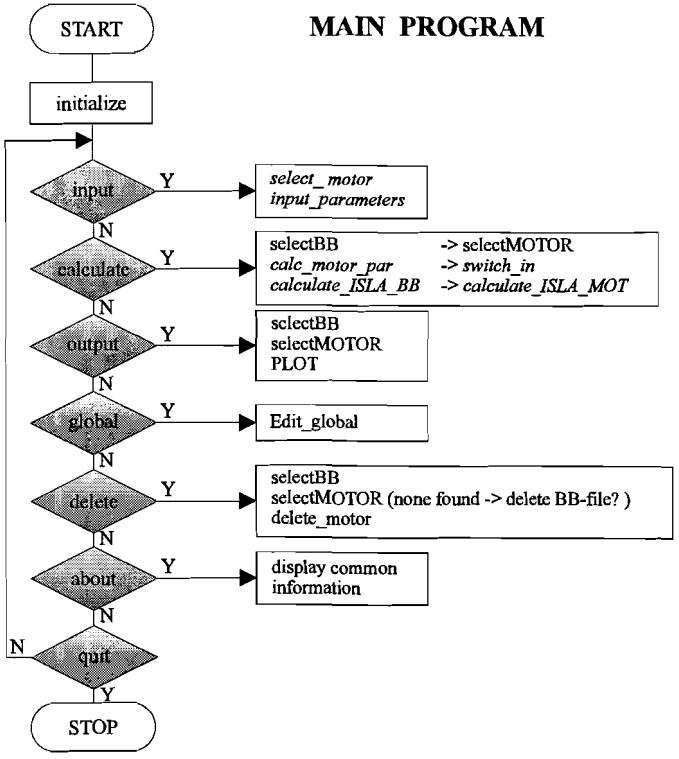
MAIN PROGRAM
START
initialize
input
Y
select_motor
input_parameters
N
calculate
Y
selectBB -> selectMOTOR
calc_motor_par -> switch_in
calculate_ISLA_BB -> calculate_ISLA_MOT
N
output
Y
selectBB
selectMOTOR
PLOT
N
global
Y
Edit_global
N
delete
Y
selectBB
selectMOTOR (none found -> delete BB-file?)
delete_motor
N
about
Y
display common information
N
quit
N
Y
STOP

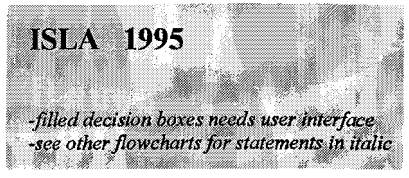
ISLA 1995
-filled decision boxes needs user interface
-see other flowcharts for statements in italic

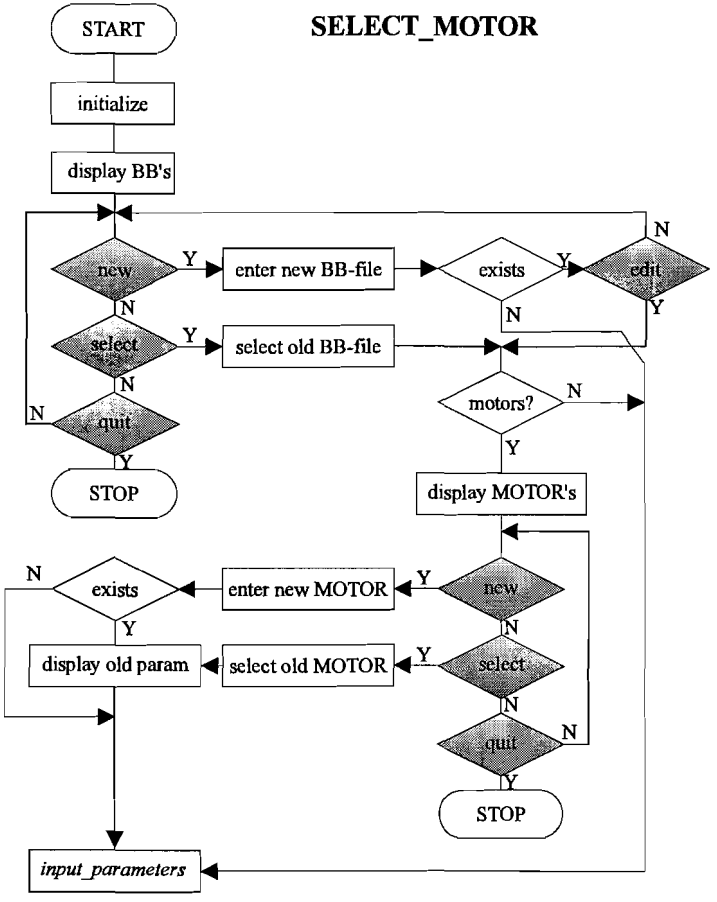
SELECT_MOTOR
START
initialize
display BB's
new
Y
enter new BB-file
exists
Y
edit
N
Y
N
select
Y
select old BB-file
N
motors?
N
N
quit
Y
Y
STOP
display MOTOR's
N
exists
enter new MOTOR
Y
new
Y
N
display old param
select old MOTOR
Y
select
N
quit
N
Y
STOP
input_parameters

INPUT_PARAMETERS

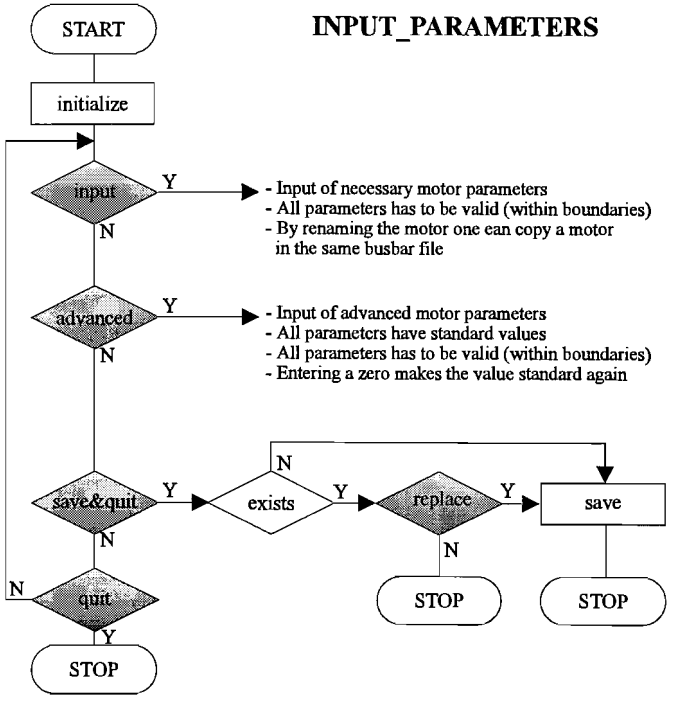

CALC_MOTOR_PAR

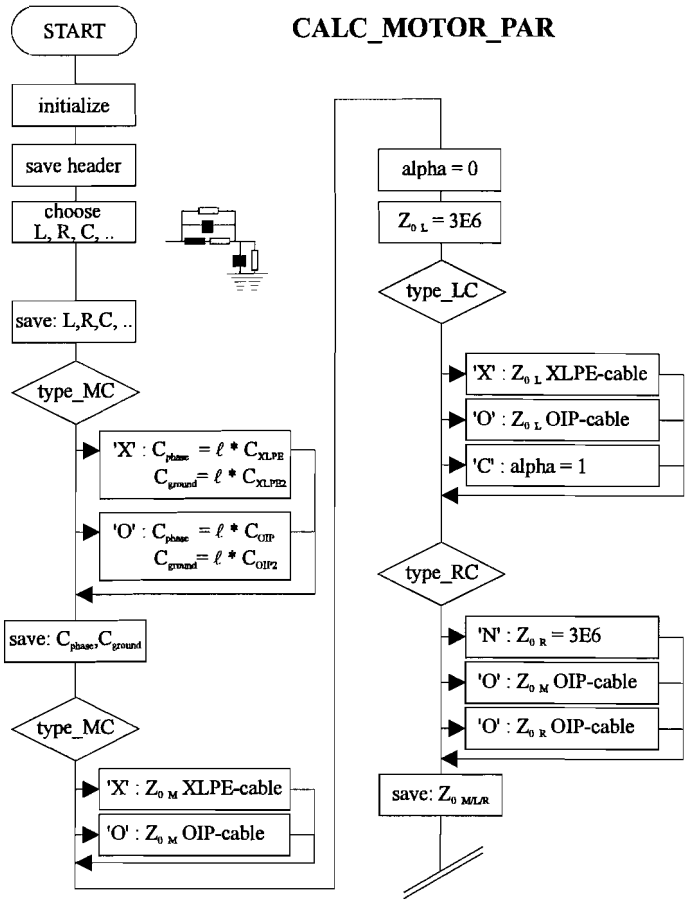

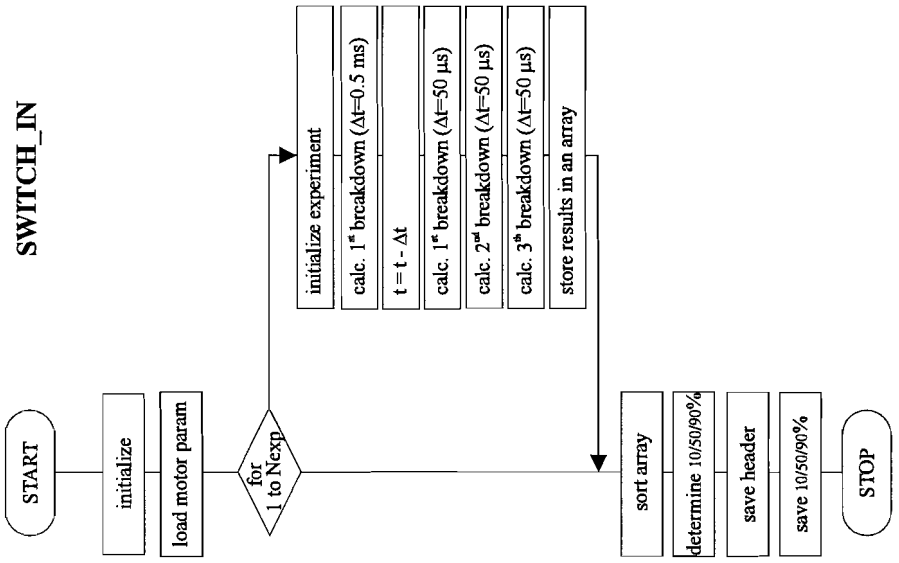
SWITCH_IN
START
initialize
load motor param
for
1 to Nexp
initialize experiment
calc. 1st breakdown (Δt=0.5 ms)
t = t - Δt
calc. 1st breakdown (Δt=50 µs)
calc. 2nd breakdown (Δt=50 µs)
calc. 3th breakdown (Δt=50 µs)
store results in an array
sort array
determine 10/50/90%
save header
save 10/50/90%
STOP

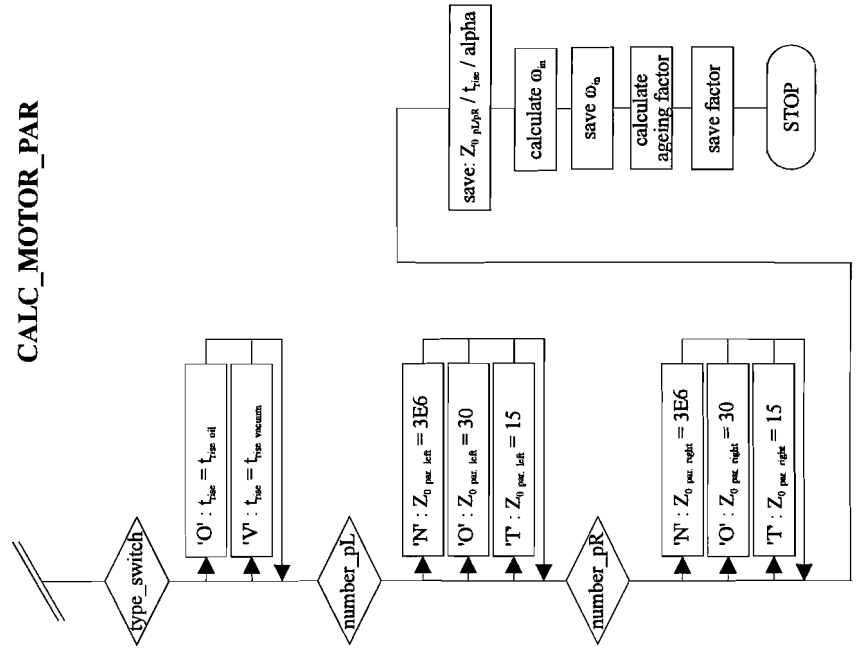
CALC_MOTOR_PAR
type_switch
'O' : t_spec = t_type oil
'V' : t_spec = t_type vacuum
number_pL
'N' : Z0 pat. left = 3E6
'O' : Z0 pat. left = 30
'T' : Z0 pat. left = 15
number_pR
'N' : Z0 pat. right = 3E6
'O' : Z0 pat. right = 30
'T' : Z0 pat. right = 15
save: Z0 pL/pR / t_spec / alpha
calculate ωm
save ωm
calculate ageing factor
save factor
STOP

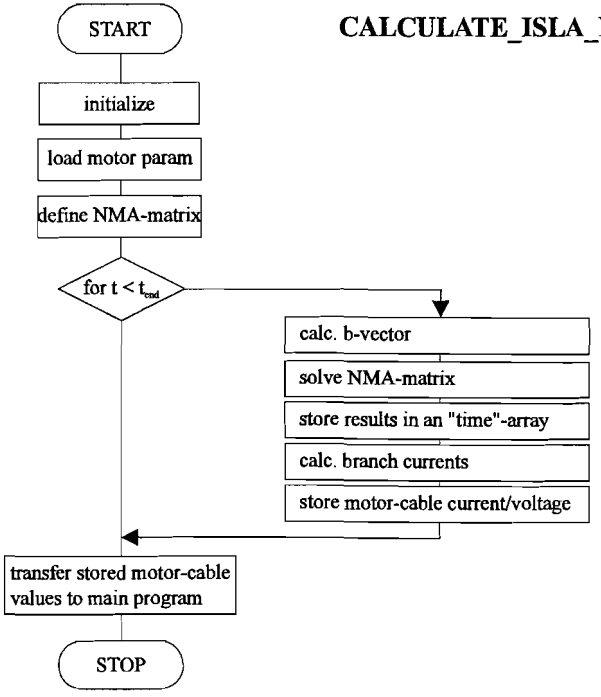

CALCULATE_ISLA_BB

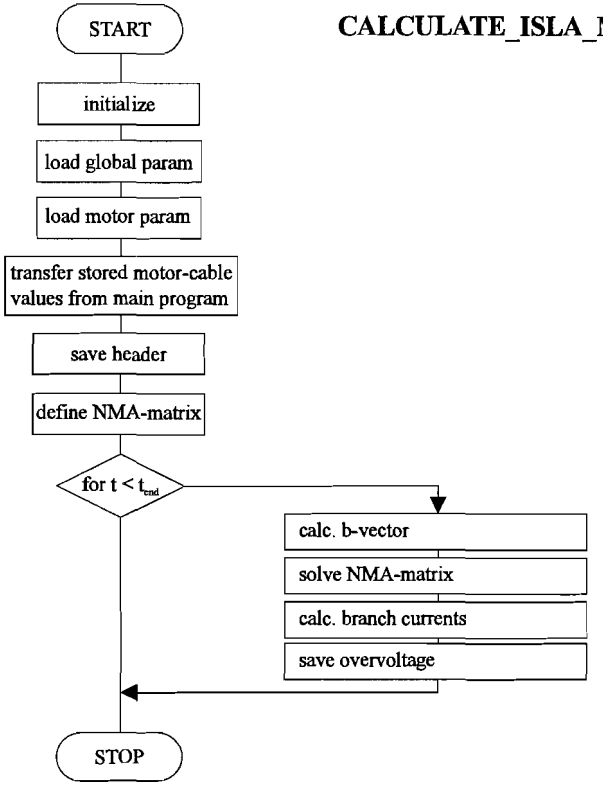

CALCULATE_ISLA_MOT